2018

DRILLABILITY OF TITANIUM ALLOY 6246

MAHROS DARSIN

A thesis submitted to Auckland University of Technology in fulfilment of the requirement of the degree of Doctor of Philosophy

School of Engineering, Computer and Mathematical Sciences

Department of Mechanical Engineering

ATTESTATION OF AUTHORSHIP

I hereby declare that this submission is my own work and that, to the best of my knowledge and belief, it contains no material previously published or written by another person (except where explicitly defined in the acknowledgments), nor material which to a substantial extent has been submitted for the award of any other degree or diploma of a university or other institution of higher learning.

Signed  Date 20/02/2018

ABSTRACT

Titanium alloys are relatively new materials that have been used extensively, especially in aerospace applications. The main properties are: a high strength to weight ratio (three times that of steel), an ability to maintain strength at elevated temperatures, excellent corrosion resistance and biocompatibility. The latter makes these alloys suitable to be used for body implants, such as for teeth and bones. However, titanium alloys are not easy to machine. They tend to behave in a springy manner due to a low modulus (Young) ratio. Their low heat conductivity makes the heat that emerges from machining mostly absorbed by the tool. Consequently, the tool loses its ability to cut further. One titanium alloy, named as Ti-6Al-2Sn-4Zr-6Mo (or Ti-6246), which has better corrosion resistance than the most widely used Ti-6Al-4V, faces the same problem when coming into the machining workshop. Meanwhile, only limited research has been conducted on the Ti-6246 alloy relating to its machinability, such as turning, milling and slab milling. Some non-conventional machining processes have been tried, such as Electrical Discharge Drilling, and Wire-EDM. There are more advantages in attempting hybrid machining by using Ultrasonic Assisted Turning (UAT) though. However, to my knowledge, no paper has been published on drilling the Ti-6246 alloy.

Drilling is a fairly simple process. However, the geometry of the drill bit or drill insert is very complicated. During drilling, a drill insert employs a different cutting speed from zero in the centre of the chisel to the maximum at the outer side (the rubbing side). This research will concentrate on the drillability of the Ti-6246 alloy. Drillability is derived from the machinability of the drilling process. It means an attempt to find the best parameters which result in the minimum force employed for drilling, with the longest tool life, whereby the minimum surface roughness and excellent roundness can be achieved. To reach the goals an extensive and systematic set of experiments will be carried out, while simultaneously the phenomena behind the process must be understood. Therefore, an understanding of microstructure and mechanical properties during the process will be studied in depth by utilising a comprehensive analysis of tools, forces, material and chips all together.

The Taguchi L-18 method was used for designing the experiments. This was followed by an ANOVA analysis of data using Minitab 17 software, where the optimum characteristic of drillability has been achieved. However, combinations of different

machining parameters and environments have been suggested due to the different criterion of the characteristics of drillability. As displayed by the chip formation the optimum result was achieved when keeping the Ti-6246 alloy in its received condition and applying a cutting speed of 50 m/min, and a feed rate 0.15 mm/rev for drilling 30 mm with a coolant. Consequently, in accordance with tool deterioration criterion, machining with a coolant, at 30 mm deep, a cutting speed of 50 m/min and a feed rate of 0.15 mm/min simultaneously, this would result in the least tool deterioration. Further, the optimal condition for drilling forces would be achieved when drilling with a cutting speed of 27 m/min, a feed rate of 0.08 m/rev on depth of only 10 mm without coolant, while the material should be HT1 treated. Lastly, the optimum surface roughness between 0.3113 µm to 0.5235 µm was achieved when drilling with these parameters: Clt_{off}, HT_{AR}, h_{10}, Vc_{35}, $Fr_{0.08}$.

ACKNOWLEDGEMENTS

Prior to acknowledging some people, I would like to praise Almighty Allah. He is the Most Gracious, the Most Merciful, and enables me to seek knowledge up to the highest level of academia in my old age. It is part of my obedience in Him and His Messenger (peace be upon him) to walk over the world to seek knowledge and to gain wisdom.

Special gratitude goes to my dearest supervisor, Associate Professor Tim Pasang for the guidance, stimulation, encouragement and patience in supervising my PhD study; especially his critical and detailed review in all my steps of research and in composing this thesis. I would also like to express my gratitude to Professor Zhan Chen as co-advisor, for his support with my work, deep discussions and suggestions on my writing and presentations.

I am grateful to my beloved mother, Siti Sholihah, for her special prayers and eternal love. I specially devote this hard work to my late father, Rotiban, for his frequent question to me during his life: "When are you going to pursue your doctorate?" Also a very big thank you to the rest of my brothers and sisters (both in blood and in-laws), for supporting my family reunion in Auckland.

To my beloved wife, Setijobudi Asri Ningrum: many thanks for encouraging me to pursue my PhD degree and your continuous prayers, support and understanding especially during critical times. To my beloved son and daughters, Khalid, A'yun and Fatimah: thanks for accompanying me and departing due to my study period.

A very special gratitude goes out to DIKTI/AUT Scholarship for providing the funding for my study.

A special mention goes to the following university staff: Jim Crossen, Jamie Ross, Mark Masterton, Thomas Jones, Tim Luton, Patrick Conor, Dave Crofts, Steven Hartley, Bum Jun, Anna Matich, Josephine Prasad, Teteh Veronika, Lesly and Leonie. It was fantastic to have the opportunity to work on most of the research with your assistance. A special gratitude to Suzanne Hardy who have proofread this thesis.

I am also grateful to my colleagues in the Centre of Advanced Manufacturing group: Doddy, Yuan, Nurul, Kourosh, Mana and Steve for having discussions, sharing information and having fun on BBQ events at Tim's & Zhan's house. A huge thank you goes to brother Sabri for helping me in developing the simulation.

And finally, last but by no means least, also to my brothers in the AUT Muslim prayer space (AUT Masjid) especially Sheikh Rafat for their brotherhood and advice that made me feel at home during my stay in Auckland.

LIST OF PUBLICATIONS

1. M. Darsin, T. Pasang and Z. Chen. *Drillability of titanium Alloy Ti-6246*. The Twenty-fifth International Conference on Processing and Fabrication of Advanced Materials XXV. January 22 – 25, 2017.
2. M. Darsin, T. Pasang and Z. Chen. *Serrated chips formation when drilling Ti-6246*. The 28th New Zealand Conference on Microscopy, January 31 – February 3, 2017.
3. M. Darsin, T. Pasang and Z. Chen. *Performance of TiAlN PVD coated carbide tool when drilling titanium alloy Ti-6246*. International Conference on Materials Science and Nano Technology, April 19 – 22, 2017. Followed by publication in MATEC Web of Conferences, Volume 109 (2017).
4. M. Darsin, T. Pasang and Z. Chen. *Drillability of titanium Alloy 6Al-2Sn-4Zr-6Mo: cutting forces point of view*. The 3rd International Conference on Precision Machinery and Manufacturing Technology (ICPMMT 2018). Auckland, New Zealand, Feb 4 - 8, 2018.
5. M. Darsin, T. Pasang and Z. Chen. *Achieving holes quality in drilling titanium alloy 6246 with TiAlN-coated carbide drill insert by Taguchi method*. Submitted to Journal of Advanced Manufacturing Technology (JAMT) (in the 2nd stage of review).
6. M. Darsin, T. Pasang and Z. Chen. *Forces perspective of drillability of titanium alloy 6Al-2Sn-4Zr-6Mo*. Submitted to Journal of Energy, Mechanical, Material, and Manufacturing Engineering (JEMMME) (in review).

TABLE OF CONTENTS

LIST OF FIGURES

LIST OF TABLES

GLOSSARY

Symbol	Meaning
α	Alpha phase
α’	Martensitic alpha phase
β	Beta phase
Vc	Cutting speed
fr	Feed rate
DoC	Depth of cut
d	Diameter of drill bit
h	Depth of drilling
HT	Heat treatment
HT1	Heat at 870^{o}C for 3 hours then followed by air cooling
HT2	Heat at 870^{o}C for 3 hours then followed by water quenching
Fz	Thrust force
Mz	Torque
HV	Hardness in Vickers scale
HB	Hardness in Brinell scale
SEM	Scanning electron microscopy
Ra	Arithmetic surface roughness
Rd	Roundness
S/N	Signal to noise ratio
Gs	Degree of serration
H	Height from the bottom to the top of the chips
C	Height from the bottom to the valley of the chips

CHAPTER 1. INTRODUCTION

1.1 Background

Titanium was found in 1790 as ilmenite ($FeTiO_3$) by William Gregor, then five years later by Martin Heinrich as rutile ore (TiO_2). Pure titanium was first successfully extracted from rutile ore by the Hunter process (attributed to A.M. Hunter, an American chemist) in 1910. It is a very high purity metal which is ductile when hot, but brittle when cold. Initially, it was mainly used as an alloying element in steel. An industrial scale of titanium production was launched in the 1940s using the Kroll process [1].

In the early 1950s, titanium alloys were developed for the applications of defence and aeronautical sectors because they have a compatible behaviour of high strength-to-weight ratio. However, since the 1960s it was proved that titanium tubing in a power plant heat exchanger cooled with sea water that there was no corrosion for several years. Therefore, their application used in the corrosion resistant environment started to increase. In fact, the application for a corrosion resistant material became the major reason for the production of commercially pure titanium (CP titanium) for non-aerospace applications in that era [2]. By 2006, world product shipments of titanium were estimated at over 60,000 metric tonnes, speeding up to 300,000 metric tonnes in 2013 (Figure 1.1), of which at least 50% was used in applications other than aerospace.

In the aerospace industry, the application of titanium alloys are used for blades and discs of compressors in jet engines, and the structure of airframes in aircraft such as in landing gear, space rockets and satellites. The aerospace industry uses it in a variety of components because it has excellent strength, light weight and is also excellent in its resistance to corrosion. Its high density and strength compared to other materials is shown in Figure 1.2. In addition, titanium alloys are compatible with the graphite fibres in polymeric composites (another high percentage usage material for aerospace components) [3]. Titanium is now broadly used for the oil and gas industry, jewellery, as an architectural, racing or sport car material and in general recreational products from golf clubs to bicycles, spikes in a sprinter's running shoes, and so on. A certain titanium alloy is now being using used for seat posts and handlebars on mountain bikes. The benefit of using this kind of titanium alloy for handlebars is associated with

a low modulus of elasticity. Its biocompatible properties have boosted its application for use in medicine as bone and dental implants, as well as prosthetic devices. In addition to its biocompatibility, the established application in the biomedical area is due to its high fatigue strength and the lower modulus of elasticity [2]. Titanium improves the quality of individual lives when it is used in eyeglasses and even in lightweight wheelchairs. The wide spread of applications are in line with the method and variety of the alloying process.

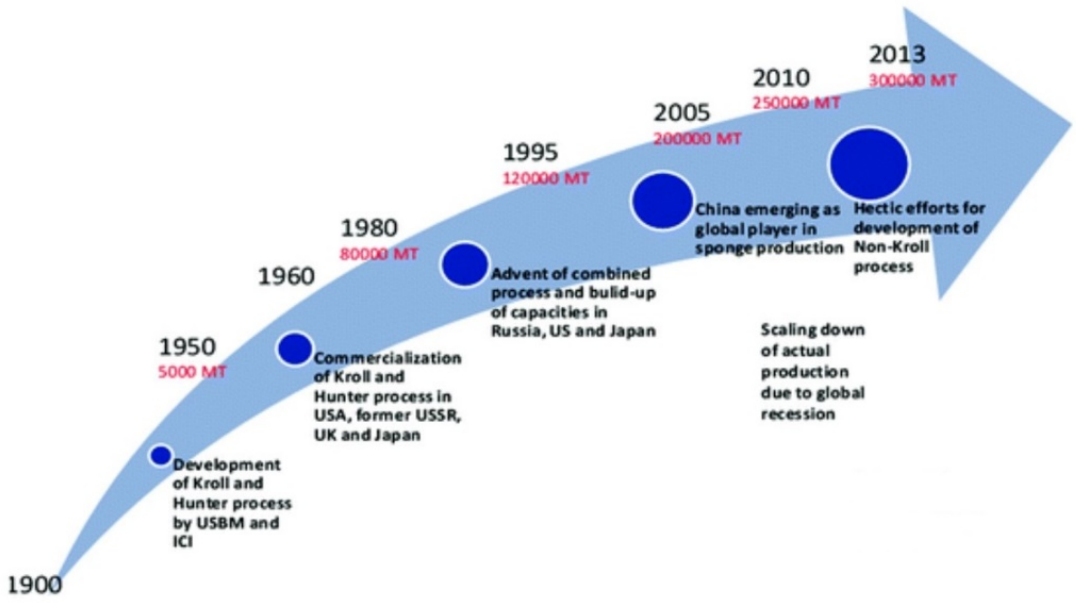

Figure 1.1 Trends in world titanium production [4].

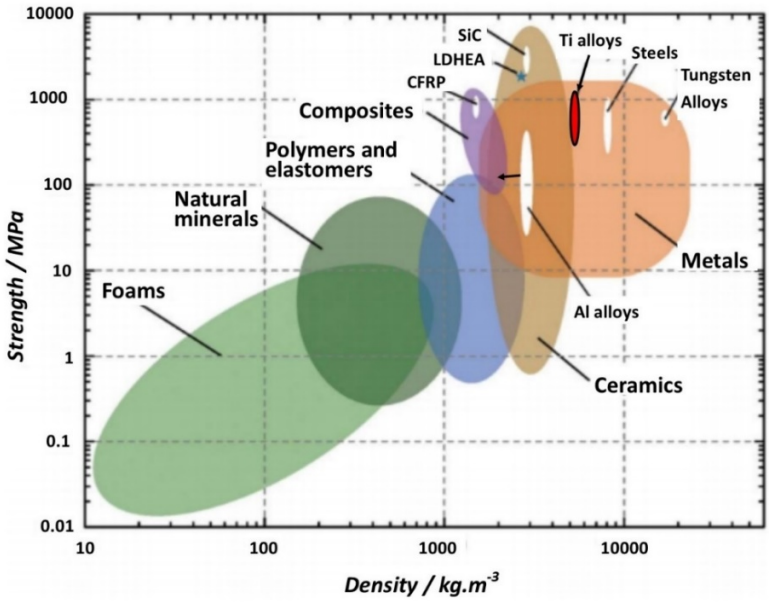

Figure 1.2 Ashby plot of strength against density of titanium alloys among engineering materials [5].

Titanium is also commonly alloyed with other elements to ensure that their mechanical properties meet the requirements of various applications. Based on the alloy type, there are four categories of titanium: (i) pure, (ii) alpha and near-alpha, (iii) alpha-beta, and (iv) beta alloy. Pure or commercially pure (CP Ti) titanium is unalloyed. They rely on oxygen (O) and nitrogen (N) as their strengthening elements. Alpha and near-alpha alloys are alloyed with some alpha stabilisers, for example aluminium, oxygen, and nitrogen that will improve the temperature as a result of which the alpha phase is stable. By contrast, beta stabilisers, for instance molybdenum and vanadium, tend to stabilise the beta phase at lower temperatures. Consequently, alpha-beta alloys are made when some alpha-favouring and some beta-favouring elements are alloyed to the titanium [6].

Ti-6Al-4V, one of the alpha-beta alloys, is the most widely used nowadays. Its outstanding properties are high specific strength, biocompatibility and corrosion resistance. It is distinctive in that it conjoins desirable properties with essential workability and good shop manufacture ability. Also, the production capability and commercial readiness leads to its usage becoming reliable and economic. Accordingly, wrought Ti-6Al-4V became the reference alloy to which other alloys should be compared when choosing a titanium alloy for a specific application [6].

Titanium alloy 6246 (Ti-6Al-2Sn-4Zr-6Mo or Ti-6246) is an alpha-beta alloy [6]. It has excellent corrosion resistance; superior to that of the most popular titanium alloy (Ti-6Al-4V) due to its 6% molybdenum content [7]. The fact that a regular and unremitting oxide layer forms instantly when exposed to oxygen makes this alloy better protected from the effects of corrosion [7]. Other advantages of Ti6246 are its very high strength-to-weight ratio (favourable for aerospace components), low thermal expansion, it is non-magnetic, has sound fatigue resistance, is able to be heat treated [8] to a minimum of 1040 MPa (higher strength levels than Ti 6Al-4V) and has reliable mechanical properties at high temperatures. This alloy is designed to combine the elevated temperature characteristic of Ti-6Al-2Sn-4Zr-2Mo with higher strength levels [9]. Due to its advantages this alloy has potential applications, especially where sea water corrosion would most likely happen. Therefore, these alloys could be used for sub-sea wellheads and well sampling equipment. Other potential applications are for oil and gas drilling tools, housing and shaft for gas and oil drilling. When the

weight-to-size becomes a major consideration this alloy is an alternative and has been used for the frame and other components of motorsport with high-performance.

Both titanium alloys (Ti-6Al-4V and Ti-6246), as are other titanium alloys, are among the not easy-to-machine metals. The machinability of titanium alloys is poor and it has been attributed to disfavoured thermal conductivity and extreme chemical reactivity. Moreover, thermoplastic instability and the tendency of chips to pile up, leads to its poor machinability. In general, 40% to 50% of titanium costs are directly related to machining. Therefore, studying machinability of Ti-6246 is valuable. Machinability is a measure of how easy a given material may be machined with a cutting tool.

General advice in machining titanium is to maintain the tool's condition (to keep the tool sharp), maintain a high feed rate (and never stop feeding), keep the cutting speed low, and use plenty of cooling fluid. Many machinability studies have been carried out on Ti-6Al-4V and less on Ti-6246. Furthermore, due to the unique nature of the drilling, not all the suggestions can be implemented. For example, cutting speed is variable from zero at the chisel (center of drilling) to a maximum at the heel of the drill bit. This is different from the case in turning or milling. Also, abundant cutting fluid cannot be applied unless the machine and the drill are designed for this purpose (through the use of coolant).

Concerning chip morphology, it is scientifically unclear as to why and how the serrated chips form when machining titanium alloys. There are two theories relating to the formation of serrated chips; adiabatic shear theory and periodical crack theory. These both contain some disadvantages or contradictions. An effort to combine those mechanisms of chip serration needs clarification due to inconsistencies in determining the degree of chip segmentation. Thermomechanical aspects of machining should be considered instead of only cutting the speed and feed rate, as already suggested by Siemers [10], that shear is deformation followed by recrystallisation. The effect of heat treatment to the strain rate and shear rate before machining and consequently to thermoplastic shear instability or crack formation, is also worth studying. The effect of BUE existing on tools should also be considered in the formation of segmented chips.

Another trend in studying machining and machinability is by modeling or simulation. There is no doubt that this method is very cheap, more flexible and more promising.

In modeling, no real material nor tool, should be bought or sacrificed for trial and error experiments. It is more flexible to change the parameters of machining without the risk of damaging the machine or operator. Furthermore, availability of commercial software with some improved capability makes the simulation a fast growing research method. For serrated chip formation, some simulation has achieved good conformity with the experiments in terms of chips forming, but still needs improvement for the heat generated and forces at work during machining. Moreover, most of the chip formation modeling is in the orthogonal cutting and in 2D format. Therefore, developing a simulation of serrated chip formation for drilling in 3D is a great challenge.

The study of drillability of Ti-6246 in this investigation is an attempt to answer the following questions:

a. How do various cutting parameters (f_r, V_c, and depth of drilling), cutting environments (dry and wet), material treatment (untreated and heat treated) affect the formation of segmented chips? Which parameters are more dominant in affecting the chip formations?

b. What and how do tools deteriorate under various drilling parameters?

c. How to achieve the best drilled holes?

d. Could chip formation in drilling be modeled in 3D?

1.2 Purpose of the Study

Drillability of Ti-6246 is the focus of this research. The term ‘drillability’ is derived from the terms of machinability [11] that implies the ability of a certain material to be machined using a cutting tool with a minimum cutting force, the best machined surface roughness, circularity and roundness, and with longer tool life. However, modeling in 3D for drilling was developed with a concern about serrated chip formations to create the foundation of drilling simulation for the next research.

1.3 Significance of the Study

As far as I know there is no published paper on drilling Ti-6246 alloy. Therefore, research on drillability of Ti-6246 should make a contribution on how to drill this

material economically and efficiently. Furthermore, the simulation/modeling of chip formation during drilling, with the existence of built-up edges, will be a foundation for the next development of simulation of the drilling process of titanium alloys.

1.4 Thesis Outline

The thesis is organised into several chapters and further into sub-chapters according to the thesis objectives.

Chapter 1 gives a general introduction about titanium, its application, the purpose of the study and significance of the study.

Chapter 2 provides a wide literature review of past research. An overview of titanium and its alloys is described briefly in sub chapter 2.1. Knowledge of machining and machinability from basic to specific in titanium alloys and more exclusively in machinability of Ti-6246 is presented in sub-chapter 2.2. Sub-chapter 2.3 is concerned with the Taguchi method and its application. Sub-chapter 2.4 provides a basic theory of simulation for machining and its application.

Chapter 3 describes the experimental procedures prior to drilling, observation during drilling, and laboratory preparation for microscopy observation. The procedure for using Minitab for analysis is presented in this chapter.

Chapters 4-6 present the experimental results followed by discussion of each study concern. Chapter 4 is concerned with chip formation. Chapter 5 discussed tool deterioration, whereas Chapter 6 is more focused on drilled holes and surface integrity.

Chapter 7 provides the overall conclusion and recommendations for future works based on this research.

CHAPTER 2. LITERATURE REVIEW

2.1 Overview of Titanium and its Alloy

Titanium has a unique physical metallurgy. Unlike other metals which have simple atomic arrangements and only have a single certain crystal lattice, titanium – as an allotropic element – has more than one crystallographic form. These are stable at an exclusive range of temperatures. At a specific temperature, which is famous as the beta transus temperature (882°C [12], or 888°C [6]), pure titanium experiences a phase transformation. It is in a lattice form of hexagonal close-packed structure (hcp) below the transus temperature and in a body-centred cubic phase (bcc) at above this temperature [see Figure 2.1]. The bcc state will remain stable until the melting point of 1687°C. The state of the hcp crystal structure is commonly referred to as the α phase, and the bcc state as a β phase. The bcc structure is established as stable only at elevated temperatures. Only when another element is being alloyed with the titanium then is it possible for the alloy to remain in the cubic structure at the lower temperatures [6].

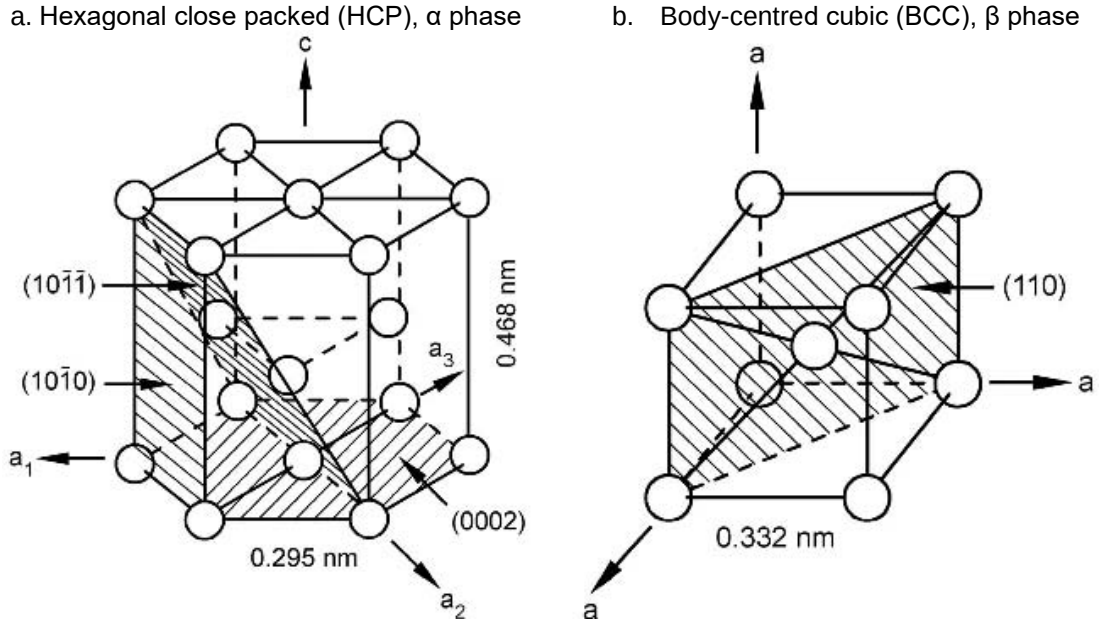

Figure 2.1. Two main crystal structures of titanium [2], [6], [13]

As an alloy in titanium, the dissolved elements can either (i) stabilise the α phase by elevating the temperature of α-β transition, (ii) stabilise the β phase by lessening the temperature α-β transition, or (iii) act only as a strengtheners of solid solutions and do not affect the temperature of transition. Titanium has high reactivity with several

interstitial elements including gases of nitrogen, hydrogen and especially oxygen. The reaction may happen below the melting point. The oxygen has a strong α-stabilising effect; therefore it decreases the transus temperature. The more interstitial elements there are the higher the strength. However, the ductility will sharply drop and the risk of embrittlement increases [12]. Some popular alloying elements and their effect is presented in Table 2.1.

Table 2.1 Common alloying elements and their stabilising effect [12]

Alloying element	Range (wt%)	Effect on structure
Aluminium (Al)	2 - 7	Alpha stabiliser
Tin (Sn)	2 - 6	Alpha stabiliser
Vanadium (V)	2 - 20	Beta stabiliser
Molybdenum (Mo)	2 - 20	Beta stabiliser
Chromium (Cr)	2 - 12	Beta stabiliser
Copper (Cu)	2 - 6	Beta stabiliser
Zirconium (Zr)	2 - 8	Neutral
Silicon (Si)	0.2 - 1	Neutral

The effect of alloying on the beta transus temperature indicates that there are four categories of titanium alloy, i.e. pure, alpha and near-alpha, alpha + beta and beta alloys. Commercially pure (CP Ti), alpha and near-alpha are generally characterised by high corrosion resistance and high weldability, but they are not heat treatable because they are single phase. The alpha + beta alloys have exceptional properties of strength and ductility if they are treated properly. They are stronger than both alpha and beta alloys. The last, beta alloys, are metastable, which have a tendency to convert to an equilibrium or balance of structure. They have higher deformability compared to alpha and alpha + beta alloys (hexagonal structure types) [13].

Apart from the four categories above, there are also titanium aluminides; an intermetallic compound of titanium and aluminium (with one or more additional alloy elements provided as well) [6]. Titanium aluminides are alloys based with three major intermetallic compounds: (i) Ti_3Al (Alpha-2 alloys), (ii) gamma TiAl and (iii) a ternary orthorhombic variant based on Ti_2AlNb [4]. Titanium aluminides are chemical compound alloys used to enhance strength, formability, and so on. Titanium aluminides have greater working temperatures than typical titanium alloys. The typical elevated temperature titanium alloys are only used up to temperatures somewhat above 500^{o}C, while titanium aluminide alloys are directly comparable to other high

temperature compatible alloys, such as well-established steels and Ni-based super alloys [13]. However, they are more expensive and usually have lower ductility and formability [6].

2.1.1 The Most Popular Titanium Alloys

For some decades, several manufacturing industries have been developing different types of titanium alloys for different applications. Among those alloys developed there are some that became popular and more widely used, such as Ti-6Al-4V, Ti-6Al-2Sn-4Zr-2Mo, Ti-6Al-2Sn-4Zr-6Mo, Ti-8Al-1Mo-1V and Ti-10V-2Fe-3Al.

Ti-6Al-4V so far is the most widely used and therefore the most popular among other titanium alloys. Its application is used widely in the aerospace industry and in medical use for artificial body parts, yet it is also used in the automotive, nautical and chemical industries [9]. Ti-6Al-4V is also used for the new technology of manufacturing integrally bladed rotors (IBR), either by using linear friction welding, i.e. direct attachment of the blades to the disc, or by machining the rotor from a single-piece forging [4]. Figure 2.2 shows a heavy Ti-6Al-4V forging for an aircraft, i.e. a landing gear. It has a combination of properties of high-strength and toughness. In addition, it has an excellent corrosion ratio [6]. Its properties are developed depending on grain refinement (during cooling from the beta phase) and decomposition of martensite formed upon quenching (by maintaining the aging at low temperature) [6].

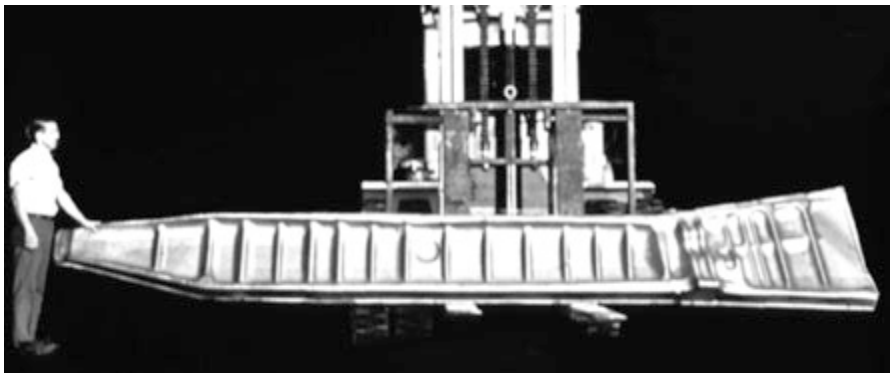

Figure 2.2 Large Ti-6Al-4V forging for the landing gear of Boeing 747 [4].

Titanium alloy Ti-6Al-2Sn-4Zr-2Mo is eminently applied mainly for higher temperature titanium alloys. Usually the modified version Ti-6Al-2Sn-4Zr-2Mo-0.08Si (Ti-6242S) is used. In comparison to the most widely used titanium alloy (Ti-6Al-4V), Ti-6Al-2Sn-4Zr-2Mo has a higher working temperature; 300^{o}C for the

former and 450°C for the latter [12]. For long term applications however, it lasts up to 425°C [9]. Therefore, it has potential in applications for higher heat resistance as used in such items as plugs and nozzles. It is also used in the application where a combination of several good properties is required, such as for gas turbine components. However, as other titanium alloys, its tribological properties are poor. Other drawbacks of this material are its low surface hardness and little wear resistance; that makes this material have restricted applications.

2.1.2 Titanium Alloy 6246

Ti-6246 alloy, by standard, comprises of 6% aluminium (Al), 2% tin (Sn), 4% zirconium (Zr), 6% molybdenum (Mo), small amounts of other impurities, and titanium as the rest of the composition. Starting from pure Ti, adding Al reduces the weight of the α phase whilst stabilising it. The 6% of Mo is added to stabilise the β phase. Sn and Zr are also stabilising elements that encourage solid solution strengthening as in superalloys.

This alloy has a few more β-stabilised properties than that of Ti-6Al-4V, therefore more β phase exists at equilibrium at room temperature. Therefore, most of the literature includes it in an α + β alloy [8], [9], [13], while others claim it is nearer a β alloy [2], [4]. However, there is one literature which says that Ti 6246 is near α alloys (sometimes called super alpha alloys), and it barely reaches to α-β alloys [6]. Its structure is alpha in low temperatures, but becomes beta in elevated temperatures. Thus, more literature stated that Ti-6246 is among the α + β group.

This alloy is heat treatable which is designed to combine the strength properties at long term elevation of Ti-6Al-2Sn-4Zr-2Mo-0.08Si with the high developed short term strength properties of a fully hardened α + β alloy. Its application is for forging parts in intermediate temperature sections of gas turbines, particularly in compressor discs and blades [12] and also for seals and airframe components. Ti-6246 is considered to be used for deep, sour-well applications [8]. It also used for short term load-carrying applications up to temperatures of 540°C, whereas a maximum working temperature of 300°C to 400°C for long term load carrying applications is recommended; less that of Ti6242S [8].

The β transus temperature of this alloy lies between 935°C to 945°C. The microstructure consequently depends on the processing and heat treatment history. A typical microstructure consists of equiaxed primary alpha grains surrounded by a partially transformed beta matrix. The microstructure strongly influences the tensile, fracture toughness and high cycle fatigue properties. A microstructure of approximately 10% equiaxed primary alpha plus transformed beta matrix consisting of a relatively coarse secondary alpha and aged beta is claimed to result in optimum combination of strength, ductility and toughness. Small secondary alpha plates have been found to precipitate in the beta phase for this alloy. When water quenching the Ti-6246 alloy from above 880°C, an orthorhombic α" martensitic structure is formed, with lath morphology. Decomposition of α" into fine α precipitates have been reported to occur for treatments between 227°C to 527°C leading to increased hardness. Above 527°C softening occurs due to growth of the precipitated α phase (up to 627°C) and re-dissolution of a precipitated α phase into a β phase [12].

Different types of microstructures can be achieved by thermomechanical treatment, i.e. (1) fully lamellar (or basket weave or Widmanstätten), (ii) equiaxed (also called globular) and (iii) bimodal (also called duplex). The β-transus temperature is the main concern for thermomechanical treatment because it becomes a separation between the single (β) field and two-phase (α+β) field.

Lamellar microstructures are formed when cooling directly carried out from above the β-transus temperature. At above the beta-transus temperature, the material consists of beta grains only. Grain of α nucleates at the grain boundaries when the temperatures drop below the transus temperature, then it grows as lamellae into the (prior) β grain [13]. The critical parameter is cooling after recrystallisation treatment, where the higher the speed of cooling, the finer the lamellae that are created (Figure 2.3).

Globular (equiaxed) microstructures consist of equiaxed particles of the primary α phase (α_p); β-phase is along the grain boundaries. Equiaxed structure, unlike the lamellar microstructure, are the result of a recrystallisation process (Figure 2.4-a). Therefore, prior to solution treatment the alloy has to be highly deformed (cold worked) in the α+β field. Following the solution heat treatment at the temperatures in the two-phase field, a recrystalllised and equiaxed microstructure is produced [Figure 2.4-b(i)]. Prolonged annealing roughens the equiaxed microstructure [Figure 2.4-

b(ii)]. The volume fraction of the primary α determined by the solution heat treatment itself [14].

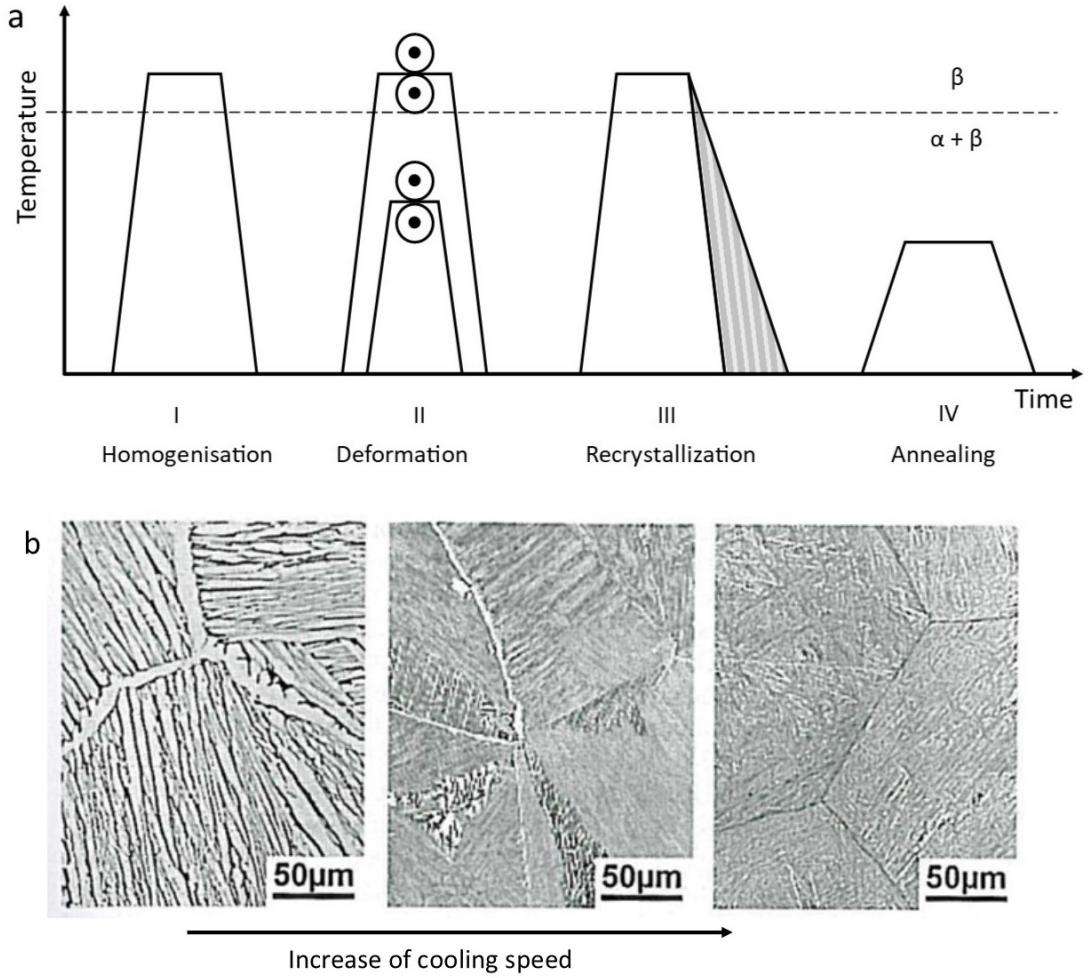

Figure 2.3. Processing route of fully lamellar microstructure (a) [4] and the effect of cooling speed on the lamellar size (b) [14].

Duplex (bimodal) can be achieved by the solution treatment in the α+β field, just below the β-transus temperature (Figure 2.5-a). Duplex structures consist of equiaxed (primary) α in a lamellar α+β matrix (Figure 2.5-b). Bimodal structures can be regarded as to be a mixture of lamellar and an equiaxed microstructure [13]. The key parameter is the cooling rate after homogenisation in the β-field, where the rate is decisive for the α lamallae size. Another key parameter is the temperature of annealing in the α+β field, where the temperature is decisive for the volume fraction of primary α phase.

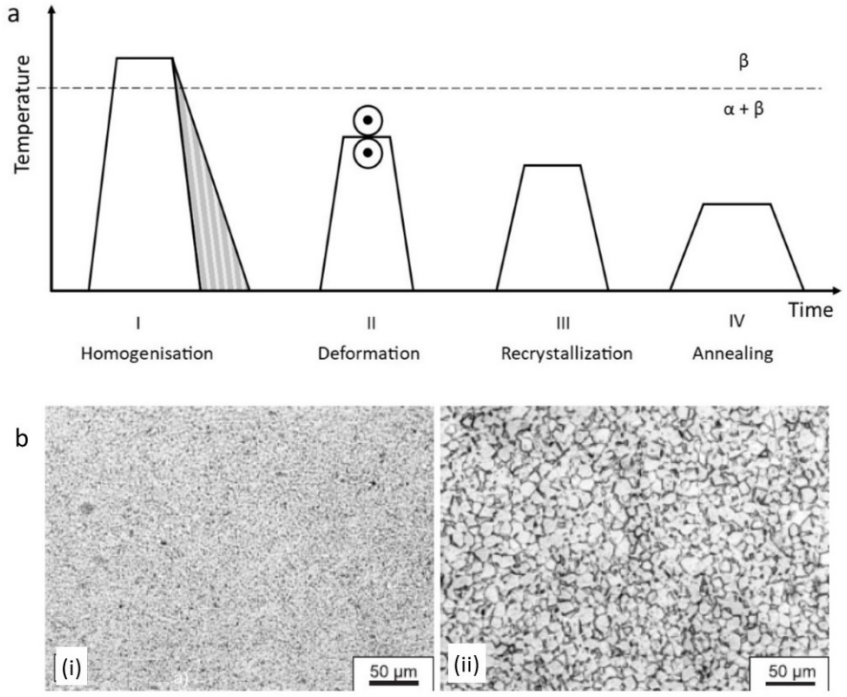

Figure 2.4. Processing route of globular (equiaxed) (a) [14]*, and the example of globular (equiaxed) microstructure: the fine one (b-i)& the coarse one (b-ii)*[13].

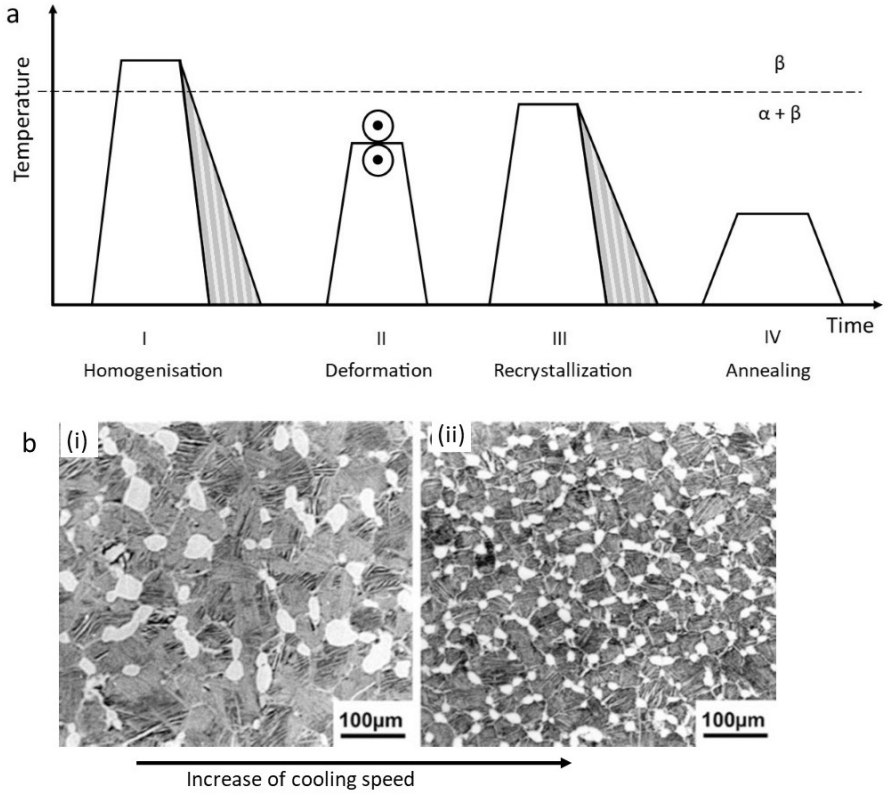

Figure 2.5. Processing route of duplex (bimodal) microstructure (a) and effect of cooling speed on the microstructure b(i) slow cooling rate, b(ii) fast cooling rate [4]

Apart from those three possible microstructures and the processes, there are two other kinds of possible microstructures which have resulted from different processes, i.e. beta processed microstructures and through-transus process microstructures. Figure 2.6-a shows a schematic of how the beta processed microstructures are produced. Compared to the previous processes, it is clear that recrystallisation (step III) is omitted to produce an unrecrystallised structure with a greatly deformed β grain boundary. From the beta deformation temperatures, the alpha layers are formed on the local shape of the grain boundaries which have already deformed [2], [4].

The through-transus process is made to alter the uninterrupted α layers at the β grain boundaries to particular globular α particles. The only difference with the β processed materials is step II (as shown in Figure 2.6-b). Special attention needs to be paid that the material has to be in the α+β phase region only for a short period before the final deformation process. That means producing the through-transus process which needs more delicate control than the β process. The microstructure is called “necklace” by CEZUS [2], [4].

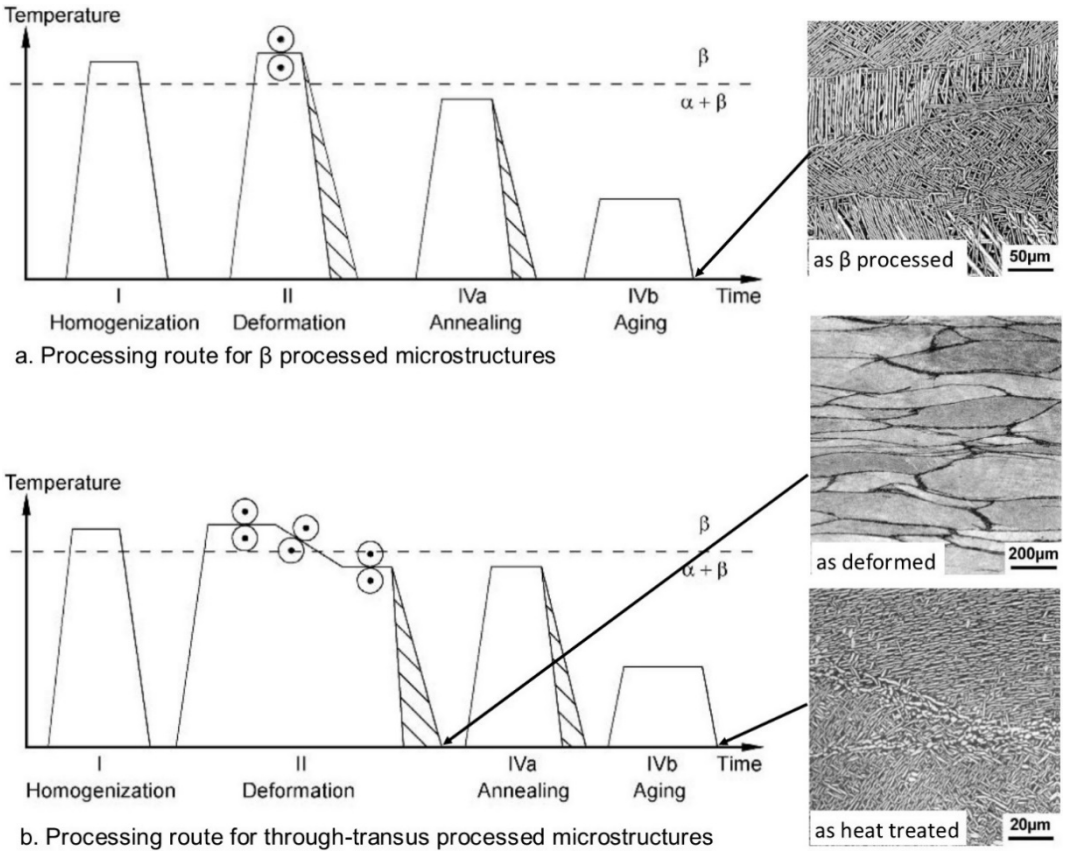

Figure 2.6. Two other alternatives for processing Ti-6246 and the potential microstructures [2].

2.2 Machining and Machinability

Machining is a manufacturing method in which the finished part is formed by removing the undesired material from a workpiece. The finished part should accomplish the requirements of form, size, and quality of surface [15], [16], [17]. In manufacturing processes, machining is usually required as the last step following other processes such as casting, forming, and welding, etc. because they usually cannot produce a fine surface quality. Overall there are two types of machining, non-conventional and conventional machining. The difference between both types of machining is in how the material removal occurs. In non-conventional machining, the material removal is with emerged energy from the tool that erodes or scrapes the workpiece. It means there is no direct contact between the tool and the workpiece. The material removal categories appear according to the type of energy utilisation needed; either by a mechanical, chemical and electrochemical or thermoelectric process [17]. Examples of non-conventional machining by thermoelectricity are: electrical discharge machining (EDM) and laser beam machining (LBM). Whereas, the mechanical removal examples are: water jet machining (WJM) and ultrasonic machining (USM). In conventional machining, a sharp tool has direct contact with the workpiece, so therefore the tool must be harder than the workpiece. Processes included in conventional machining are turning, milling, broaching, shaping, planning and drilling.

Drilling is a hole-making machining operation using a drilling tool. Drilling is one of the most extensively used for material removal in the machining sector. This process is specialised for making a hole or enlarging it, as the finished hole or a basic one will be continued by other processes such as threading, chamfering or honing. It is a fundamental process and contributes to 40% to 60% to the whole machining process of the structural frames of an aircraft (Brinksmeier, 1990 in [18]). In conventional machining, the drilling machine ranges from the most sophisticated computer-controlled or multiple-spindle machines to hand-held electric or crank-driven drills [19]. For non-conventional machining, laser beam machining (LBM) or wire-EDM (wire electrical discharge machining), these are the most common methods to make a hole.

Twist drilling is the most common hole-making method [20]. In the case of a twist drill, dimensional precision of both sides also determine roughness of the machined surface [21]. A twist drill can be composed of a single drill or a body and a drill insert fixed at the end of the body. However, basically the angles and planes for a twist drill are the same as shown in Figure 2.7-a. The cutting edges are the main part that cut the material. Before the cutting process takes place, the chisel touches the material. However, if the chisel is not sharp, it will press the material. In order to reduce the chisel width, the inner cutting lips are ground (thinning tool) (Figure 2.7-b). Flutes produced in a helical form are the way the chips move out and the way the cutting fluid comes in. The helix or rake angle (γ) describes the angle of the cutting face relative to the work. A rake angle is varied along the cutting edge (Figure 2.7-c), therefore the chip pattern is affected by this angle. A clearance angle (α) will give space (and to avoid friction) between the flank surface with the bottom drilled surface. In regards to an angle point ($2\emptyset$), drilling cannot be categorised as orthogonal cutting, but is rather considered oblique cutting. However, from the B-B view the drilling process is considered an orthogonal cut (Figure 2.7-b and 2.7-c).

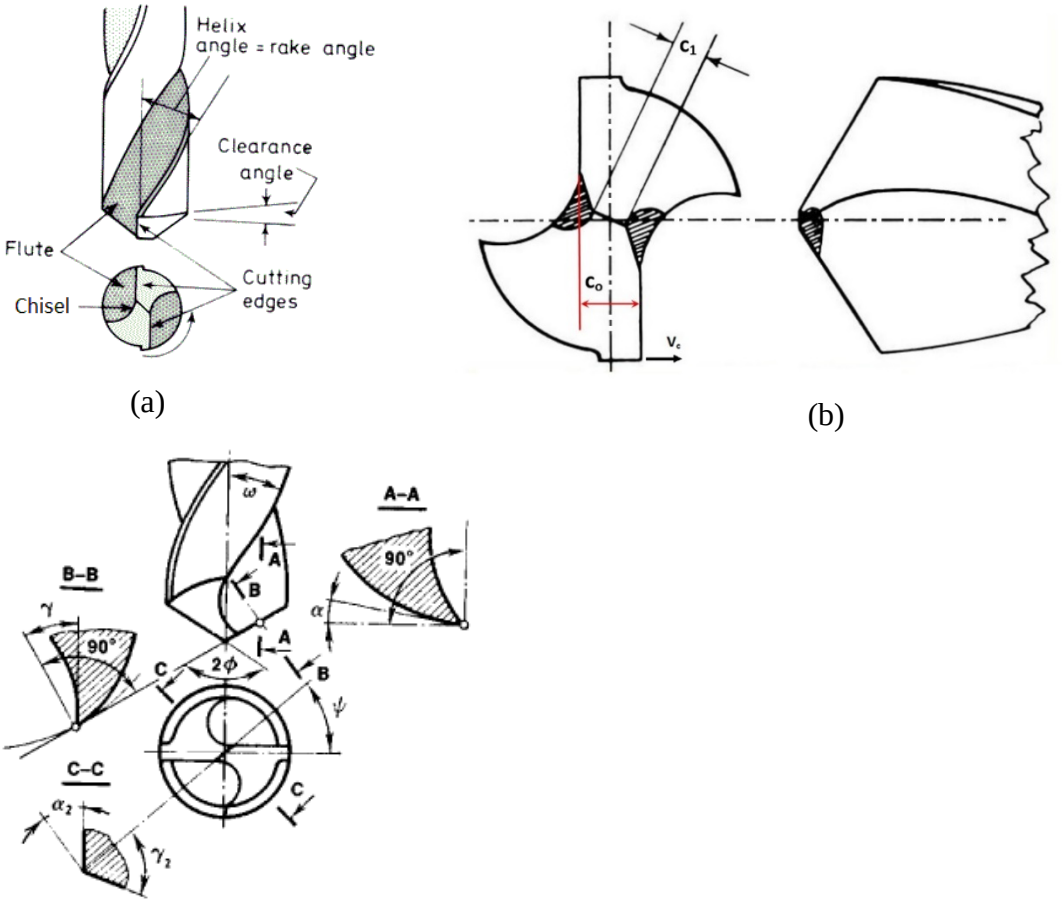

Figure 2.7. Parts and angles of a twist drill (a), thinning of chisel (b) and cutting view of a twist drill bit (c) [22].

There are two main forces at work on the tool tip; the thrust force (Fz) and torque (Mz) as an effect on the feed rate (f_r) and linear cutting speed (V_c) which is applied to the drill. Mainly the thrust force (more than 50%) has an effect on the works of a chisel [23], while torque is influenced by speed rotation and the diameter of the drill. The chip formed due to shear force ($\tau_{cutting}$) deforms the material then separates it. Heat is generated during machining, mainly due to the shear at the primary zone and friction between the rake plane of the tool and the chips which move along. An (exaggerated) ideal element of chip pattern for drilling is depicted in Figure 2.8-b. It is in a cone form with the height equal to radius (half of the insert tool diameter) and the depth of cut equal to half of the feed rate (DoC = fr/2). The form and size of total deformation of the chips, in regard to shear deformation the primary and secondary shear deformation of the chips before and alongside the tool face, depend on:

a. Workpiece material;

b. Material and geometry of the tool;

c. The drilling speed (Vc) and feed rate (f_r);

d. The type and method of cutting fluid application.

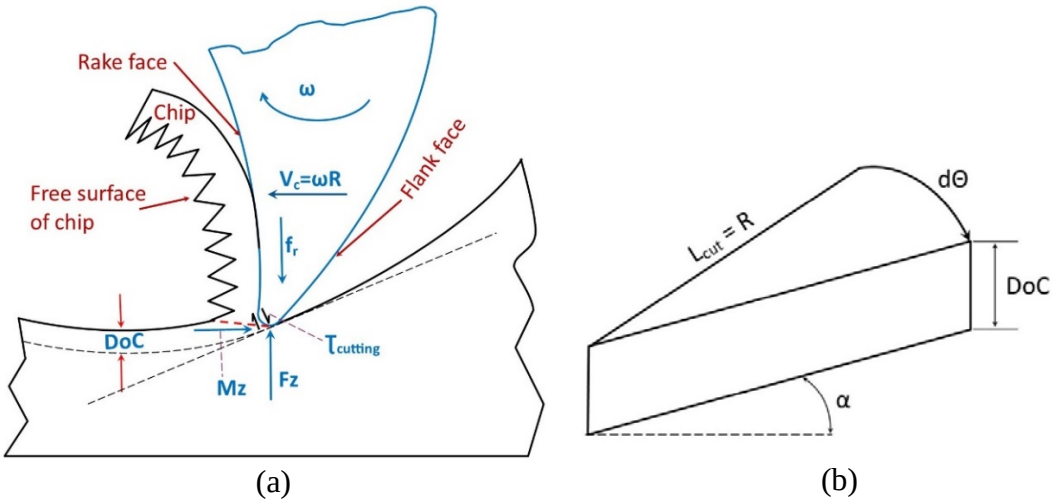

Figure 2.8. Mechanics of drilling; (a) Orthogonal view of drilling, (b) element of single cut chip

2.2.1 Tool Materials for Machining Titanium Alloys

Many tool materials, both coated and uncoated, have been developed and used to machine titanium alloys. It is reported that tool delamination, when using PVD coated with TiN, happened instantly after 5 seconds [18]. A rapid tool wear was experienced by most of the developed cutting tools when machining titanium alloys due to high reactivity with the machined material; there is no exception with very high grade tools such as diamond, ceramic and cubic boron nitride. The uncoated WC/Co or straight carbide tools have shown their superiority by the majority of studies' results for machining titanium alloys, especially for turning and milling. Nevertheless, for drilling Ti-6Al-4V, studies have proven that the PVD-TiAlN coated carbide tool has shown its superiority over the uncoated carbide [24]. By contrast to other researchers, Pramanik [25] stated that carbide based tools (such as carbide and binderless CBN) and diamond based tools (such as sintered diamond and natural diamond) seem to have sound compatability for machining titanium alloys.

2.2.2 Research on Drilling Titanium Alloys

To my knowledge, there are no published articles on drilling Ti-6246. Most of the published papers on drilling were on Ti-6Al-4V. Some of them are summarised in the following paragraphs.

Cantero et al. [26] used a TiN carbide coating tool for drilling Ti-6Al-4V with a cutting speed of 50 m/min and a feed rate 0.07 mm/rev. They varied the method of drilling; in the first group, the tool and workpiece were cooled after each individual drilling and the second group series of eight holes were machined with no suspension between drillings. They found that the holes were not different even after the tools were broken. There were also microstructure changes and consequently the hardness changed as an effect of the drilling (Figure 2.9). The hardness of machined surfaces increases until the depth of about 300 microns, which was fairly deep. Lastly, they found that the tool material adhered to the machined surface and vice versa, where elements of part of the material was stuck on the tool tip [26].

Rahim et al. [27] compared drilling of Ti-6Al-4V and Ti-5Al-5V-Mo/Fe. The latter alloy is considered a low production cost titanium alloy. The tool material was K grade uncoated WC/Co with a diameter of 6 mm. They found machining of both materials resulted in an identical tool life. Nevertheless, Ti-6Al-4V demonstrated a better machinability than Ti-5Al-5V-Mo/Fe, due to the fact that the previous material had the slower rate of tool wear than the latter. This result contradicts the previous researcher's conclusion [28], where surface roughness is improved by increasing the cutting speed.

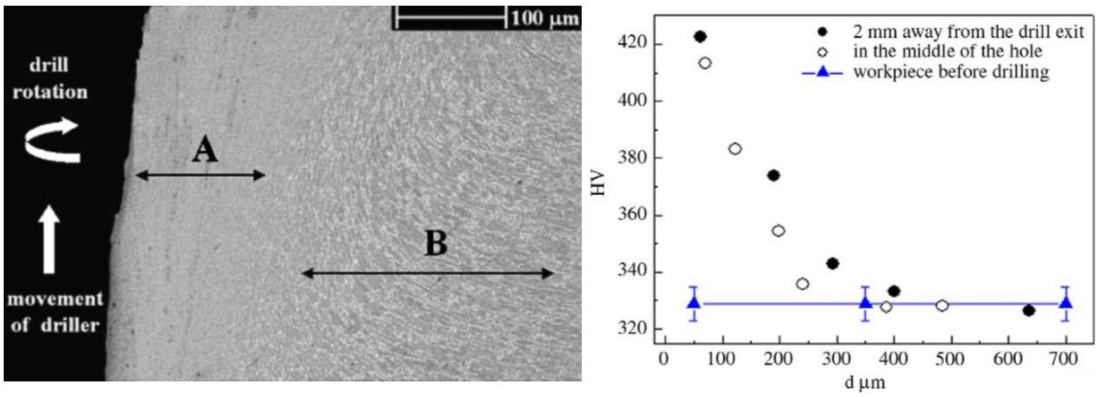

Figure 2.9. Microstructure change and hardness change as effect of drilling [26].

Cantero et al. [26] and Rahim et al. [27] have two similarities in their result, i.e. metallurgical alteration and mode of tool deterioration. Metallurgical alteration occurred on the drilled surface and was more severe with increased time and cutting speed. Deformation goes by the track of the drill rotation. They found that the tool deterioration mode was chipping or microchipping at the corner edge of the drill. At this corner edge a high temperature emerged, therefore, an adherent layer was formed. Along with the increase of the temperature, the adhered layer became weaker and could not bear the high compressive stress. Consequently, it might have pulled out some elements of the tool together with the moving chips. Examples of tool failures are shown in Figure 2.10.

Sharif & Rahim [18] compared uncoated carbide and TiAlN PVD coated carbide tools in drilling Ti-6Al-4V. They varied the cutting speed of 25, 35 and 55 mm/min and the feed rate of 0.06 mm/rev and water soluble coolant of 6% at a flow rate of 19.4 litre/min. They concluded that a coated tool has slower flank wear than an uncoated one, with the best tool life at a cutting speed of 25 mm/min. Therefore they recommended this TiAlN PVD coated tool for drilling titanium alloys. The same authors compared the performance of a TiAlN (mono-layer) with two kinds of supernitride (multi-layers) coated carbide tools [24]. The TiAlN coated carbide tool underperformed compared to the supernitride tool as shown in Figure 2.11. It might be due to the fact that TiAlN coating has a lower content of aluminium than that of a supernitride coated tool. The higher content of aluminium in the supernitride coated sample enhanced thermal and wear protection. The same research group has made comparisons between the point angle of three drills, i.e. 116.5, 120, and 133.4^{o}. Their observation indicated that surface roughness and subsurface deformation were both the best at an angle point of 133.4^{o}. Furthermore, the microhardness was not affected by the drill point angle [29].

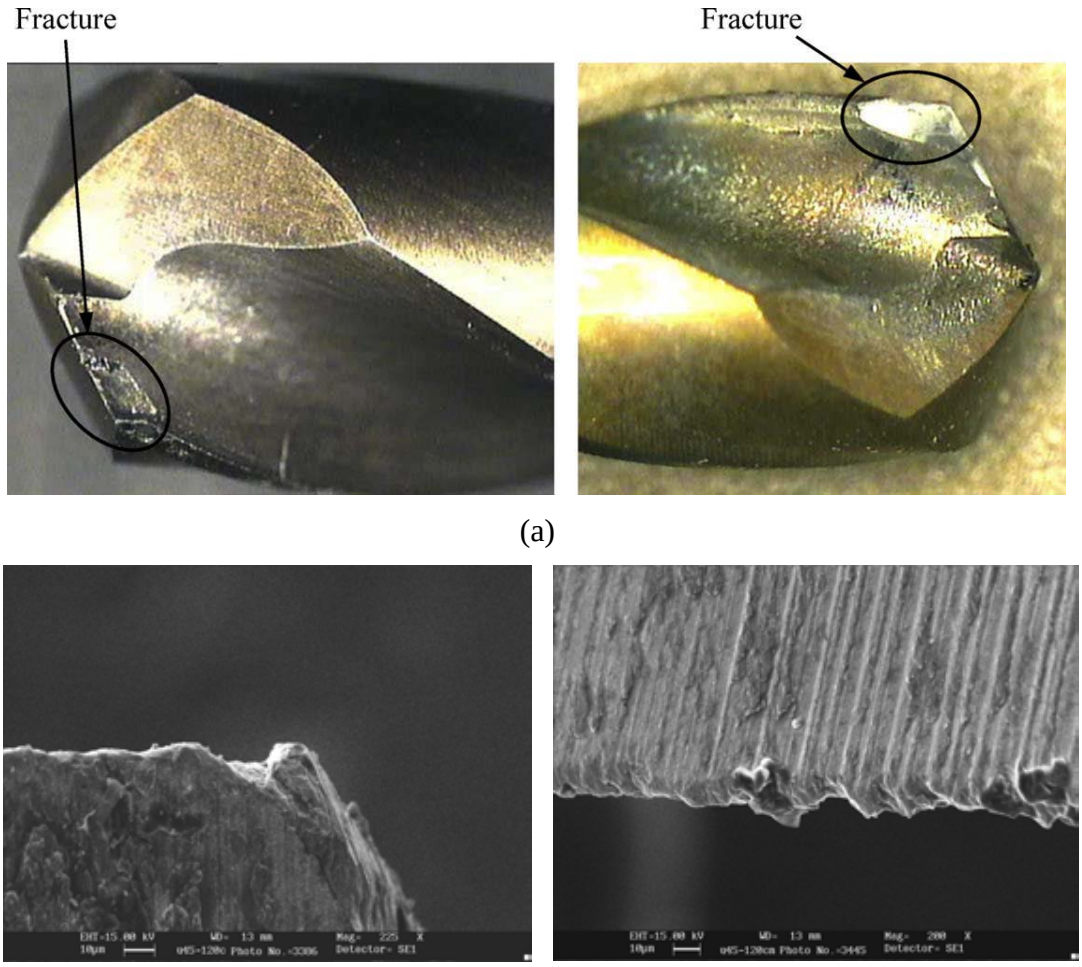

Figure 2.10. Typical drill failure: (a) Fracture at the edge corner of tool with different method of drilling [26]*; Microchipping observed using SEM by Rahim et al.*[27] *at Vc 45 m/min for (b) Ti-6Al-4V, and (c) Ti-5Al-4V-Mo/Fe*

Prabukathi et al. [30] used a statistical method to optimise the parameters for drilling Ti-6Al-4V with solid carbide (K200 drill diameter of 5 mm). They quantified that the thrust force was 92.7% as affected by the feed rate and only 5.6% by spindle speed. Meanwhile, torque was affected by 82% of the feed rate and only 10% by spindle speed. Their method was the Weighed Sum Optimisation Technique for Multiple Object Optimisation. Apart from forces, they also observed the holes diameter, circularity and exit burr. The quality of the drilled holes, especially hole sizes and circularity, were influenced by the number of experiments as shown in Figure 2.12. The more the holes were drilled, the more the deviation from the drill diameter and consequently the circularity.

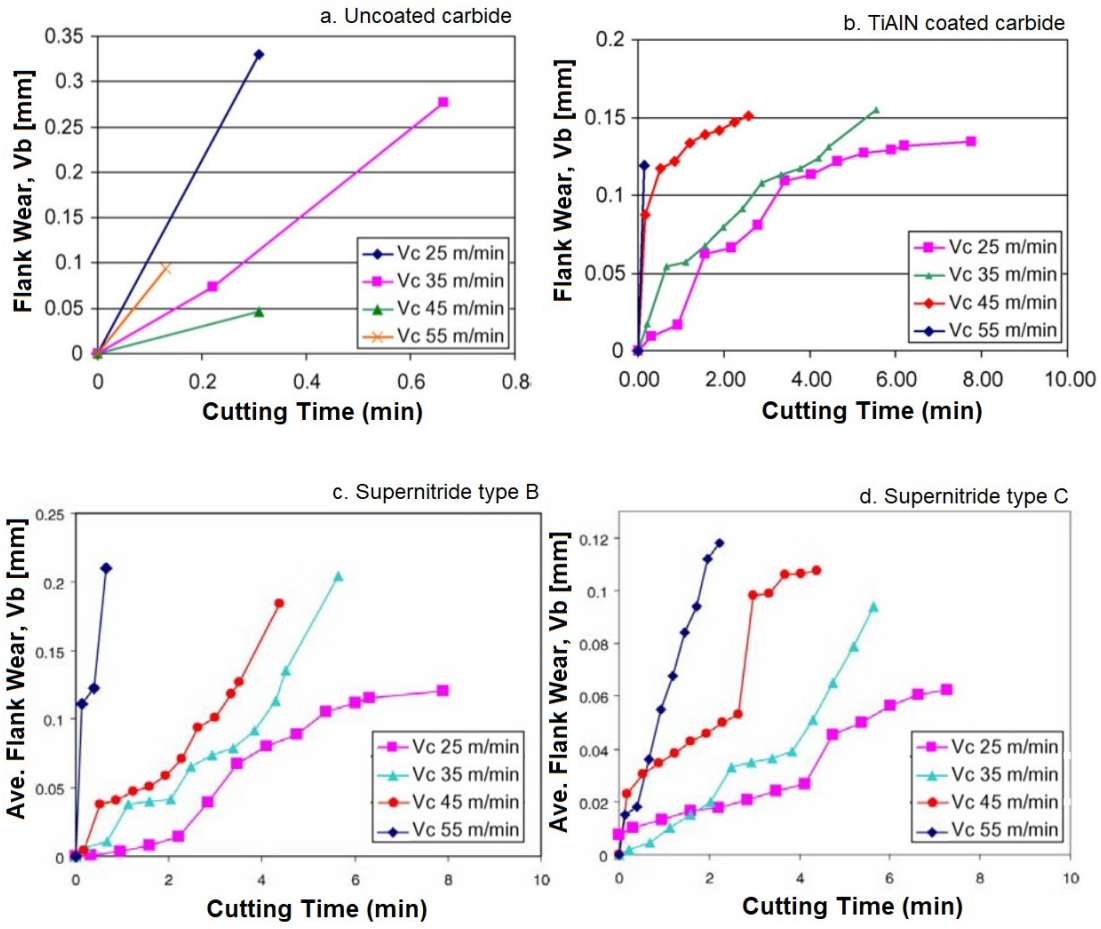

Figure 2.11. Flank wear of drilling using different tool materials: (a) uncoated carbide [18], *(b) TiAlN coated carbide, (c) supernitride type B and (d) supernitride type C* [24].

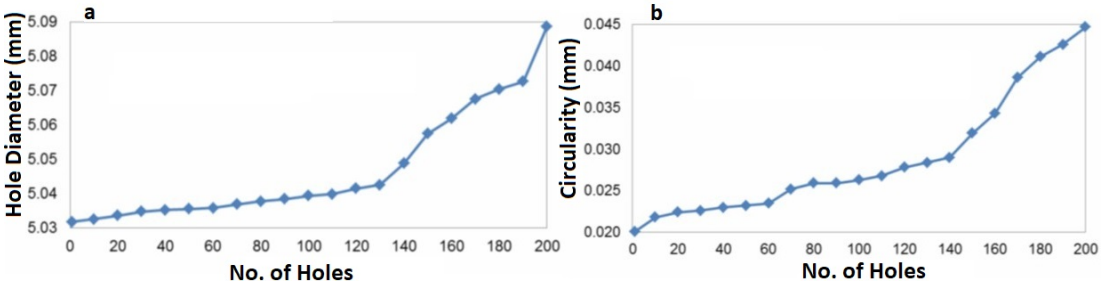

Figure 2.12. Hole diameter (a) and circularity (b) in tool life experiments [30].

2.2.3 Machining and Machinability of Ti-6246 Alloy

In terms of machinability, Ti-6246 alloy in the as-forged condition is similar to that of annealed Ti-6Al-4V and Ti-6Al-6V-2Sn [31]. In the solution treated and aged condition, its mechanical properties are equivalent to Ti-6Al-6V-2Sn for the same heat treated condition. As a general reference Ti-6246 can be beta solution treated at 985^{o}C, and aged at 595^{o}C [31].

Like other titanium alloys, Ti-6246 alloy is not easy to machine. The phenomenon is due to its high heat hardness, where only limited tools are recommended for machining it. Only the carbide & binderless CBN (the carbide based), and sintered diamond & natural diamond (the diamond based) [25] and uncoated- and PVD TiAlN coated-WC/Co carbide [18] cutting tools are considered satisfactorily suitable for machining titanium alloys. Its low heat dissipation rate makes the most of the heat generated during machining which is absorbed by the tool and consequently weakens it [32]. The heat distributed to the tool and chips, and absorbed by the work material are 80%, 10% and 10% respectively [32]. Its high affinity towards other materials results in the formation built-up on the tool then reduces the surface quality of the machined surface. In addition, Pervaiz et al., [32] suggested using a cutting tool and tool holder which had a high conductive property.

Machining on Ti-6246 has been carried out by different researchers, by means of turning and face milling. Some non-conventional machining has also been tried, such as EDM Drilling and WEDM. Lastly, hybrid machining has also been tried by using Ultrasonically Assisted Turning (UAT).

Turning of Ti-6246 has been performed by Rihova et al. [33]. They focused on the wear mechanism of dry turning with a standard coated tool TK 2000. The depth of cut was varied between 0.05 to 0.2 mm with a cutting speed from 20 to 300 m/min. Observation of the flank face showed notch and abrasion wear, while on the rake face experienced crater, micro-cracking and a built-up layer (Figure 2.13). Micro- cracks formed when using DoC 0.2, Vc 160 and DoC 0.2, Vc 200.

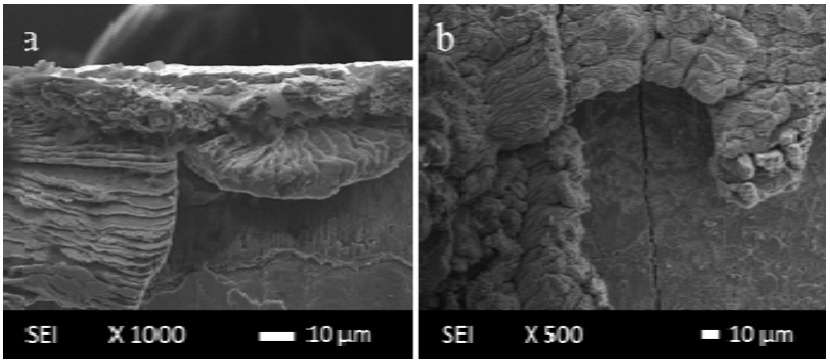

Figure 2.13. SEM images of different wear mechanisms (a) build-up edge formation, (b) microcrack formation [33].

Sharif et al. [34] performed face milling on Ti-6246. They compared machinability with both a sharp and chamfered tool. The cutting speed has no significant effect on tool life with a chamfered tool; however a low cutting speed results in better tool life for a sharp tool (Figure 2.14). Similar (non-uniform) flank wear on both tools is displayed at the initial machining, but it was higher in the chamfered tool. The researchers argued that chipping acceleration and flaking of the cutting edge caused by unstable cutting as a consequence of a chamfered tool subsequently means a negative T-land.

Using wire-EDM on Ti-6246 has been compared with conventional milling [35]. The main focus of this research was observing the fatigue life after machining. Statistically, there was minimal difference in the performance of fatigue of the material between WEDM and the flank milling (Figure 2.15). Variation in the fatigue life of both machined surfaces is in likelihood due to differences in the residual stress state.

Muhammad et al. [36] have performed modeling for Ultrasonic Assisted Turning (UAT) for machining Ti-6246, then compared the built model with experiments. They found parameters that would be used for the next experiments. Later on, they compared conventional turning (CT) and ultrasonic assisted turning (UAT) for the machining of Ti-6246 and Ti-676-0.9La (the modified Ti-6246) [37]. An obvious lessening of the cutting forces was observed for both alloys as an effect of vibration application. There was a significant reduction of 74% in the tangential component of the cutting forces at a speed of 10 m/min in both alloys. Therefore, the UAT diminished the radial component force by 59% for Ti-6246 and 74% for Ti-676-0.9La.

Apart from turning, face milling, wire EDM and UAT there are no published papers regarding the conventional drilling of Ti-6246; therefore drilling was chosen for this research.

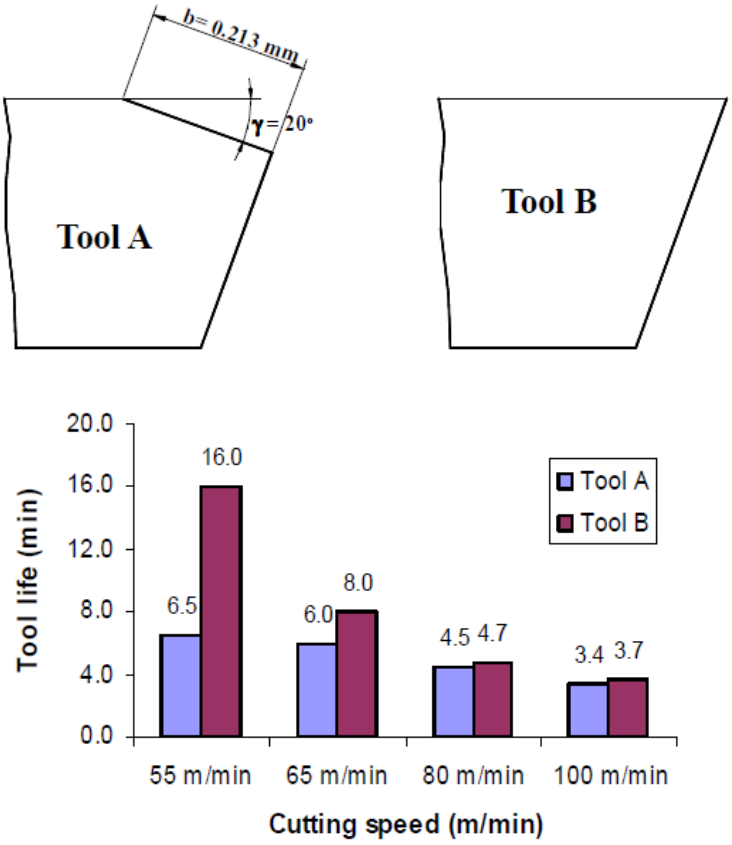

Figure 2.14. Performance comparison of two different designed tools in face milling of Ti-6246 at assorted cutting speeds and feed rate of 0.1 mm/tooth [34].

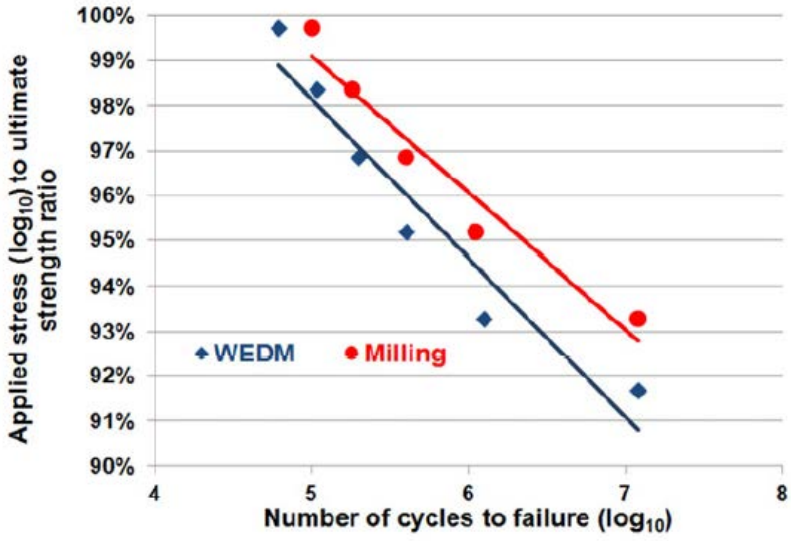

Figure 2.15. Fatigue curve plots for Ti-6246 specimens [35].

2.2.4 Heat Treatment and Temperature Related Treatment of Ti-6246

Stella et al. [38] performed heat treatment on the Ti-6246 alloy. It was heated with different temperatures above the beta transus, followed by water quenching. There

were two possible microstructures after water quenching following the solution treatment: (i) α and retained-β, or (ii) α and α' martensite, with a little β, reliant on the temperature of solution-treatment. The heat-treatment temperatures determined the relative amount of the phases. Different acting from steel, the α" martensite did not harden the material appreciably. On the other hand, a significantly hardened material resulted from aging. It transformed the a" and β to a smooth α + β needle-like structure.

Machinability of Ti-6246 with Ti-6Al-4V and Ti-54M after heat treatment have been compared by Armendia et al. [39]. Ti-6Al-4V and Ti-54M underwent three types of heat treatments, i.e. mill anneal, beta anneal and duplex anneal, and only the mill anneal for Ti-6246. Figure 2.16 shows that in machining Ti-6246 the mill anneal treatment did not have a significant impact. While in the beta annealed sample the machinability of Ti-6Al-4V and Ti-54M was considerably lower than the as forged sample. When comparing those three charts there seems to be a conflict because they compared flank wear with different cutting speeds, i.e. at 80, 90 and 60 m/min for Ti-6Al-4V, Ti-54M and Ti-6246 respectively. Furthermore, there was no explanation as to why the Ti-6246 was treated differently from the other two alloys.

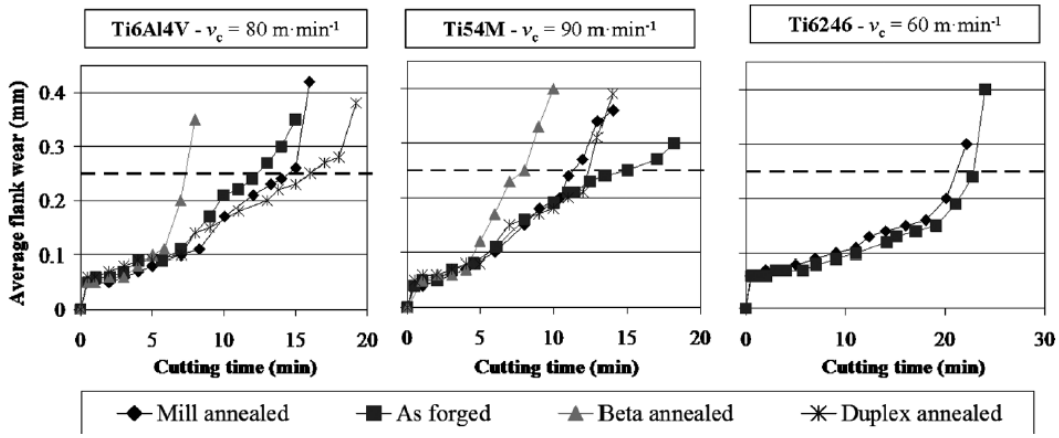

Figure 2.16. Comparison of machinability of three different α+β alloys as forged and after heat treatments [39].

According to Gill and Singh, applying Deep Cryogenic Treatment (DCT) on Ti-6246 material before EDM drilling enhances the MRR due to the improvement of its heat dissipation capacity [40]. However, it increases the rate of tool wear. The kerosene dielectric decomposed into carbon and hydrogen due to an electric spark from EDM. Then the machined material was penetrated by the carbon to form a TiC layer, which

has a higher melting temperature compared to the untreated alloy. Therefore, it needed a higher force to remove the TiC layer.

2.2.5 The Effect of Rare Earth Elements

Recently, rare earth elements have been added to titanium alloys. Preceding a successful addition of lanthanum (La) to Ti-6Al-4V [41], La had also been added to the Ti-6246 [42]. A La_5Sn_3 intermetallic phase was formed when lanthanum and tin came into a reaction. In order for the lanthanum to be able to be added, 3% of zirconium replaced the 2% of tin. The new alloys formed a matrix of Ti-6Al-7Zr-6Mo-0.9La (Ti-676-0.9La) which contains precipitation of pure metallic lanthanum and have a fairly low melting temperature compared to a titanium Ti-6246 alloy. The addition of lanthanum improved the machined surface, reduced the force and resulted in the chips having a shorter break when applied in conventional machining. In continuing this research, Muhammad et al. [37] have used the same material for machining in pure conventional turning and conventional machining with ultrasonic assistance. Lanthanum particles precipitated at the grain boundaries (Figure 2.17-a). Chips of Ti-676-0.9La were discontinuous in both types of machining. Due to high temperatures during chip segmentation, the lanthanum particles which exist at the localised deformation zone were melted, thus resulting in material separation in the chips in comparison to the original Ti-6246. This is shown in Figure 2.11-b&c.

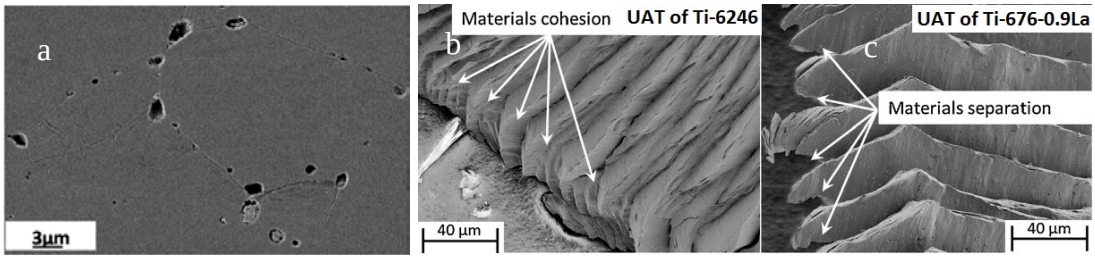

(a) (b) (c)

Figure 2.17. Particles of lanthanum precipitated at grain boundaries (a); Chips of different materials: Ti-6246 (b) and Ti-676-0.9La (c); both chips are of ultrasonic assisted machining [37].

2.2.6 Chip Characteristics

Ostroushko et al. [43] performed chip root studies on Ti-6246. A quick stop device was used. Quick Stop Device (QSD) is an apparatus to experimentally study the deformation zone in the chip root. The method is to retract the tool rapidly from the

workpiece which thereby freezes the process. They found that the chip patterns were influenced by the machining parameters, e.g. the cutting speed (Vc) and depth of cut (DoC). Most of the conditions resulted in segmented chips, except for a low cutting speed (20-40 m/min) and low DoC (0.05-0.2 mm), which results in continuous chips, whereas combining the medium Vc and lowest DoC, or lowest Vc and high DoC results in transition chips (Figure 2.18). Between each slices of the segmented chips there was a shear zone. The shear zone width increases with an increase in the cutting depth.

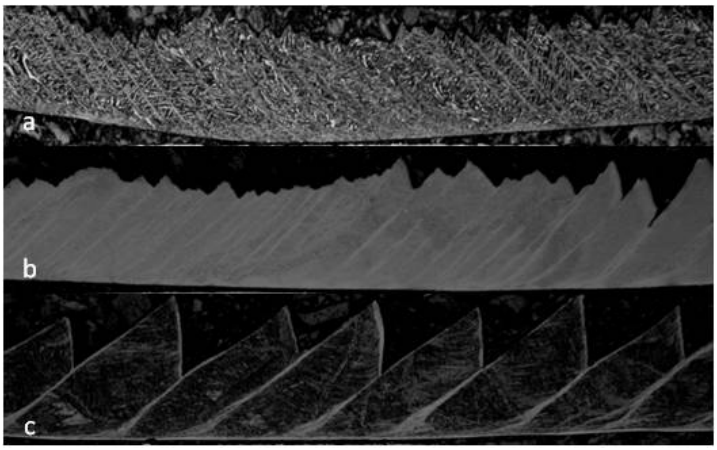

Figure 2.18. Chip pattern of Ti-6246 as an effect of machining parameters: (a) continuous, (b) transition and (c) segmented [43].

If it is compared with Ti-5333, the chip morphology is similar [44]. At a lower cutting speed (10-20 m/min) they were continuous, while at a cutting speed of 40 m/min the chips were segmented and the shear band was clearly visible, as shown in Figure 2.19.

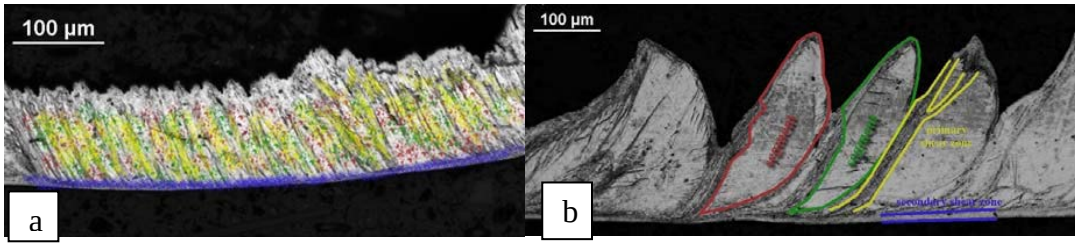

Figure 2.19. Cross-section of chips formed during orthogonal cutting of Ti-5333. (a) continuous chips – no localised deformation is visible; (b) segmented chip – segments and shear bands are clearly visible [44].

The segmented chip is typical of chip patterns of α+β titanium alloys. There are shear bands between chips, and these shear bands are thermally shortened and crack or separate at the end. That was demonstrated by Joshi et al. [45] when they compared three types of titanium alloys [α, α+β, β rich (α+β)] with an increasing β fraction. In

their research, Ti-5.26Al-3.03Sn, Ti-6Al-4V and Ti-4.1Al-3.3V-3.9Mo were chosen as examples of α, α+β and β rich (α+β) titanium alloys respectively. They applied Vc of 73 m/mi, fr of 0.11 mm/rev and DoC of 1 mm.

Although the trend of the formation of segmented chips was the same, the category of the cutting speed was different. The cutting speed between 20-40 m/min was considered to be low and was not able to form a serrated chip in Ostrouskho et al. [43], while according to Rokicki et al. [44] at Vc 40 m/min the serrated chips had already formed. For different materials it would need different cutting speed limits to form a serrated chip. Ti-55531 and Ti-6Al-4V for both Vc of 20 and 65 m/min formed a serrated chip but the latter shows a greater tendency than the former [46]. For a higher cutting speed, generally most of the researchers agreed that a serrated chip is formed, even though the materials are different. For example, Ti-5333 for Vc 20 m/s or 1200 m/min [47].

Komanduri [48] explained that the mechanism of chip formation of Ti alloy is not directly affected by the cutting speed. Nevertheless, the cutting speed influenced the process overall, including the temperature of the tool, tool wear, and generation of a secondary chip. Subsequently, the author corrected his opinion that there was a critical cutting speed for the existence of a thermoplastic instability (adiabatic shear). In the case of Ti-6Al-4V, it is at Vc 0.15 m/s or 9 m/min [49].

The segmented chips occurred through ductile fracture when applying a high cutting speed. Figure 2.20 is comprised of void nucleation, growth and coalescence as an indication of the thermal softening degree within the primary zone [50]. Consequently, with a low cutting speed, there was a breakdown inside the upper region of the primary zone which occurred through cleavage and resulted in a continuous chip. This is in contrast to what Wang & Liu [51] suggested, that cleavage failure occurs at an ultra-high cutting speed.

Regarding shear band formation, Siemers et al. suggested that it is driven by a deformation process followed by recrystallisation of the structure [47]. It involved a high temperature (above 800^{o}C primary shear zone in machining Ti-6Al-4V). Therefore, thermal conductivity of the material contributes to the formation of serrated chips. The degree of segmentation reduces with raising thermal conductivity of materials [52]. Serrated chip dimensions for non-titanium alloys are also closely

related to the force [53], [54] and it is affected by tool wear [55] but there has not been any reported in the titanium alloys.

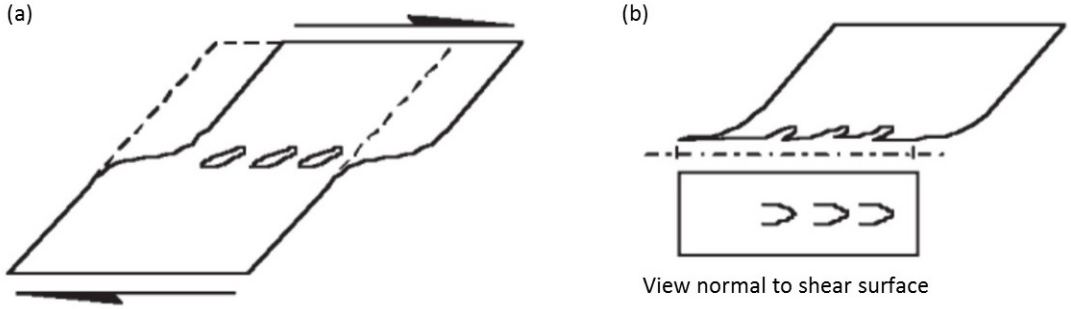

Figure 2.20. A simple representation of a sheared element: (a) nucleation and growth of voids, (b) a normal view to the shear failed surface [50].

Until now, there have been two theories of how serrated chips were formed, both arguing supported by their evidence. First is the adiabatic shear theory, which proposes that recurrent thermoplastic shear volatility happening within the primary shear zone results in serrated chips. The shear volatility happens if the rate of thermal softening surpasses the strain rate and strain rate hardening. The heat generated by severe plastic deformation in the primary zone is unable to dissipate due to the shear process that takes place instantly; a theory introduced by Komanduri [48]. Another theory is that of the periodical crack, which argues that cracking at the free surface is the commencement of serrated chips then propagating into the tool-chip area. A catastrophic shear happens as a result of a regular crack that weakens the primary zone. [56].

Both theories have their own limitations; the adiabatic or catastrophic theory is most suitable for ductile material, while the periodical crack theory is suitable for brittle material. Wang & Liu [51] tried to combine these two theories. They explained that when the cutting speed is very high the serrated chip is a result of the ductile fracture and the adiabatic shear which produces serrated chips. Instead of using a critical cutting speed when a serrated chip would probably occur, they introduced cutting load (cutting speed times feed rate) versus degree of segmentation (the comparison between the vertical distance of peak and valley of a serrated chip towards the maximum height of a serrated chip). However, they were inconsistent when trying to create a line of separation between a serrated and a continuous chip region by choosing a different degree of chip segmentation. In conclusion, a more comprehensive and methodical

exploration about the formation of serrated chips involving analytical and experimental investigation should be carried out in order to create a link-connection between existing knowledge and the reality of the facts.

The theory of adiabatic shear suggests that the shear was started from the tool's vicinity to the free surface side, whereas the periodic crack propagation theory suggests it is from the opposite direction. The former theory has been supported by experiments on titanium alloys and hardened steel, whereas there are no papers supporting the latter theory for titanium alloy applications. Therefore, I will use the first theory with some modification and deeper analysis regarding further parameters influencing the formation and propagation of instability in the shear band.

Looking more closely at the shape of chips, we found irregularities either in continuous, segmented or transitional chips (Figure 2.21). Segmented chips are classified as either a periodic or aperiodic saw tooth [50]. A non-periodic segmented chip has similar characteristics to continuous chips. The difference in the thickness or form of chip has been recognised but there is no adequate reason for their cause(s). Figure 2.21 shows the example of the chip thickness differences.

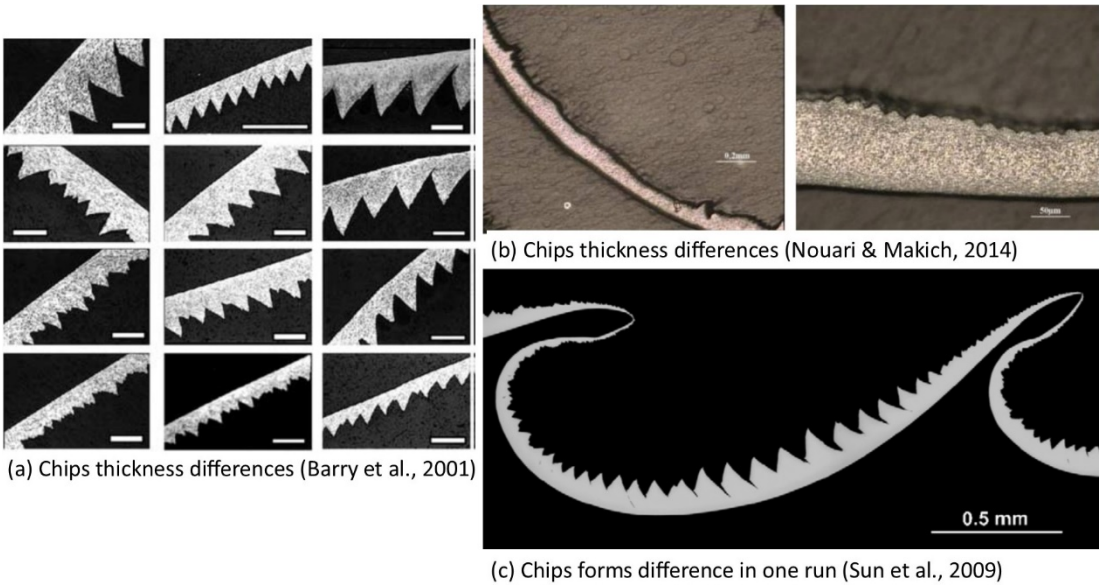

Figure 2.21. Chip thickness (a) and (b) differences from different literatures and (c) chips form difference in one cut [45],[49],[56].

2.2.7 Built-up Edge in Machining Ti-6246

Built-up edge formation is a very common occurrence in machining titanium alloy due to its affinity to most of the tool materials [25], [26]. A built-up edge does not occur

in other material, such as steel, when machined at high speeds [57]. There are three categories of built-up edge depending on where they stick on. Built-up edge (BUE) sticks on the edge of the tool, a built-up layer (BUL) on the lip of the rake layer, and flank build-up (FBU) sticks on the lip of the flank side [58]. In the drilling process, regardless of the material used, built-up edge formation is unavoidable due to different cutting speeds along the tool lips [57].

A BUE forms in machining due to high compressive stresses and high temperatures in the tool/chip interface. A complete contact (mechanical interlocking) occurs in all surfaces of the tool including the hills and valleys due to plastic deformation of the work material. A BUE is formed typically at moderate temperatures. At high temperatures, material recovers its ductility, therefore inhibiting crack formation. Regarding work material, a BUE formed when material had two or more phases. For single-phase material regardless of the cutting conditions it behaved as a uniform mass in the machining zone, resulting in a separation between the chips and the tool [58].

There is no explanation from the previous researcher regarding the effect of a BUE in the formation of serrated chips. Most of the research studying segmented chip formation is on hard or hardened steel with a high cutting speed, therefore there is less possibility of forming a BUE. An existing BUE on the tool-chip interface will change the tool dimension and coarsen the tool surface consequently increasing the cutting force due to friction. Therefore the studying of built-up edges relating to segmented chip formation is important when studying the drillability of Ti-6246.

2.3 Tool Deterioration

Tool deterioration encompasses all the changes in the cutting part of a tool caused by the cutting process [14]. Two major classes of deterioration are distinguished, i.e. tool wear and chipping. Further, the ISO defines tool wear as a change in shape of the cutting part of the tool from its original shape, resulting from progressive loss of tool material during cutting. However, chipping or brittle fracture is the occurrence of cracks in the cutting part of a tool followed by a loss of small fragments of tool material during cutting.

Tool deterioration is a measure for machinability. When the tool deteriorates it means the tool has achieved the end of its life and has to be replaced to continue the

machining. One method to improve tool performance is by coating the tool substrate. One of the coatings that results in an excellent performance is TiAlN. It appears to be compatible for machining abrasive and difficult-to-machine materials [59]. There are two ways of applying TiAlN on the base tool material: by physical vapour deposition (PVD) and chemical vapour deposition (CVD). TiAlN coating has strong chemical stability, low thermal conductivity and high wear resistance at 900^{o}C. The TiAlN coating increases the surface hardness to approximately 3400-3600 HV and improves the resistance to abrasive wear [46]. Other researchers [59], [60] proved that the Al element incorporated in TiAlN coating forms the superficial layer Al_2O_3 to improve wear resistance and to enhance chemical stability.

In machining hard metals, PVD TiAlN has shown it has better performance than TiN and TiCN [61]. TiAlN also possessed perfect tribological properties compared to the TiN, AlTiN and CrAlN coating [62]. In a wear abrasion test, it is proved that the erosion rate of TiAlN tool coating has the smallest in comparison to that of CrAlN, TiN and Cr with a value of 7, 13, 18, and 38 ($x10^{-3}$ µm/s) respectively [62]. TiAlN coated tools have been used for machining hard metals such as Inconnel 718 [63], AISI 4140 steel [64], AISI 4140 hardened steel [65], and titanium Ti-6Al-4V [66]. Hao et al. [63] found that in machining Inconnel 718 the tool life of a TiAlN coated carbide tool could last for 29 minutes at a cutting speed of 20 m/min, then drop to 3 minutes only when the cutting speed was 45 m/min [63]. Khrais and Lin [64] found that a TiAlN coated carbide tool can stand for up to a maximum cutting speed of 410 m/min when machining AISI 4140 steel. More than this cutting speed will lead to premature failure [64]. Kumar et al. [65] concluded that the performance of TiAlN was better than that of TiCN when machining hardened steel AISI 4340 in terms of lower wear resistance and smoother surface finish.

In drilling Ti-6Al-4V, the most common type of drill failure was fracture [66] and microchipping [67]. Ti-6246 has been machined using conventional machining methods, such as turning [32] with notch and abrasion wear on the flank face, while micro-cracking and a build-up layer appear on the rake face. The tool displayed flank wear upon milling [62].

2.4 Taguchi Method

For years engineers and scientists have performed one-factor-at-a-time (OFAT), an experimental method that keeps all factors or variables fixed except for one. There is a potential risk by using the OFAT experiment as it does not reveal what will happen to the response variable and what is the significant effect of those factors if some were changed simultaneously. The drawback of OFAT is that the interaction between factors cannot be estimated [68]. Another drawback of the OFAT technique is that there is no warranty upon the repetition of experimental results [69]. Therefore, in studying two or more factors, a statistically designed experiment that modifies several factors simultaneously will be more efficient.

Design of experiment (DOE) was developed to overcome the difficulties when using OFAT. DOE is an official mathematical technique for systematically designing and performing scientific studies that alter experimental variables simultaneously in order to ascertain their influence of a certain response. DOE is a vigorous statistical technique to study the impact of numerous variables concurrently. By using DOE it is possible to disclose the connection between the various factors influencing a process and output of the process. Furthermore, the optimum conditions, the most affecting factors and the potential combination and collaboration among factors can be studied following the analysis [70].

Taguchi designs use orthogonal arrays to study how different parameters influence the response mean and the variance. It also detects how well the process is performing. In testing all possible combinations, orthogonal array test pairs of combinations differ from the factorial design. The design is balanced; therefore all factor levels are weighted similarly. Consequently, each factor can be reviewed autonomously, so the influence of one factor does not influence the estimation of others. In the end it will trim down the time and costs related to the experiment if fractioned designs are used [71]. The fractional factorial design means experimental design consists of a wisely chosen fraction (subset) out of the full factorial design. Therefore, only an adequately chosen fraction of the factor combinations is required to be run [72].

In designing the experiments, the Taguchi method uses a table which consists of a table and column. The column corresponds to selected factors and each factor consists of at

least two levels. Each row related to an experimental run. In the Taguchi method some combinations are omitted in order to efficiently find the factors with minimal trials.

A Taguchi design is concise, smart and is best used for three existing conditions: (i) where the number of factors (variables) are between 3 and 50, (ii) where there are limited interactions among variables, and (iii) where only a few variables contribute meaningfully. The Taguchi experiment design is brief, neat and derived from a full factorial design (FFD). In FFD, all possible combinations of factors and levels are fully tried. Therefore, it is effective in some conditions: (i) when the number of factors and levels are small, (ii) when the experiments are not time-consuming and (iii) when the cost of experiments is low [69].

Some researchers have proven that using the Taguchi method would sharply reduce the number of experiments with an equivalent result. They have obtained a comparable result by using the Taguchi method only using 16 trials in comparison to that of the Full Factorial Design (FFD) using 288 trials [73]. In a recent publication, it was proven that using the Taguchi method has saved about 89% of experimental runs (from 81 experiments according to traditional DOE, to 9 runs by the Taguchi method) [74]. Furthermore, they found that the best combination of input variables of both DOE produced similar results. The only difference was from the parameter with a negligible contribution.

The Taguchi method has been successfully applied in optimising machining parameters, such as milling of composites [75], milling of steel [76], or turning [77]. Sometimes to maximise the results, the Taguchi method is combined with an analysis of variance (ANOVA) [78] or response surface method (RSM) [79].

Many researchers using the Taguchi method in their design experiments used numeric values in their parameters. However, it is possible to use non-numeric values as parameters in this method. Khanna used heat treatment as one parameter for titanium cutting [79] and Kowalczyk used different types of tools for the precision turning of titanium [80].

Parameter design is used in the Taguchi method to achieve optimum process while using multiple performance characteristics. According to some literatures such as M. Nalbant et al., [81], there are some steps in using the Taguchi method:

a. “Identify the performance characteristics and select process parameters to be evaluated.
b. Determine the number of levels for the process parameters and possible interactions between the process parameters.
c. Select the appropriate orthogonal array and assignment of process parameters to the orthogonal array.
d. Conduct the experiments based on the arrangement of the orthogonal array.
e. Calculate the total loss function and the S/N (signal to noise) ratio.
f. Analyse the experimental results using the S/N ratio and ANOVA.
g. Select the optimal levels of process parameters.
h. Verify the optimal process parameters through the confirmation experiment.”

With the Taguchi method, the arrays are arranged so that the number of experiments necessary are significantly fewer compared to the traditional design approach. A lost function is generated to evaluate the deviancy between the experimental values and the desired values. In the next step, this lost function is then transferred to a signal-to-noise (S/N) ratio. The loss associated can be minimised by maximising the S/N ratio [79]. The S/N ratio represents the characteristics of performance which can be differentiated into three categories: lower-the-better (LB), the higher-the-better (HB) and the nominal-the-better (NB) as presented in equation 2.1 to 2.3. The Minitab 17 program is usually employed for computing the S/N analysis to find out the S/N ratio for each level of process parameters.

$$\left[\frac{S}{N}\right]_{HB} = -10\log\left(\frac{1}{n}\sum_{1=1}^{n}\frac{1}{y_i^2}\right) \quad \text{(2.1)}$$

$$\left[\frac{S}{N}\right]_{LB} = -10\log\left(\frac{1}{n}\sum_{1=1}^{n}y_i^2\right) \quad \text{(2.2)}$$

$$\left[\frac{S}{N}\right]_{NB} = -10\log\left(\frac{\bar{y}}{s_y^2}\right) \quad \text{(2.3)}$$

In drilling, it is preferable to have a lower surface roughness which is an indication of better performance. Therefore, an LB performance characteristic would be adopted for this research for surface roughness. For force analysis, the lower the forces that work, the better the process. Therefore, LB performance would be used for force analysis. Other characteristics of performance would be chosen according to the nature of the output measured. The significance of each set of parameters is studied further using a statistical analysis of variance (ANOVA). A prediction of the optimal combination of

process parameters will hopefully be achieved through both an S/N and ANOVA analysis. To ensure that the parameter design will result in the optimum process, a confirmation experiment should be carried out.

2.5 Modeling of Machining

Numerical modeling, or better known as simulation, is making an impression in machining studies. To some extent, modeling of machining has been broadly used in predicting tool temperatures and forces during machining, tool deterioration, chip formation and machined surface generation. Modeling highly contributes to reducing the experiments that are needed for optimising the cutting condition, tool geometry and other parameters such as tool choice and its coating method. Its attraction is driven by the fact that none of the analytical models were able to predict with adequate precision which are satisfactory conditions for a practical machining situation. A well-developed machining simulation would enable good compatability with the experiments in terms of temperature, stress and strain distribution. Consequently, it would promote the attenuation of machining costs and even further costs when optimisation is carried out experimentally. Machining simulation would lead in future research when its development has revealed the phenomena and is able to optimise the machining condition.

Some software is commercially available for performing simulation in machining such as, ANSYS, ABAQUS, DEFORM and ADVANTEDGE. In modeling, researchers specialise in different aspects of machining: forces, heat, chip formation, or tool deterioration. The further development of machining simulation has to include the dynamic behaviour of the machine tool within it [82]. The model was then compared to the result of experimentation or the real measurement while machining. Among the most difficult to be carried out is the modeling of serrated chip formations.

In modeling chip formations, there are some aspects that will influence the sensitivity or the results of analysis: the model of approach, the mess fineness, mass scaling and the failure criterion used for element deletion.

The first factor that influences sensitivity of the modeling result is the model of different approaches. ABAQUS provides three possible models of approach: the Lagrangian (LAG), and the Arbitrary Lagrangian-Eularian (ALE) formulation.

Subsequently, Zhang et al. [83] compared both models of approach and added the Coupled Eularian-Lagrangian (CEL) formulation. They concluded that only the LAG model was able to present the serrated chip formation model, while two other models could not, as depicted in Figure 2.22. In the previous research, it was also stated that an ALE approach is suitable for continuous chips, whereas LAG is better for non-continuous chips [82] .

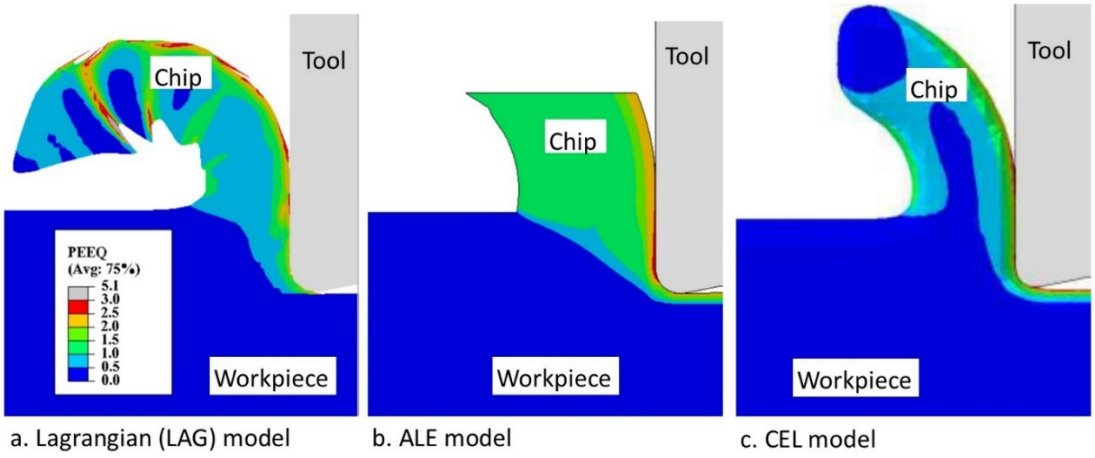

Figure 2.22. Comparison of equivalent plastic distribution in different model of approach [83].

The second factor that would impact the simulation quality is the fineness of meshing. However, the finer the mesh; the better the quality of simulation. Fine mesh would take more time in computing or running the simulation. Therefore, different types of meshing could be applied; smooth mesh at the cutting area and coarser mesh in the rest of the part. In other words, the density of the element number would be increased at the machining area. The mesh size would also be different between the tool and the workpiece. When the concern is of chip formation, the workpiece cutting area has to have finer mesh than the tool [84]. Otherwise, the tool mesh should be finer if the tool deterioration is the main concern [85]. Figure 2.23 shows the fineness of two types of mesh for different purposes.

The third factor which may influence the quality of modeling is mass scaling. This approach is to scale the masses of elements with small edge lengths, which governs the critical maximum time step size. This cannot be exceeded in an explicit dynamic analysis [82]. Mass scaling would reduce the calculation time or the running process, from 170 hours to 10 hours [86]. It also simplifies the requirement for the computer needed for running the program. However, applying mass scaling would multiply the

force needed for it to work. Figure 2.24 shows the dependence of the cutting forces on the mass scaling, governed by the predetermined minimum time increment. The time step higher than 5e-8s leads to an increased mass scaling and unrealistically high cutting forces.

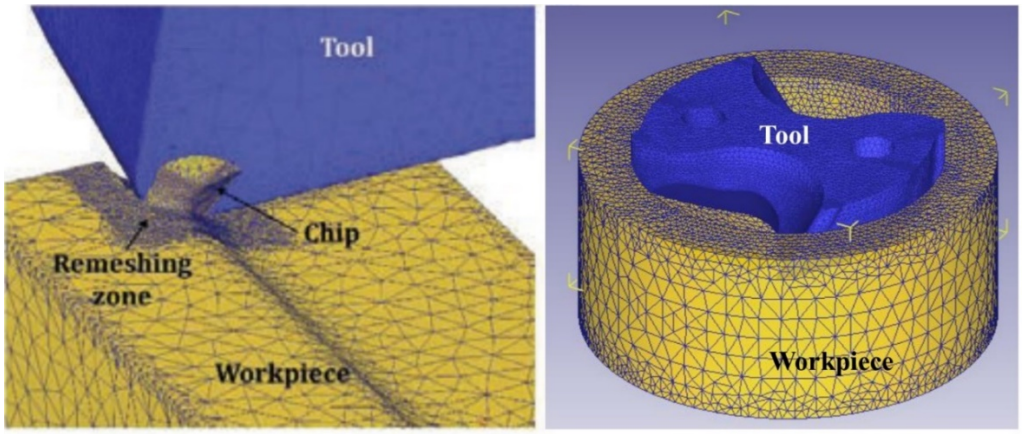

a. Finer workpiece mesh [68] b. Finer tool mesh [69]

Figure 2.23. Finer mesh in cutting part of workpiece (a) and in tool (b) due to different concerns of the study

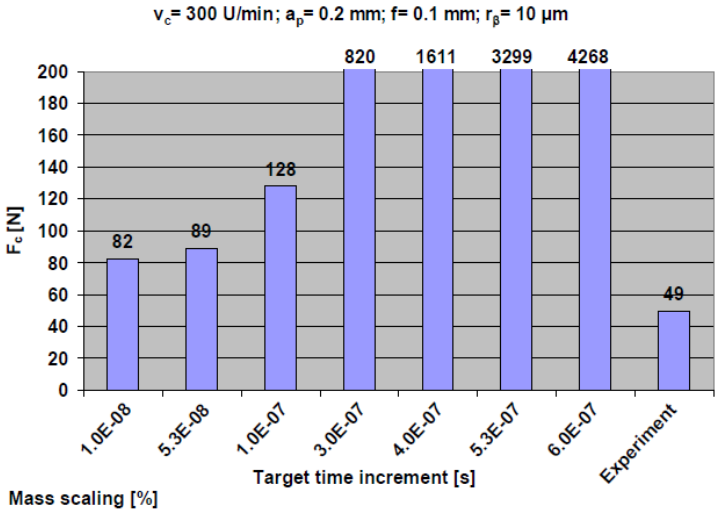

Mass scaling [%]

start	0.002	0.547	1.935	17.394	30.924	54.817	69.585
end	0.018	0.556	1.994	32.091	59.932	101.72	122.51

Figure 2. 24. Cutting forces vs. mass scaling/minimum time increment [86].

The fourth factor which most likely influenced the sensitivity of simulation is the failure criterion used. Most of the machining modeling was used by Johnson-Cook's constitutive model (J-C), which is an implementation of isotropic hardening. However, the J-C constitutive model has been criticised for neglecting the coupling effects of strain, strain rate and temperature. It is also lacks the ability to capture some important

behaviour during high strain and a high strain rate [87]. Furthermore, the J-C damage model could not imitate the serrated chip form.

The J-C material law is usually used when three conditions are most likely to occur: (i) dynamic problems with high strain rates (ii) temperature effects which adopt a Von Mises model yield criterion and, (iii) an isotropic hardening rule. This law relates flow stress (σ) with other variables as presented in the equation 2.4.

$$\sigma = [A + B(\varepsilon)^n][1 + Cln\frac{\dot{\varepsilon}}{\dot{\varepsilon_0}}][1 - \left(\frac{T - T_{room}}{T_{melt} - T_{room}}\right)^m] \quad \text{.....(2.4)}$$

In the above equation, ε represents the plastic strain, $\dot{\varepsilon}$ is the strain rate (s^{-1}), and $\dot{\varepsilon_0}$ denotes the reference plastic strain rate (s^{-1}). T, as usual, represents the workpiece temperature (^oC) and T_{melt} is the melting temperature of the work material (1595^oC); T_{room} is the room temperature (20^oC). Other constants relate to mechanical and physical properties of materials; the yield strength (MPa) is denoted by A; the hardening modulus (MPa) is coded by B, C symbolises the strain rate sensitivity coefficient; n is a symbol for the hardening coefficient; and m is the thermal softening coefficient.

Calculation of the failure (D) is carried out for each element and it is defined by the following equation:

$$D = \sum \frac{\Delta\overline{\varepsilon^p}}{\overline{\varepsilon^p}^f} \quad \text{.....(2.5)}$$

In the above formula, $\Delta\overline{\varepsilon^p}$ exemplifies the increment of equivalent plastic strain, and $\overline{\varepsilon^p}^f$ represents an equivalent to strain to fracture. Fracture is admitted when D=1; if it occurs the related elements are deleted from the computation.

In modeling serrated chip formations, the J-C convention has been modified by Calamaz et al. [88] with better results in showing the degree of chip segmentation, as can be seen in Figure 2.25. This model is well known as the TANH model, an abbreviation of Hyperbolic Tangent function.

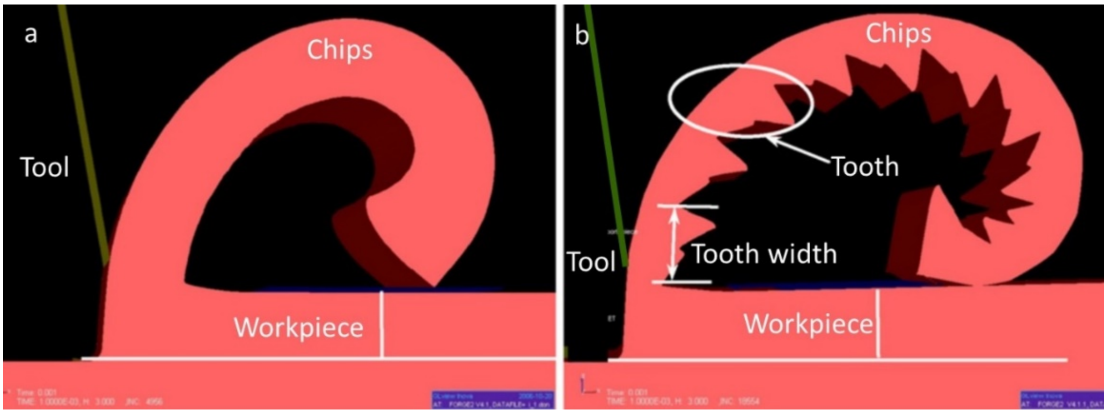

Figure 2.25. Comparison between chip formations in modeling using conventional J-C model (a) and modified J-C (TANH) (b) model [88].

The new model introduced the strain softening effect, as presented in equation 2.6. The presentation of conventional J-C equation and the flow stress increase are alike at a low temperature. However, further than the provided strain, the flow stress begins to decrease then is nearly constant after a certain time. The effect of the strain, strain rate, and temperature on the flow stress was considered by the Calamaz model. Furthermore, the Calamaz model also takes into account the hypothesis of dynamic recovery and the mechanism of recrystallisation.

$$\sigma = [A + B(\varepsilon)^n]\left[1 + Cln\frac{\dot{\varepsilon}}{\dot{\varepsilon}_0}\right]\left[1 - \left(\frac{T - T_{room}}{T_{melt} - T_{room}}\right)^m\right][D + (1 - D)\tanh\left\{\frac{1}{(\varepsilon + S)^2}\right\}] \quad (2.6)$$

With

$$D = 1 - \left(\frac{T}{T_m}\right)^d \quad \ldots\ldots (2.7)$$

$$s = \left(\frac{T}{T_m}\right)^b \quad \ldots\ldots (2.8)$$

The TANH formula takes penetration on the reducing hardness of the material (also called strain softening), which permits the chips to be in a segmented form in orthogonal cutting. Nevertheless, this behaviour is detected in case recrystallisation occurs, and dynamic recrystallisation (DRX) only occurs within the adiabatic shear band (ASB). In another words, the differences in material presentation in the flow stress curves depend on whether DRX happens or not. Figure 2.26 shows the strain-stress curve which is influenced by DRX and dynamic recovery. Conventional J-C represents cold deformation, whereas TANH includes dynamic recrystallisation.

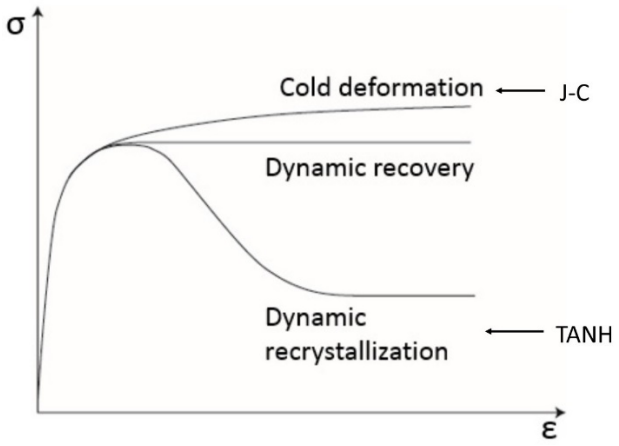

Figure 2.26. Pattern of typical flow stress curves [89].

This resulted in better conformation of the real chips. A recently published paper [90] also took advantage of implementing the TANH model in comparison to the conventional J-C model (Figure 2.27) by presenting more detail of the elements linking two successive teeth.

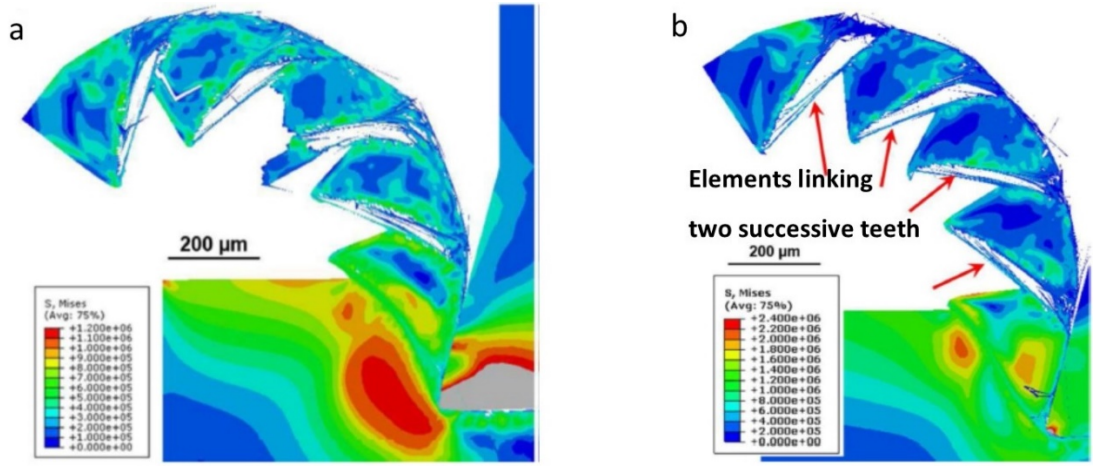

Figure 2.27. More improvement in the detail of chip formation when applying the TANH model (b) in comparison to a conventional J-C model [90].

To conclude, the difficulties in modeling serrated chip formations starts from an ambiguity in understanding the physical and thermomechanical phenomena behind it. Workpiece material plasticity is usually represented by the Johnson-Cook (J-C) model, which accounts for strain hardening and the strain rate as well as temperature effects on flow stress. In addition, the J-C damaged model was incorporated to calculate the effective plastic strain for initiating material damage and consequently enable chip formation from the bulk workpiece [91]. However, the J-C damaged model could not imitate the serrated chip form. The inclusion of the strain softening effect in the

conventional J-C damaged model by Calamaz has improved the serrated degree to be closer to the real one. However, most of the modeling of the serrated chip formation is in 2D and limited to orthogonal cutting.

Due its specific characteristics, no single simulation of drilling has been successfully depicted in 3D using ABAQUS or DEFORM. The only 3D model published on drilling for chip formations was carried out using ADVANTEDGE [92], yet due to some restrictions, the materials used for tools and workpieces were not specified. Furthermore, it was not clear what type of chips were formed, and whether or not it was able to show the serrated form (Figure 2.28). For that reason, modeling using ANSYS, ABAQUS or DEFORM 3D for serrated chip formation during drilling is an advantage.

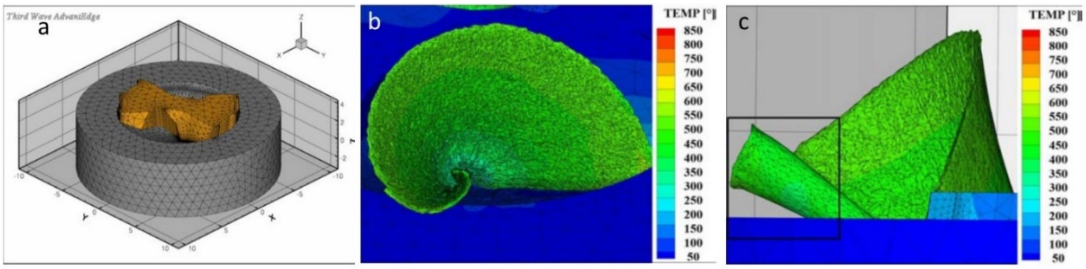

Figure 2.28. Modeling of chip formation in 3D: tool-workpiece model (a), formed chips in 3D (b), close view of chips (c).

CHAPTER 3. METHODOLOGY

There are two main stages in this research:

I. Stage 1: Detailed drilling experiments (experiments, measurements, microscopy, metallography, analysis);

II. Stage 2: Modeling of chip formations with regard to BUE formation in drilling.

3.1 Material

The material investigated was titanium alloy 6Al-2Sn-4Zr-6Mo (Ti-6246), in the form of a rod with a diameter of 56 mm. The nominal chemical composition of this material consists of four main alloying elements and some minor ones (cumulative, less than 0.4%) as presented in Table 3.1. The chemical composition of the material used in this investigation is presented in Section 4.1.

Table 3.1. Nominal chemical composition of Ti-6246 [6]

Work material Ti-6Al-2Sn-4Zr-6Mo	**Alloying elements, wt.%**				**Impurity limits, wt.% max**				
	Al	Sn	Zr	Mo	N	C	H	Fe	O
	6	2	4	6	0.04	0.04	0.0125	0.15	0.15

3.1.1 Shape of Workpiece Material

Prior to heat treatment and drilling, the workpiece material was machined to a rectangular shape according to the proposed drilling depth and to fit with the fixture. The dimension of the workpiece was 25 mm (width) x 25 mm (length), with a depth of 15 mm, 35 mm and 50 mm (Figure 3.1).

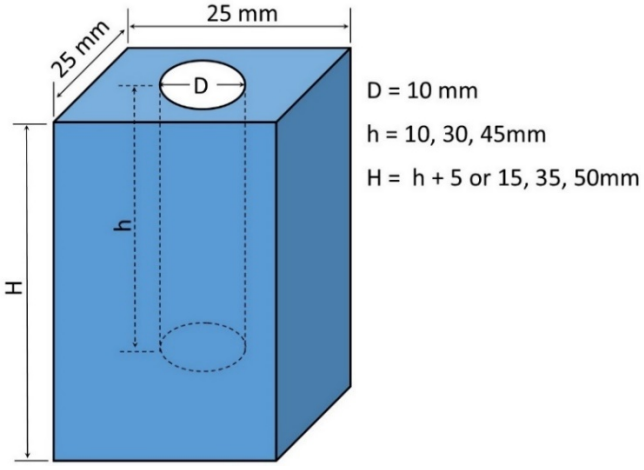

Figure 3.1. Dimension of the workpiece material.

3.1.2 Heat Treatment of Ti-6246

The idea was to find the best mechanical properties of Ti6246 (lowest hardness) to improve drillability. Three temperatures of heat treatment were chosen, i.e. below Ms, between Ms and beta transus, and above beta transus as indicated in the following figure. The Ms line (the dashed-line) is where the martensite will potentially be produced during cooling. Consequently, the beta transus line is the temperature where β changes to α+β on cooling. Each type of alloy has their own Ms and β temperature.

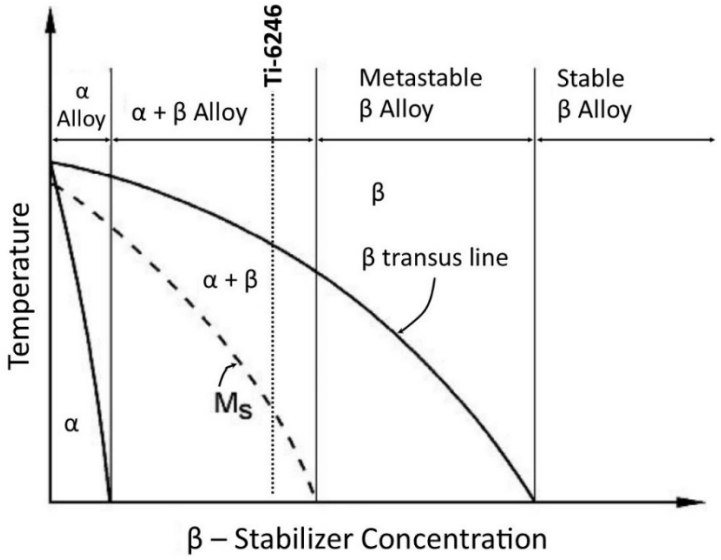

Figure 3.2. Pseudo-binary section through α β isomorphous phase diagram (from [2] with modification).

The beta transus temperature for this alloy is 935ºC [93] or 940ºC [2]. Prior to determining the Ms temperature, we should calculate the molybdenum equivalent number (Mo eq.) according to the following formula [94]:

$$Mo(eq.) = 1.0\,[Mo] + 0.22[Ta] + 0.28[Nb] + 0.44[W] + 0.67[V] + 1.25[Cr] + 1.25[Ni] + 1.7[Mn] + 1.7[Co] + 2.5[Fe]$$

Mo (eq.) of Ti-6246 = 6%.

An Ms temperature is then predicted according to information obtained from Froes (2015), as shown in Figure 3.3. Froes [95] believes that the Ms temperature is related to the alloy content and not to be altered by the quenching rate. The Mo (eq.) of 6% is between 5.75% and 7.1% which corresponds to temperatures of 680ºC and 585ºC respectively. Interpolation of these values results in an Ms temperature of Ti-6246 which is 662ºC.

The temperatures for heat treatment were determined to be 595°C, 870°C and 985°C, which represents the temperatures below Ms, between Ms and beta transus, and above the beta transus temperatures respectively (Figure 3.4). The samples were solution treated for 3 hours at each temperature to ensure that heat and microstructure maintained equilibrium throughout the blocks. Following solution treatment, the samples were cooled with either furnace cooling (FC), or air cooling (AC), or water quenching (WQ).

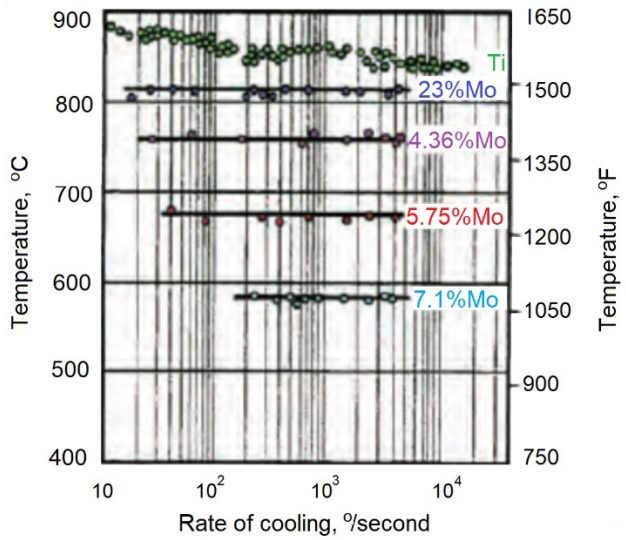

$$\frac{T-680}{585-680}=\frac{6-5.75}{7.1-5.75}$$

$$T-680=0.185185(-95)$$

$$T=680+(-17.5926)$$

$$T\approx 662^{o}C$$

Figure 3.3. Effect of cooling rate on martensite-start (Ms) [95].

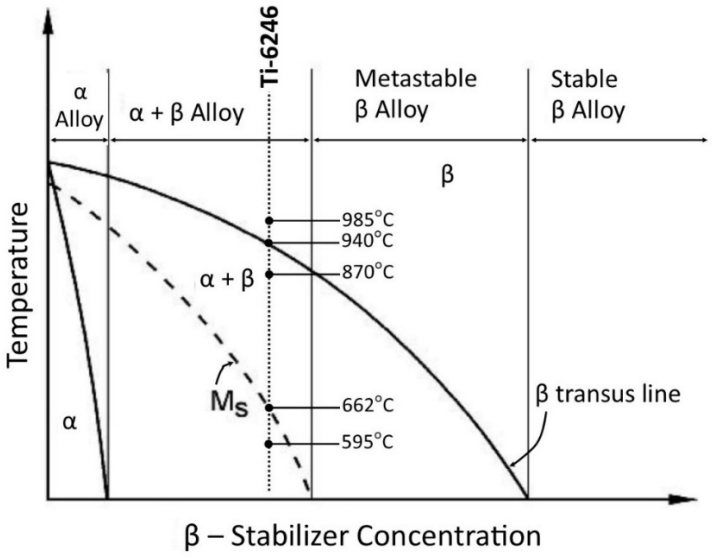

Figure 3.4. The determined temperature for heat treatment.

Following the heat treatment, nine experimental trials were carried out as shown in Table 3.2.

Table 3.2. Temperatures of heat treatment and the cooling methods

No	Temperature of heating (°C)	Cooling method
1	595	AC
2	595	FC
3	595	WQ
4	870	AC
5	870	FC
6	870	WQ
7	985	AC
8	985	FC
9	985	WQ

AC: air cooling; FC: furnace cooling; WQ: water quenching

3.2 Tool

The tools used in these experiments were insert type drills made of Tungsten carbide with TiAlN coated by the PVD (physical vapour deposition) technique. The insert was available in the market with the designation IC908 Sumocham diameter of 10 mm. The insert was mounted on the drill body. The configuration of the drill is presented in Figure 3.5.

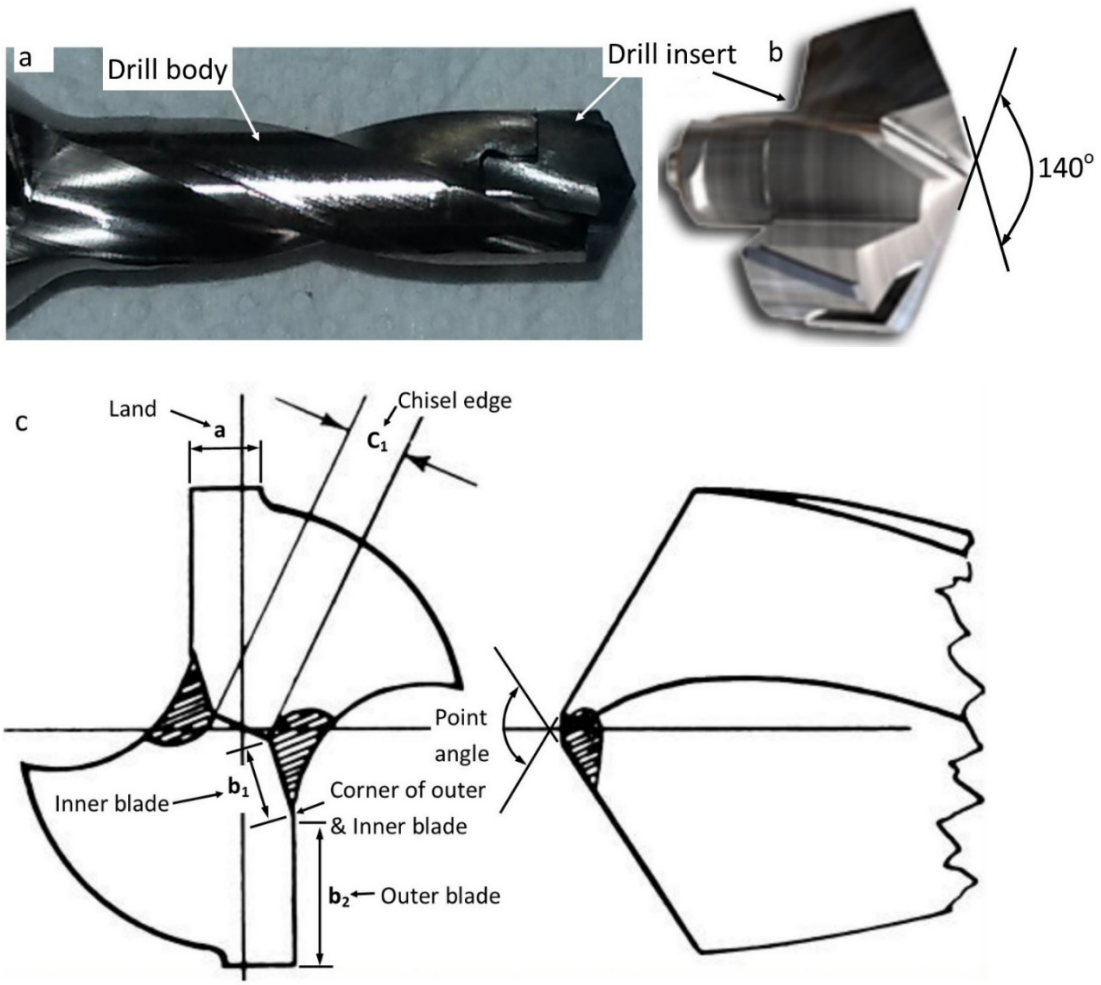

Figure 3.5. Tool picture and its configuration; (a) insert mounted on the drill body, (b) drill insert, and (c) simplified tool nomenclature.

3.3 Design of Experiments

To find the best practice, five parameters with different levels were applied for drilling Ti-6246 alloy including coolant application, heat treatment (HT), depth of drilling (h), cutting speed (Vc), and feed rate (fr). Each of the parameters had three levels, except for the coolant which had two levels only. The low and high levels of the cutting speed and feed rate were chosen within the recommended value from the tool manufacturer for drilling titanium [96]. Three levels of depth for drilling were chosen based on the potential application this material has for medium to thick components and the capability of the drilling and drill shank to hold the drill insert. Table 3.2 shows the detail of the parameters and their level.

Table 3.3. Variation of drilling parameters and their level

Machining Parameters	Level		
	Low	Medium	High
Coolant	off	-	on
Heat Treatment	AR	HT1	HT2
Depth of drilling (mm)	10	30	45
Cutting speed (m/min)	27	35	50
Feed rate (mm/rev)	0.08	0.11	0.15

For the drilling with a coolant, the synthetic coolant to water ratio 1:10 of HOCUT 795B made by Houghton Australia was used with a flow rate of 0.02 l/s through a nozzle. The nozzle was directing the coolant to the drill bit/hole. This coolant is readily available in the university workshop. The tool, workpiece, fixture, coolant nozzle and dynamometer were arranged prior to drilling, and the dynamometer was connected to a PC outside the CNC machine (Figure 3.6).

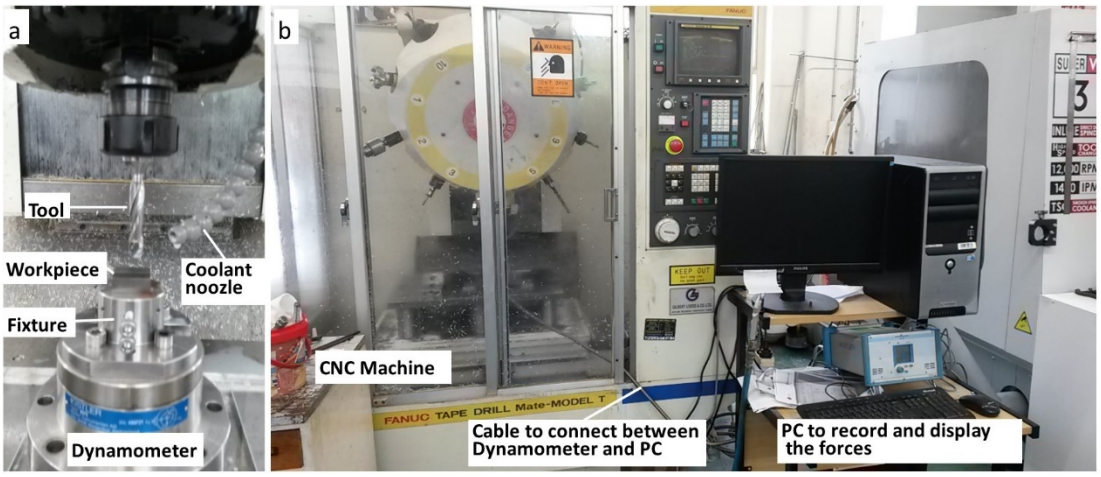

Figure 3.6. Set up for the drilling on the CNC machine: (a) arrangement of tool and workpiece, dynamometer, fixture and coolant nozzle; (b) whole arrangement to connect between CNC machine and a PC for measuring and recording the forces.

The Taguchi experiment design was chosen for running all of the experiments. If the full factorial design (FFD) was chosen, it would need 2x3x3x3x3=162 experiments. Therefore, Taguchi L18 with two levels of single factors and four other factors with three levels were used for designing the experiments, as shown in Table 3.3. All parameters were designed as orthogonal to each other, which means there was no

interaction between any two of the factors. Each factor is independent of each other. Therefore, the result of one run of experiments should be adequately reliable without any repetition. The limited availability of the material was also another reason why the repetition was not carried out. L18 means only 18 experiments are needed to complete all variations. In the Taguchi method the three levels of parameters were designated as low, medium and high. It is also possible to apply both quantitative numeric numbers and non-numeric as the levels of parameters [79], [80]. In this research, the depth of drilling, cutting speed and feed rate were numerical, whereas the variations of coolant and heat treatment were non-numerical.

Table 3.4. Design experiment of Taguchi L18 array

Experiment	Coolant	HT	h	Vc	Fr
1	1	1	1	1	1
2	1	1	2	2	2
3	1	1	3	3	3
4	1	2	1	1	2
5	1	2	2	2	3
6	1	2	3	3	1
7	1	3	1	2	1
8	1	3	2	3	2
9	1	3	3	1	3
10	2	1	1	3	3
11	2	1	2	1	1
12	2	1	3	2	2
13	2	2	1	2	3
14	2	2	2	3	1
15	2	2	3	1	2
16	2	3	1	3	2
17	2	3	2	1	3
18	2	3	3	2	1

A comprehensive study of chips (pattern and morphology), tools (wear or deterioration), hole dimensions (roughness and roundness) and forces would be carried out based on the measured/recorded output. An Analysis of Variance (ANOVA) was used to check the significance of each parameter to the output. Minitab 17 software was used to create the Taguchi design, followed by the analysis and then also the ANOVA results.

3.4. Measurement of the Output Parameters

3.4.1 Force Measurement

Prior to drilling, a workpiece block was clamped into a fixture which is mounted on a Kistler dynamometer to measure the forces worked during drilling. The dynamometer was connected to a PC outside the CNC machine to monitor the process. Four forces were recorded, i.e. Fx, Fy, Fz and Mz (Figure 3.6).

3.4.2 Hardness Measurements

Two types of hardness measurements were performed; one using Rockwell and another with micro Vickers. Hardness of the block samples were measured using a Rockwell hardness machine with a load of 150kg. Vickers micro hardness, with a load of 25g, was used to measure the hardness of the chips, and 100g for measuring the interface area adjacent to the drilled holes after drilling; both with a dwelling time of 10 seconds. Prior to measuring with micro hardness, the samples were hot mounted using a mounting press. The parameters used for hot mounting were: (i) heating at 180^{o}C for 7 minutes on a pressure of 25kN; followed by (ii) cooling for 4 minutes. The mounting media was a thermosetting plastic (polyFast) in a cylinder of 30 mm in diameter. The mounted samples were then ground gradually from 180, 500, 1200 and 2400 grit then mirror polished. While, for the Rockwell measurement, the samples were only ground and polished.

3.4.3 Procedure of Observing Tool Deterioration

The state of the drill heads was observed using a Scanning Electron Microscope (SEM) prior to and after drilling. To get the constant position observations, a fixture was designed and manufactured from an aluminium block. They are illustrated in Figure 3.7.

3.4.4 Microscopy Preparation for Chips Observation

The chips from drilling experiments were carefully collected for further analysis. From each run the chips collected would be categorised into the three stages of drilling, i.e. at the starting, at the middle and at the end of drilling. The chips were mounted and observed with an optical microscope and SEM.

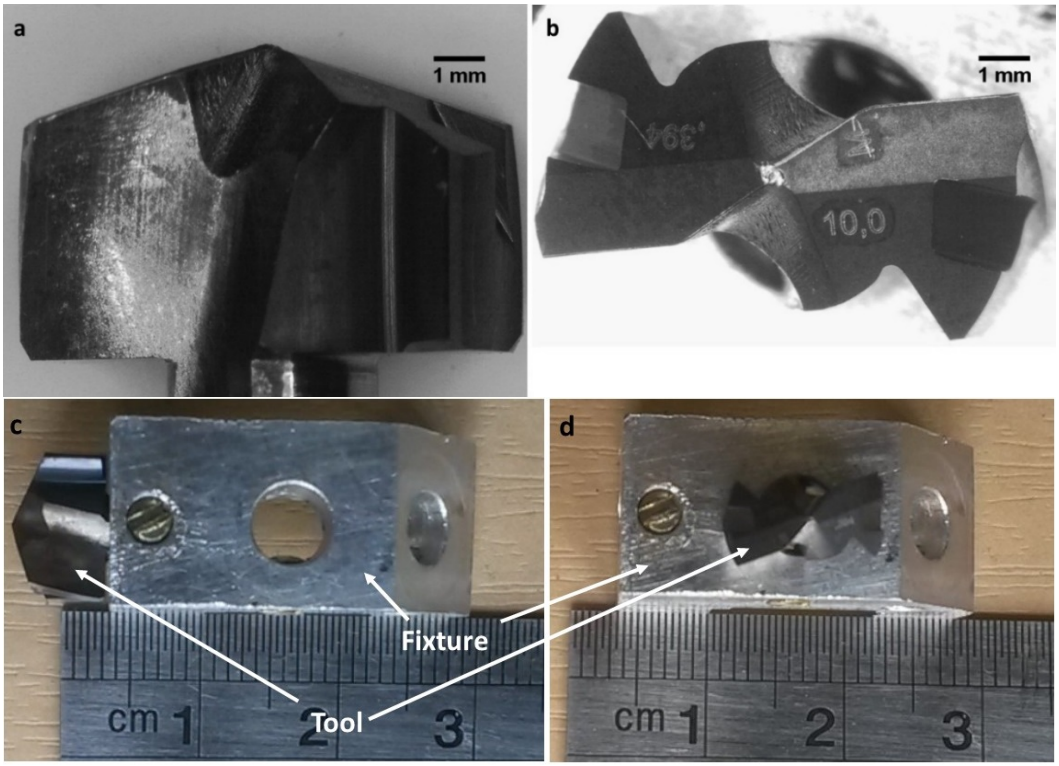

Figure 3.7. Drill insert photos: (a) rake view and (b) flank view. Drill bit position on the fixture for observation using Scanning Electron Microscope (SEM): (c) rake view and (d) flank view.

3.5 Modeling of Chip Formations in Drilling

ANSYS was used to simulate the formation of chips in this investigation. The model of the drill insert was made with SOLIDWORKS software. The model was simplified from the original shape to reduce the number of elements and nodes in the meshing step. However, the main parameters of the drill insert were kept the same as the original, such as the point angle 140^{o}; tool rake angle which was a helical flute angle 30^{o}; the primary clearance angle 7^{o}; and noose radius 0.05 mm (Figure 3.8). The model of the workpiece (which is simpler), was made directly in ANSYS.

Some steps would be carried out accordingly, from setting up the material properties to running the job in the drilling simulation, after developing the drill and workpiece. Material properties of both the tool and workpiece were inserted in the material section in ANSYS, such as density, Young's modulus, and Poisson's ratio.

Mesh was applied differently in both the tool and workpiece. As the simulation was concerned with chip formations, the workpiece mesh was designed to be smoother

than the tool. In the interactive step, the tool was set as rigid and the workpiece as a Johnson-Cook's constitutive model (J-C) material constitutive and damage model.

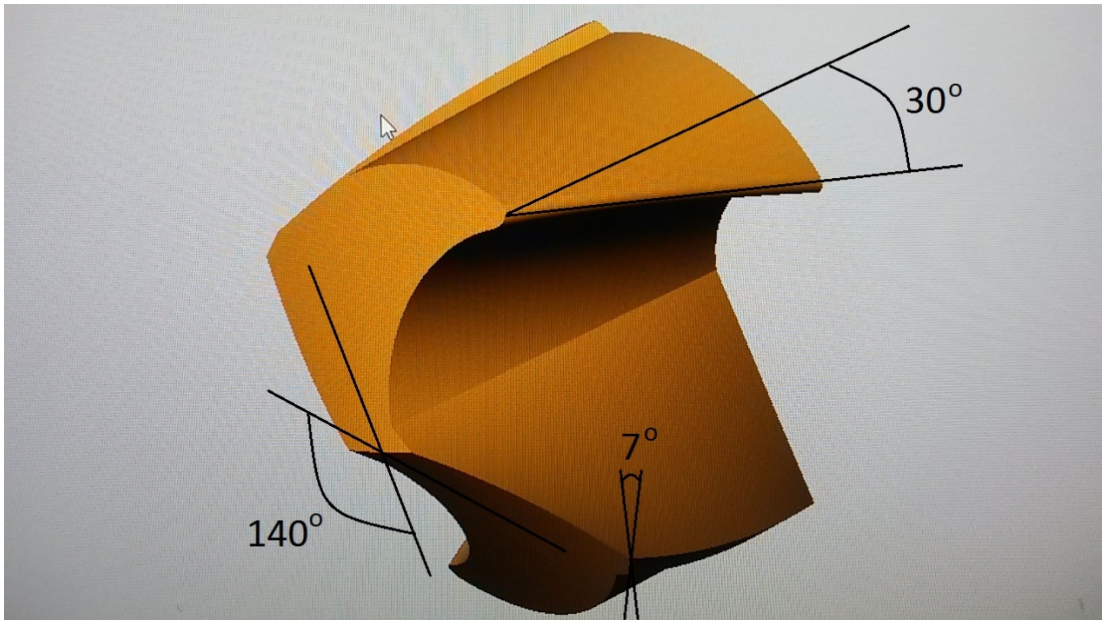

Figure 3.8. Drill model made with SOLIDWORKS then imported to ANSYS.

The boundary condition for the workpiece was set as fixed supports at the four vertical sides of the block, which means there would be neither linear nor rotational movement on those sides. Accordingly, the tool was rotated and moved down to the workpiece with a certain speed. A real linear and rotational speed could not be implemented directly in the simulation due to some restrictions of time to set. Otherwise, the time needed would be too long.

CHAPTER 4. ANALYSIS OF CHIP FORMATIONS

4.1 Chemical Composition, Microstructure and Hardness of the Blocks

Prior to the discussion about the chips, we would like to present the chemical composition of Ti-6Al-2Sn-4Zr-6Mo. This includes the microstructure and hardness of the blocks as a result of heat treatment variations in comparison to the as received material. The result of chemical composition of the OES (Optical Emission Spectroscopy) test in comparison to the literature and EDS (Energy Dispersive X-ray Spectrometry) results are shown in Table 4.1. The EDS result has an average of three times greater the measurements of different areas. The results would be different if measurement was taken on the points base. It seems that the result from one point to another is quite different and might result in the wrong conclusion that material was not homogenous. Therefore, it is suggested to measure on the area base instead of the point base. Both EDS and OES have resulted within the literature except for a significantly different in-weight percentage composition of aluminium at a value of 0.19% beyond the maximum value according to Boyer [8] of the OES one. Otherwise, other elements which the alloy was composed of were at the industrial standards of USA and Japan [8]. The EDS results are comparable to that of the OES. The slightly different result between EDS and OES may be related to the method for observations. The EDS did a non-destructive analytical method for surface elemental analysis. It is one of the electron microscopy techniques used for semi-quantitative analysis using the backscattered electron mode [97]. Whereas, OES was able to analyse the quantitative information regarding changes in elemental composition of the material being observed [98]. Both the complete EDS and OES tests are presented in Appendix C and D.

Table 4.1. Chemical composition of the material used as two methods test

Work material	**Alloying elements, wt.%**				**Impurity limits, wt.% max**				
Ti-6Al-2Sn-4Zr-6Mo	Al	Sn	Zr	Mo	N	C	H	Fe	O
According to Donachie et al. [6]	6	2	4	6	0.04	0.04	0.0125	0.15	0.15
According to Boyer et al. [8]	5.5-6.5	1.75-2.25	3.5-4.5	5.5-6.5	0.04	0.04	0.0125	0.15	0.15
EDS Test Result	6.2	2.0	4.3	6.2	-	-	-	-	-
OES Test Result	6.69	2.18	4.09	5.85		0.012		0.062	

The microstructure of each of the treatments is shown in Figure 4.1. The hardness comparison among different heat treatments is presented in Figure 4.2. The solution treated sample at a temperature of 985^{o}C resulted in lamellar microstructures. At a slower cooling rate the lamellae were increased in number, therefore producing a clearer grain boundary (ex β grain). The other heat treatments resulted in equiaxed (globular) microstructures with a different fineness. In the heat treated sample at a temperature of 870^{o}C, the cooling speed affected the grains/microstructure. The faster cooling rate (WQ) resulted in a finer microstructure than that of slower one (FC). So, at a treatment temperature of 585^{o}C the cooling rate did not affect the microstructure.

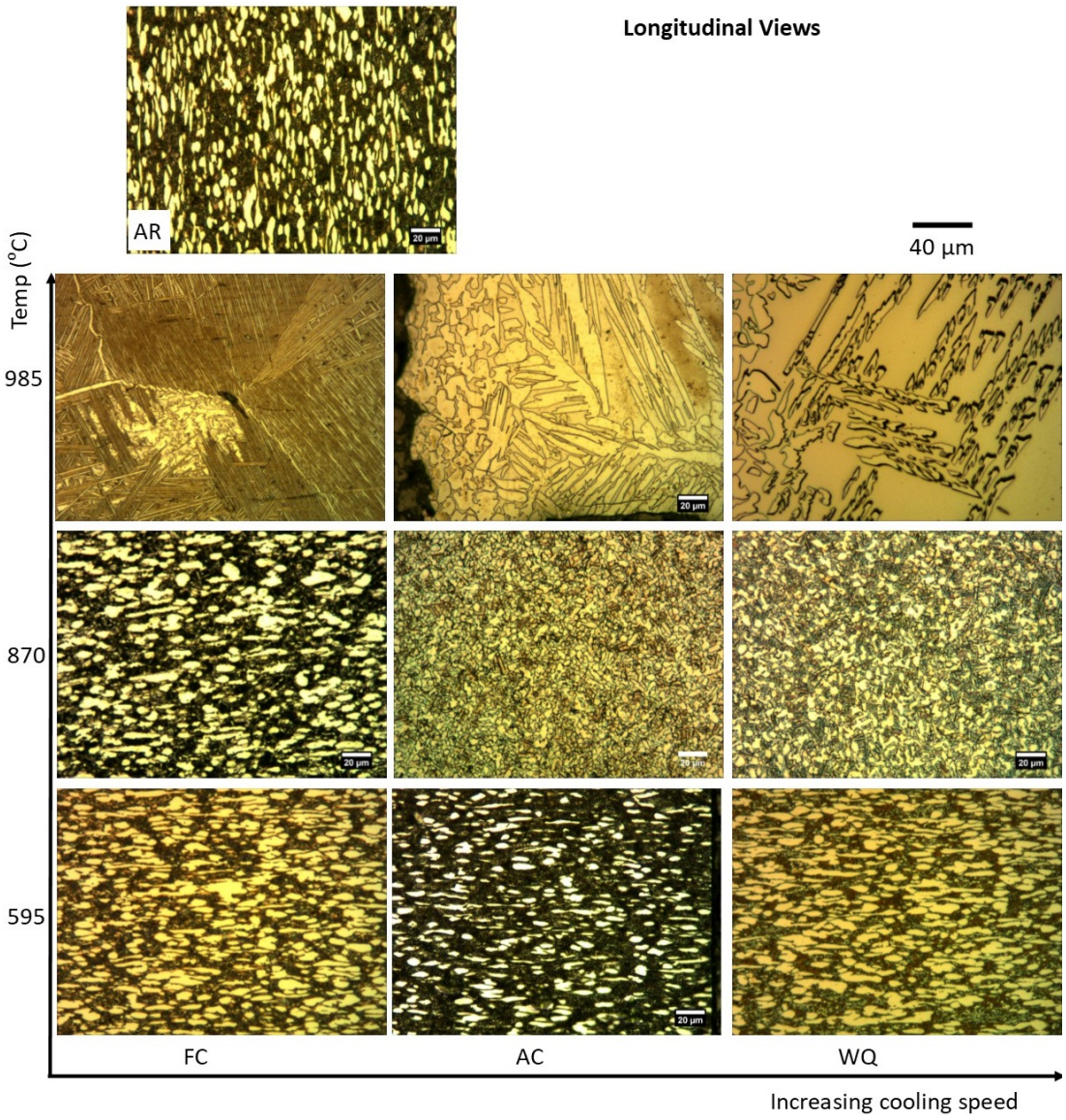

Figure 4.1. Microstructure comparison of three different heat treatment conditions.

The heat treated materials were compared to that of the as received (AR) sample. Based on the lowest hardness test results in Figure 4.2-a&b, both sets of data lead the researchers to choose 870°C/3h-WQ as the best alternative, as shown by the arrows. The third alternative for the heat treatment would be 870°C/3h-FC (based on Figure 4.2-a) or 595°C/3h-WQ (based on Figure 4.2-b), as shown by the oval circle. However, the microstructure of both heat treatments seems like the as received one (see Figure 4.1). Therefore, we chose the heat treatment of 870°C/3h-AC which resulted in a smoother grain that may lead to better drillability. The designation and the meaning of these three conditions were (i) AR (as received), (ii) HT1 (heat treated at 870°C for three hours followed by air cooling), and (iii) HT2 (heat treated at 870°C for three hours followed by water quenching) – these were rearranged for simplification. These three conditions provide different microstructures and hardness. The HT2 had the lowest hardness result among other trial specimens. Therefore, according to the general requirement of conventional machining, it should be easier to machine compared to the other two conditions, and hopefully improve the machinability/drillability of the material.

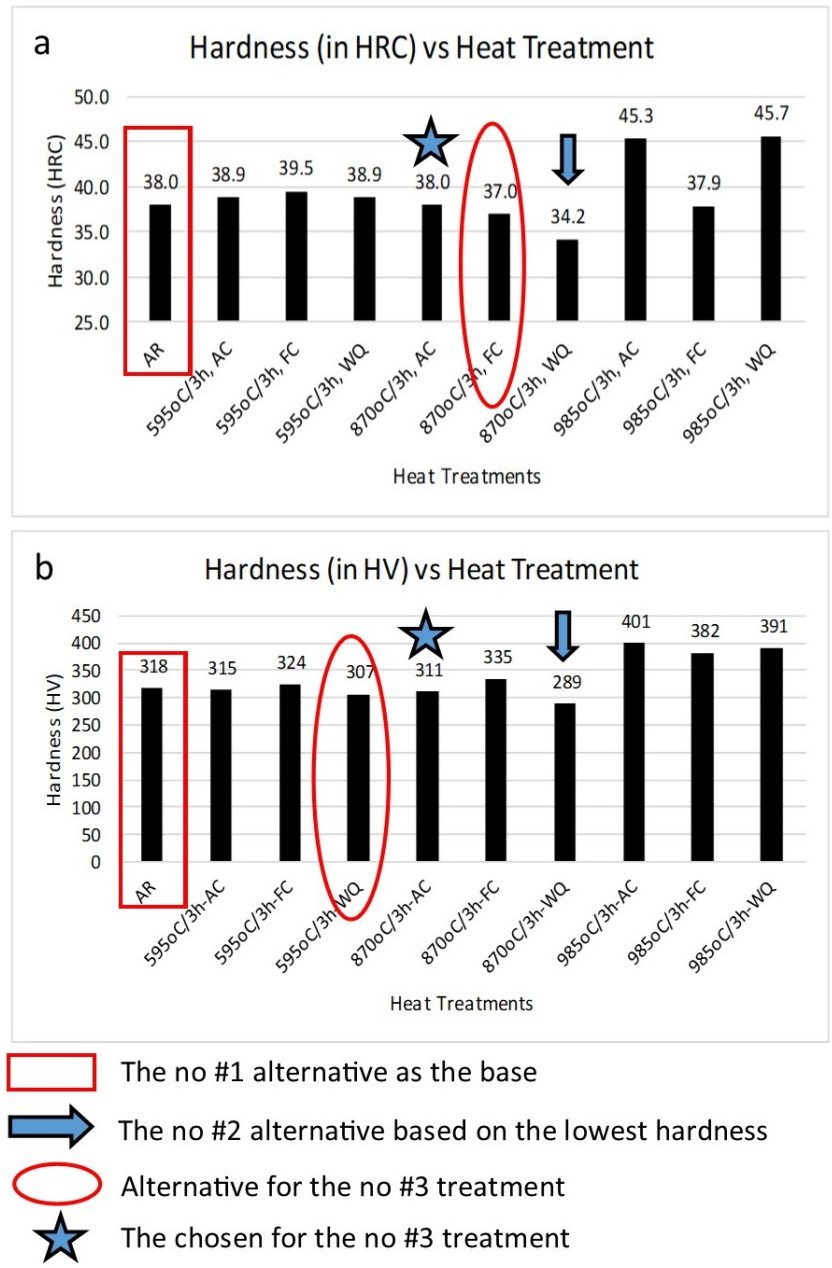

Figure 4.2. Comparison of hardness from three different heat treatments and the chosen heat treatments for the next experiments.

4.2 Chip Patterns

An example of chips collected from one drilling experiment is presented in Figure 4.3-a. A sample of one piece of a 'single' chip for observation is shown in Figure 4.3-b. A sample of a complete mounted chip of one run which was ready for a micro Vickers hardness test as well as microstructural analysis (optical and SEM) is presented in Figure 4.3-c.

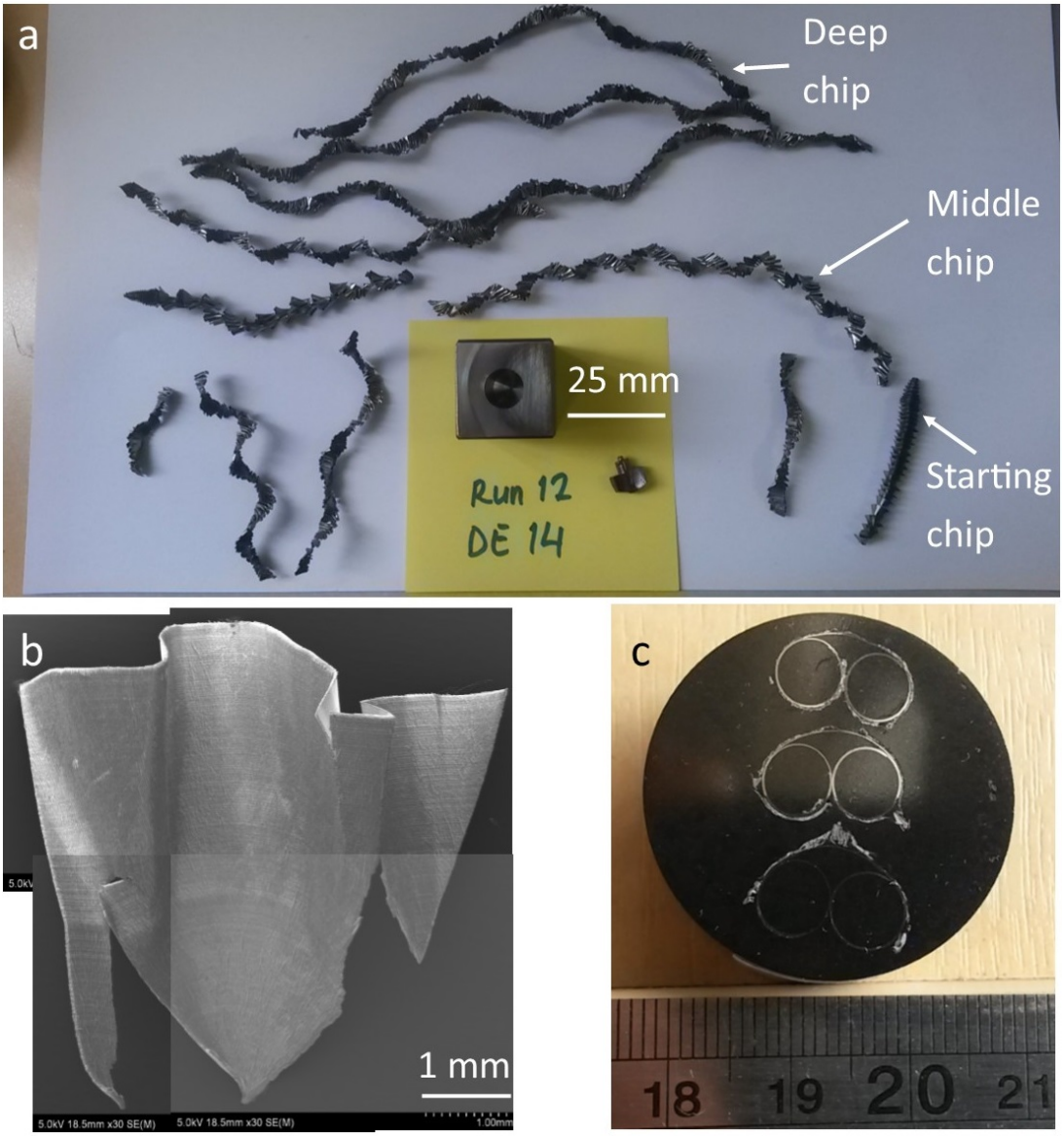

Figure 4.3. Chip preparation for SEM observation. (a) Collected chips of one run; (b) a typical chip with three areas; (c) mounted chips for metallography and microscopy analysis.

After collecting all of the chips from the different parameters applied in the drilling, we could recognise that the chip forms were influenced by the stages of drilling, as shown in Figure 4.4. At the early stage of drilling, the chips were conical spiral in shape regardless of the parameters used for drilling and the treatment of the workpiece prior to drilling. Changes in shape were then evident as the drilling continued depending on the drilling parameters. Most of the high feed rate (0.15m/min) resulted in a segmented, conical spiral of chips that were broken just before they grew into a long-pitch shape by the wall of the drilled hole due to its insufficient ductility. Moreover, by applying cutting fluid these segmented chips become shorter. The low

feed rate (0.08 m/min), on the contrary, resulted in long and nearly unbreakable chips during drilling. At a high cutting speed the chip forms were a helical spiral. With a high feed rate the chips were thicker but the helical spiral shape was still obvious. The deeper the drilling the greater the tendency to form zigzag chips that were buckled and densely folded because it may have been hard to find the way out through the flutes. This tendency can be found on the drilling of a 10 mm depth only when the chips were long and not broken, which is the last third of the whole of the long chips. When drilling got deeper the zigzag chips were denser. On the contrary, the zigzag chips were not formed in drilling at a 10 mm depth when applying a feed rate of 0.15 mm/rev with coolant. The changing of the chips may related to the tool deterioration as mentioned by Sultan el al. in drilling stainless steel [99]. It may also be related to friction. At the early stage it experienced lower friction than the subsequent chips. The latter tended to have restrictions with the slowed chips which were previously produced (Kahng & Koegler in Ke, et.al.[100]).

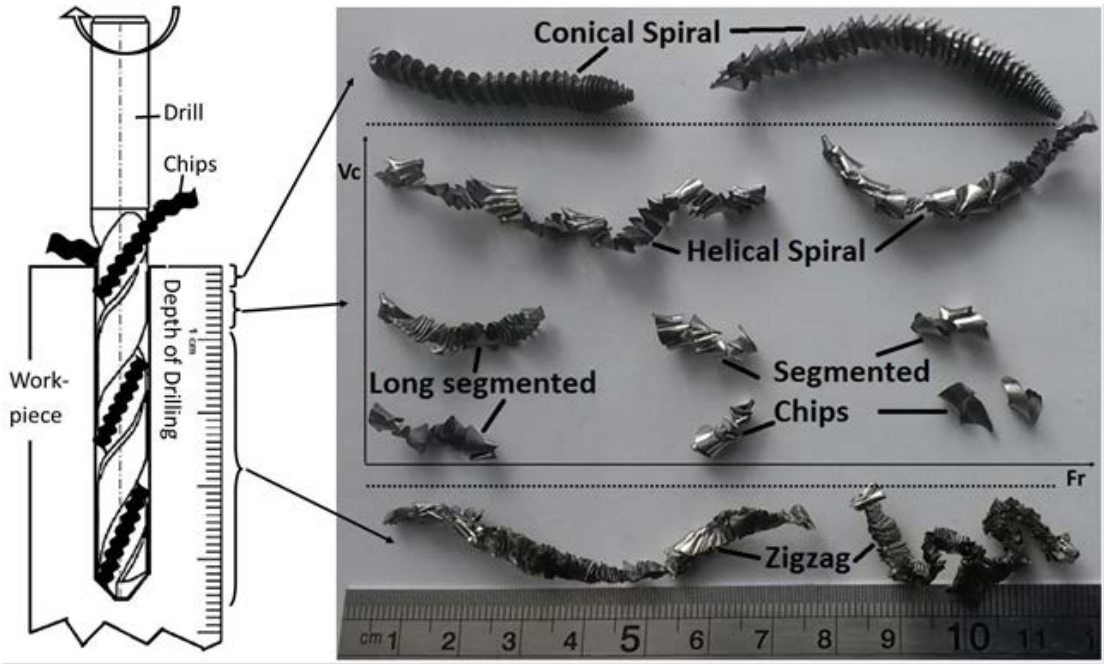

Figure 4.4. Form of chips from different stage of drilling.

A closer look at the chips with SEM revealed that there is a different profile between the two chip surfaces; that is the free surface of the chip (side of the chip that has no direct contact with the tool during drilling) and the drilled surface of the chips (the side of the chips that has been in contact with the tool during drilling) as shown in Figure 4.5. In general, the form of the chip is a zig-zag, as in Figure 4.5-b. The drilled surface

is smooth with a regular pattern line of scratches (Figure 4.5-c). The scratches should be due to friction between the tool and the chips. The free surface of the chip however, has a very dense teeth comb appearance, as in Figure 4.5-a. Between the teeth there is a connection, around the base or near the vicinity of the drilled surface. Another experiment beyond the L-18 Taguchi design; different heat treatment results have also been carried out and the result is presented in Appendix A.

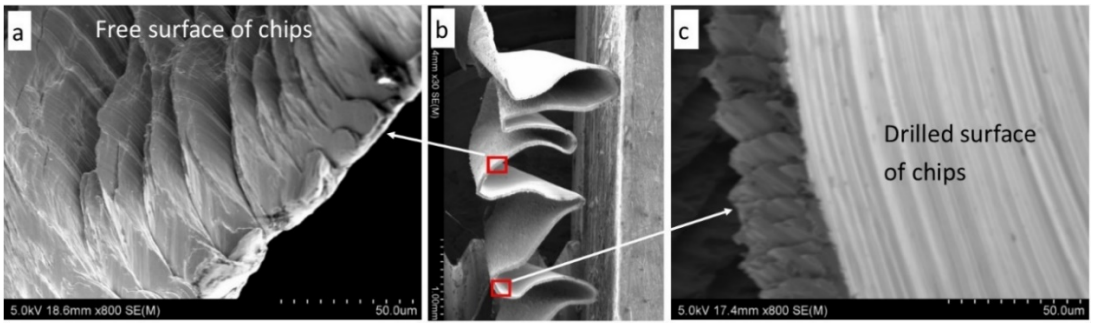

Figure 4.5. General appearance of chips: zig-zag or wavy form (a), smoother with traces of scratches at the drilled surface (b) and very dense comb teeth like appearance at the free surface (c).

Chips were formed from many single cones as an effect of using a different cutting side of the drill bit and operating different cutting speeds along the cutting blades. The peripheral chip is the result of an outer blade cutter, whereas central chips are cut by an inner blade (Figure 4.6-a). This single chip was bent at about one third near the bottom (narrow side of the cone). The bend was due to a change of blade orientation between the inner blade and outer one (Figure 4.6-b). A longitudinal view with SEM shows that the segment chips were different at the outer, inner and mid samples (Figure 4.6-b&c).

Further observation of these chips using an optical microscope shows that although there were different forms, their microscopic patterns were mostly the same, i.e. serrated (or saw tooth or segmented), as can be seen in Figures 4.8 and 4.9. These chips consisted of segments between the shear bands. Variations of drilling parameters, heat treatments and an application of coolant will cause a different size of each segment. The results were identical to what was reported in [101]. They found that most of the chosen combinations of cutting speed and feed rates resulted in segmented chips. As the exception, continuous chips were found when machining with low cutting speeds and a low depth of cut (in the case of drilling depth of cut (DoC) = Fr/2). The microscopically continuous chips were not found in our experiment results. It may be

due to the applied parameters (Vc and fr) which are between the values recommended by the drill bit manufacturer.

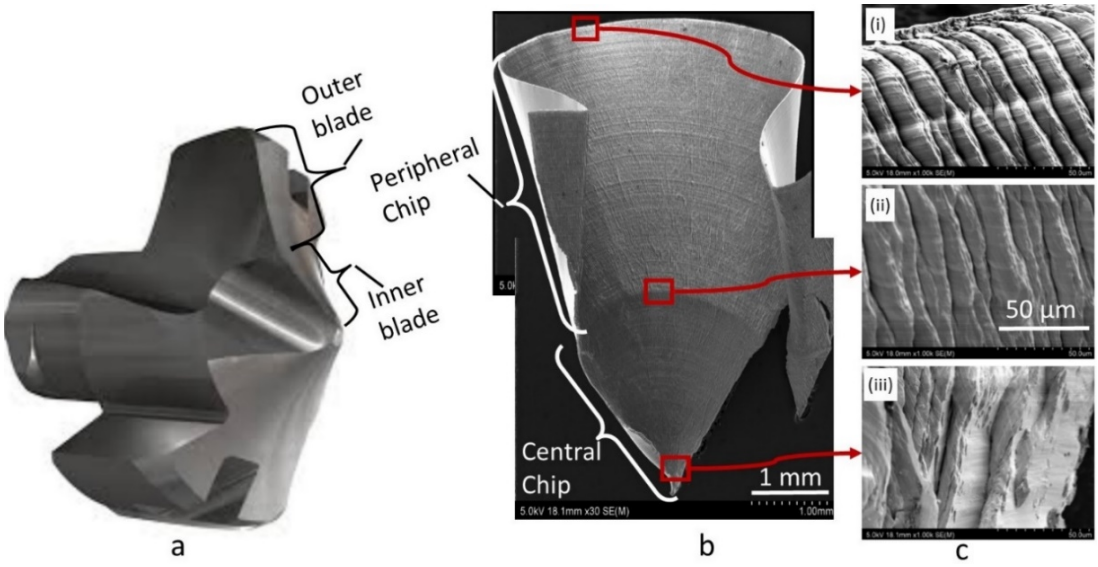

Figure 4.6. Illustration of a drill head with two blades (a), a single chip (b), SEM of chip patterns in different sections (c).

4.3 Microstructure and Hardness of the Chips

The as received (AR) material is most likely in the forged condition followed by annealing, according to its similarity to the one in ASM Metals Handbook Volume 9, as depicted in Figure 4.7-a [102]. The elongated 'primary' alpha grains (light) in aged transformed beta matrix containing acicular alpha.

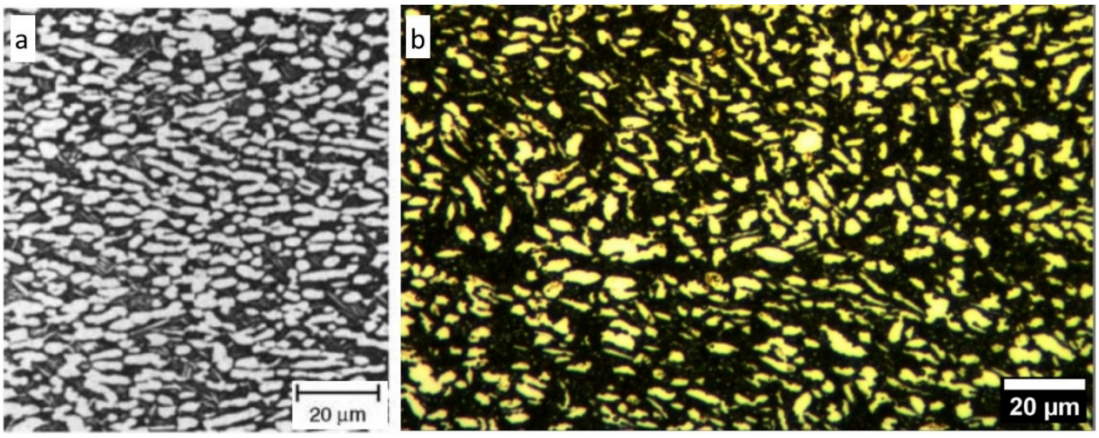

Figure 4.7. Comparison of microstructure of Ti-6Al-2Sn-4Zr-6Mo: (a) as forged and followed by heat treatments [102] *and (b) as received condition (AR).*

The hardness tests on the chips were carried out after polishing and light etching to highlight the position of indentations among the chip lines. An example of a hardness test result on a chip from experiment 18 of HT2-ed material is presented in Figure 4.8. The hardness values were quite different among the indentations; however, there was no tendency to show that certain points or positions had greater hardness over the others. Therefore, the hardness of the chip was calculated as the average value from all points; in this example the hardness is 256 HV.

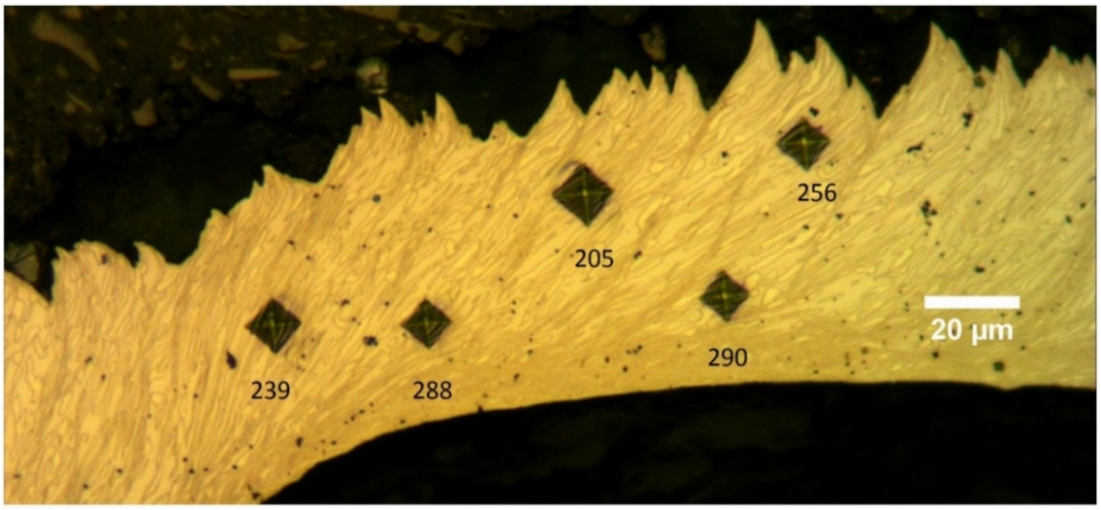

Figure 4.8 Micro Vickers hardness test on chips after light etching of HT2 treated.

The microstructure and hardness of Ti-6246 as received (AR), after HT1 and HT2 are presented in Figure 4.9-a, b, and c respectively. The hardness of block AR, HT1 and HT2 are 318, 311 and 289HV correspondingly. There is a decrease in hardness of chips compared to their original condition; except for the AR, the hardness was not changed.

In Figures 4.9-a1, b1, c1, the grains were elongated at the shear band area. The elongation of grains was also observed at the bottom of the chips, which are usually called ‘secondary shear areas.’ The deformation of chips during machining involves strain-softening, a behaviour where the shear resistance (or shear stress) reduces with continuous development of plastic shear strains [103]. This phenomenon was revealed and proved by adding to the previously understood phenomena, i.e. strain rate hardening as well as thermal-softening phenomena. When strain phenomenon was added to the existing material model, it resulted in better conformity between the model and the real chips [88], [90], [104].

The SEM observation results (Figure 4.10) show more clearly that the chips experienced grain elongation. The microstructure of the chips (Figure 4.10-b) were intentionally compared to two views, i.e. longitudinal (Figure 4.10-a1) and transversal (Figure 4.10-a2) because the chips were ploughed from the original material; not exactly as longitudinal, nor transversal. It was affected by the point angle of the drill tip (140^{o}) and also the fact that the drilling did not use orthogonal cutting. The grains that experienced elongation were in all sections of the chip segment, not only the ones in the primary and secondary shear bands. It was also obvious in Figure 4.11-b that all of the grains were elongated in all sections of the chips.

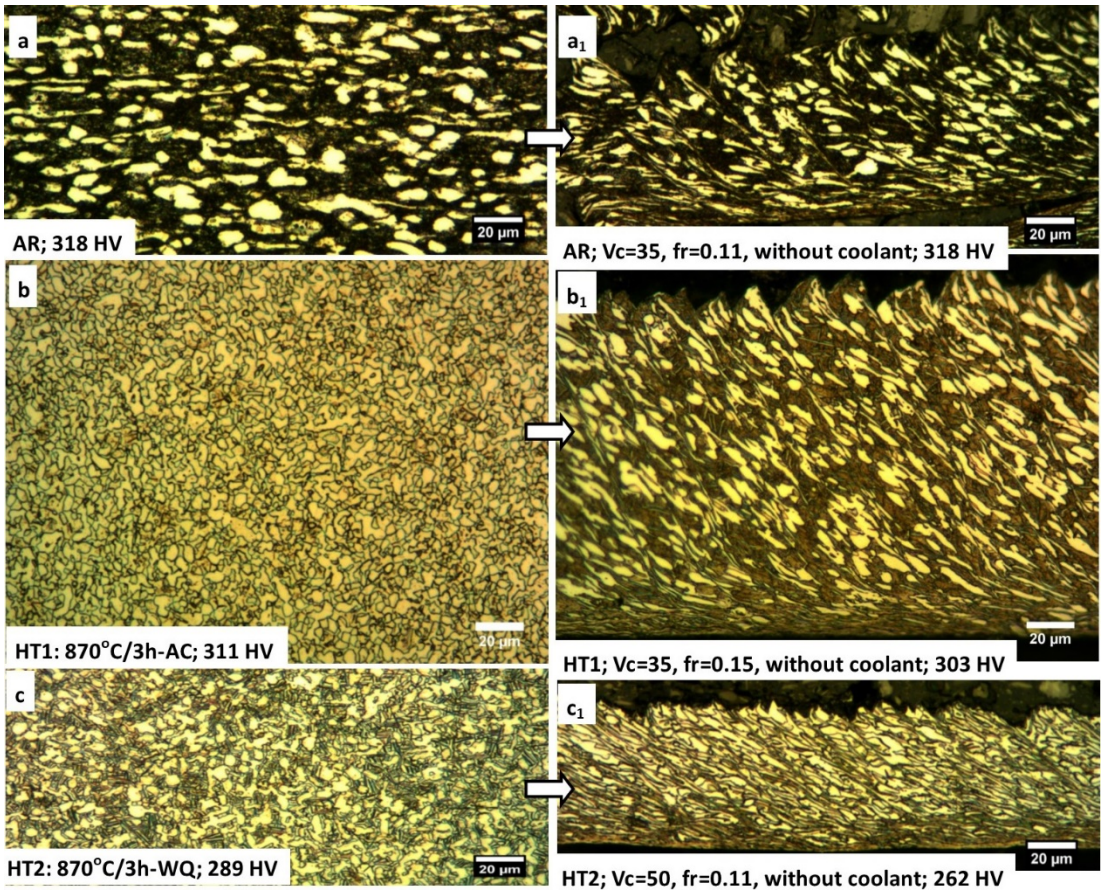

Figure 4.9. Microstructure and hardness after drilling with different machining parameters.

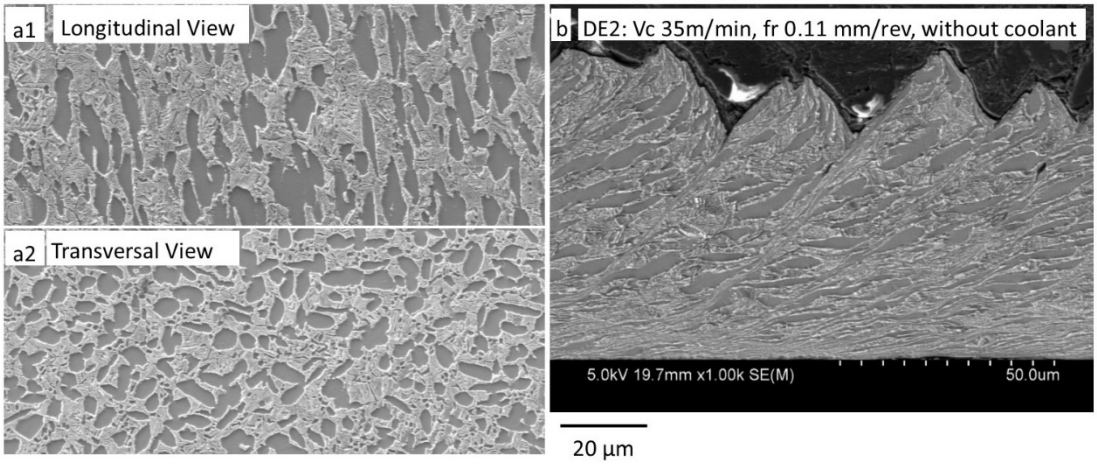

Figure 4.10. Microstructure changing before (a1 & a2) and after drilling of AR material (b).

4.4 Mechanism of Chip Formation

There are two main forces at work on the tool tip. These are thrust force (Fz) and torque (Mz) caused by the feed rate (fr) and the linear cutting speed (Vc) applied by the drill (Figure 4.11-a). The thrust force was mainly (more than 50%) caused by working with a chisel [11], while torque is influenced by speed rotation and the diameter of the drill. The chip was formed due to the shear force (τ cutting) that deformed the material then separated it (Figure 4.11-a). The serrated chips were caused by periodic thermoplastic shear instability happening within the primary shear zone. The shear instability happens when the rate of thermal softening exceeds the strain rate and strain hardening. The heat generated by a severe plastic in the primary zone was not able to be dissipated due to the fact that the shear process occurs in a very short time. Figure 4.11-b shows clearly the primary shear zones (between chip segments) and the secondary shear zone at the bottom of the chip. The pattern of elongated grains clearly shows that the chip experienced shear deformation.

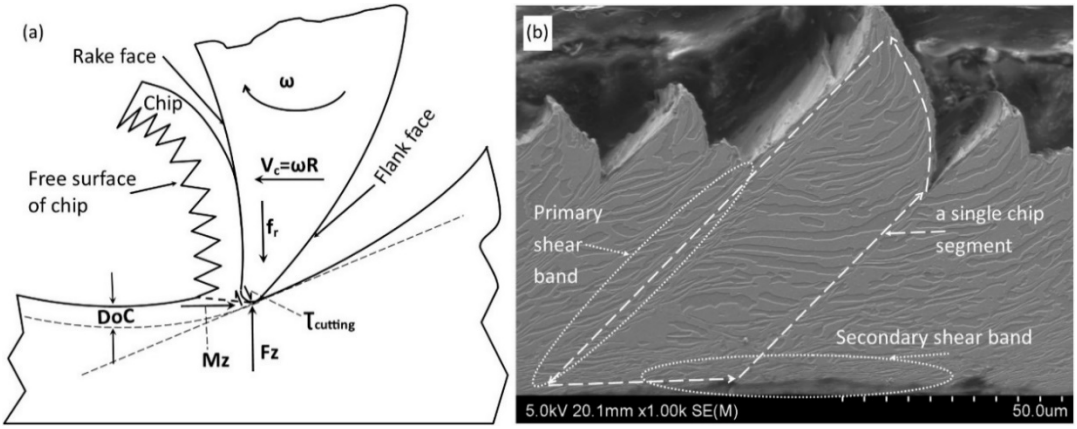

Figure 4.11. Mechanics of chip formation in drilling (a) and a SEM image of a serrated chip (b).

4.5 Serrated Degree of Chips and Taguchi Analysis

For quantitative characterisation of serrated chips, the serrated degree (Gs) of chips is defined by Wang and Liu [51], Zang et al.[60], and Liu et al. [105] as

$$Gs = \frac{H-C}{H} \times 100\% \quad \text{(4.1)}$$

Where, H and C are the height from the bottom of the chips to the top and the bottom of the segmentation, respectively, D represents chip segment thickness. The illustration of the degree of serration is presented in Figure 4.12.

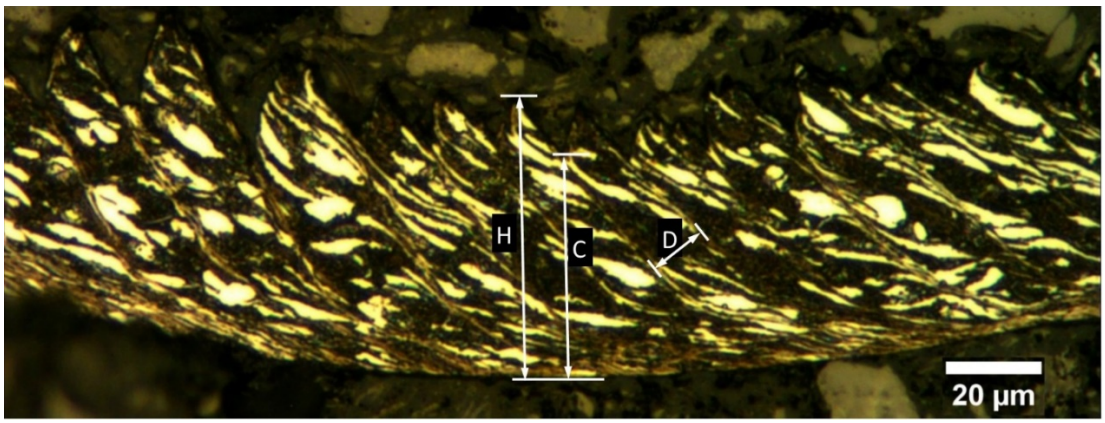

Figure 4.12. Degree of serration illustration [105].

There is a slight difference in chip formation between different cutting speeds on the as-received (AR) samples (Figure 4.13-a & d). We found that a serrated degree, Gs, is 0.16 of the cutting speed 35 m/min compared to 0.31 of the cutting speed of 50 m/min. A higher cutting speed would slightly increase the degree of serration. The result is in

conformity with what was achieved by Zang et al., that there was a mutual correspondence between the segmentation degree with the cutting speed [60]. Meanwhile, different feed rates have increased the degree of serration twice from 0.16 to 0.34 of the feed rate 0.11 mm/rev and 0.15 mm/rev respectively (comparison of Figures 4.13-a & b). The chip thickness (D) was also increased significantly from 20.8 to 44.8 µm. Applying a coolant during the drilling did not affect either the value of the degree of serration or the chip thickness (Figure 4.13-a & c). The highest degree of serration (0.34) and widest chip segment (44.8 µm) was achieved by applying Vc 35 m/min, and Fr 0.15 mm/rev without coolant in drilling the AR block (Figure 4.13-b). On the contrary, the same parameters would result in the lowest degree of serration (0.09) and fair chip segment (around 20µm) when drilling the HT1 block (Figure 4.9-b1). It may be related to less hardness of the HT1 material. After drilling the hardness of the chips decreased further. Usually the softer the material, the easier it is to be deformed without cracking. The degree of serration, to some extent, is associated with a possibility of cracking. The higher the degree of serration, the more likely it is to crack.

According to Wang & Liu, heat accumulation leads to the occurrence of locally serrated chips at lower cutting speeds. This happened because slip deformation plays the most important role. However, at high cutting speeds, adiabatic shear becomes the dominant mechanism, which leads to the formation of fully serrated chips [51]. Locally serrated chips means the difference between the top of the chip to the bottom of segmentation is relatively small; fully serrated chips mean this value is fairly big.

Feed rate in drilling is defined as a tool's distance travelled during one drill (or spindle) revolution. In other words, how deep the drill goes through in one revolution. It is also related to the volume of material removed or being chipped. The higher the feed rate the thicker the chips, or, the bigger the teeth of the serrated chips. Therefore, increasing the feed rate would increase the serrated degree.

In this research, an external coolant application was used and it is generally understood that one of the disadvantages of drilling is its difficulty for the coolant to reach the tool-chip interface by the external coolant method because the coolant has to collide with the chips on the way out. Therefore, the coolant did not relatively change the chips formed or the degree of chip serration.

The overall analysis of the chips was done using the Taguchi method, as shown in Table 4.2. Taguchi uses the S/N (signal to noise) ratio to measure the performance characteristic which deviates from the desirable value. The term 'signal' represents the desirable value (mean) for the output characteristics and the term 'noise' represents the undesirable value for the output characteristics. Out of three quality characteristics, the higher the better (HB) was chosen for analysis of the degree of serration (Gs). The higher the Gs means the easier it is for the chips to break because the smaller area is bonded between the segments of chips in comparison to the whole chip thickness. Usually the shorter chips are preferable in machining.

The characteristic of the quality of the 'higher the better' was calculated according to the equation 2.2 in Sub Chapter 2.2. The higher degree of segmentation means the higher possibility of the chips being broken. Vice versa, the lower the degree of segmentation it tends to create a long chip, which is undesirable as the chips can tangle along the drill body and have to be removed manually [100]. The S/N ratio values are listed in Table 4.2 for parameters of the degree of serration (Gs). The values in the Gs row were obtained from calculating the average of about 20 Gs in each experiment. As the characteristic of the quality of the 'higher the better' was chosen, the highest value of Gs was desired. The S/N value was generated by Minitab 17 by comparing the signal (controllable factors or the parameters which were included in the experiments) and noise (uncontrollable factor). Differing from the measured values (in this case is Gs) the S/N ratio is not affected by the chosen quality characteristic. It is always the higher the better, which means minimising the effect of the noise factors.

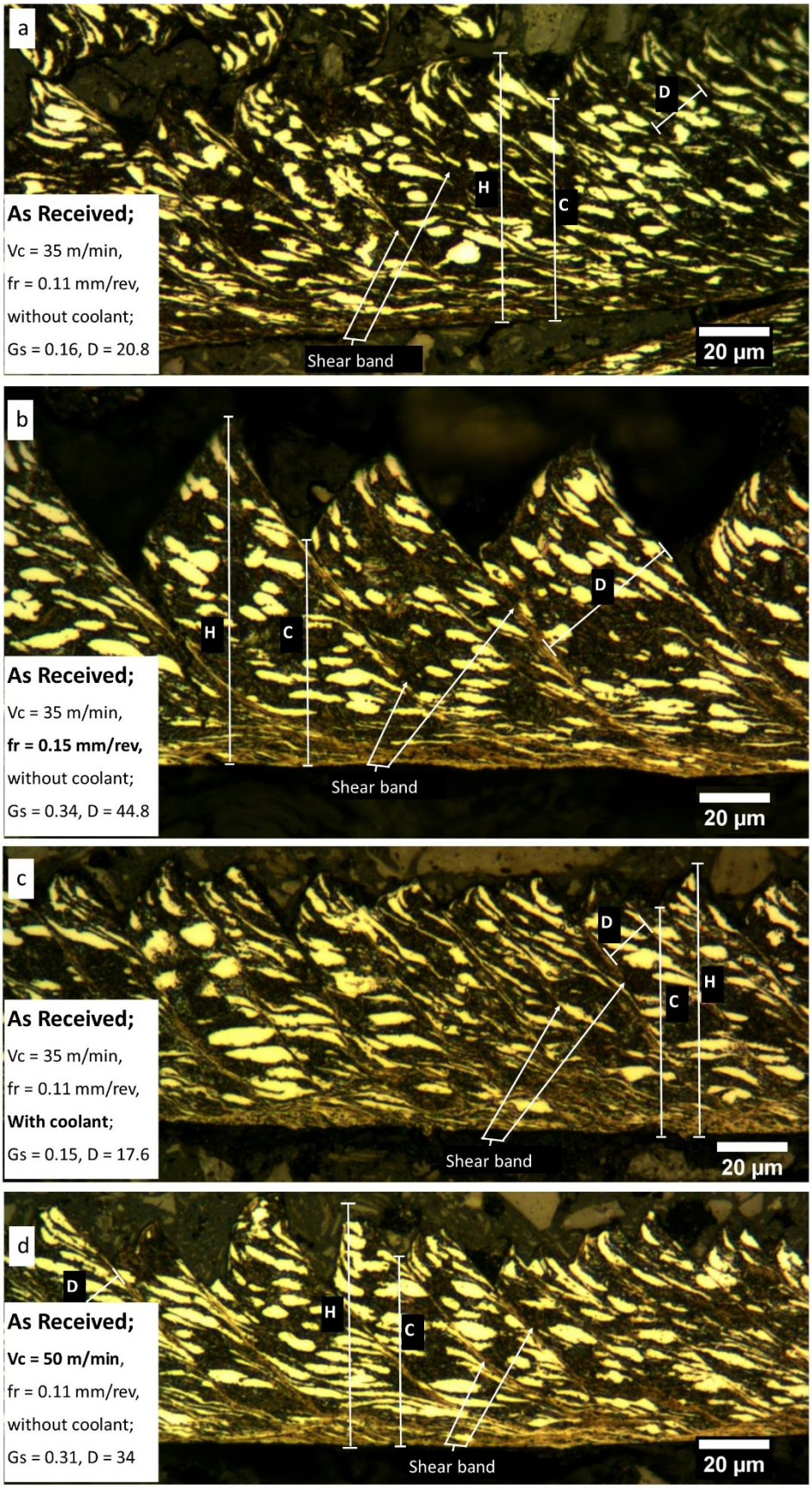

Figure 4.13 Serrated degree of chips from different drilling parameters on the AR samples.

Table 4.2. L18 Orthogonal Array, Experiment result and S/N ratio

DE	Clt	HT	h	Vc	fr	Gs (%)	S/N Gs
1	Off	AR	10	27	0.08	11.1	20.9
2	Off	AR	30	35	0.11	14.8	23.4
3	Off	AR	45	50	0.15	21.2	26.5
4	Off	HT1	10	27	0.11	8.7	18.8
5	Off	HT1	30	35	0.15	10.0	20.0
6	Off	HT1	45	50	0.08	14.0	22.9
7	Off	HT2	10	35	0.08	18.0	25.1
8	Off	HT2	30	50	0.11	14.7	23.4
9	Off	HT2	45	27	0.15	8.7	18.8
10	On	AR	10	50	0.15	44.6	33.0
11	On	AR	30	27	0.08	20.2	26.1
12	On	AR	45	35	0.11	16.4	24.3
13	On	HT1	10	35	0.15	9.7	19.8
14	On	HT1	30	50	0.08	15.7	23.9
15	On	HT1	45	27	0.11	9.1	19.2
16	On	HT2	10	50	0.11	12.0	21.6
17	On	HT2	30	27	0.15	14.3	23.1
18	On	HT2	45	35	0.08	14.3	23.1

Clt: coolant applied; HT: heat treatment; h: depth of drilling; Vc: cutting speed; fr: feed rate

Table 4.3 demonstrates the response table for the S/N ratio for 'higher is better' which was acquired for diverse parameter levels. This table was obtained from Minitab 17 after generating the S/N ratio and choosing the 'Gs' as the response. The 'Delta' row values were gained by subtracting the highest and the lowest S/N value of each factor. The higher the value of the delta means the higher the effect of the factor to the measured value (Gs).

Table 4.3. Response Table for Signal to Noise Ratios of Gs

Level	Clt	HT	h	Vc	fr
1	22.28	**25.70**	23.18	21.14	**23.68**
2	**23.79**	20.90	**23.45**	22.75	21.77
3		22.51	22.47	**25.21**	23.66
Delta	1.51	4.80	0.98	4.07	1.91
Rank	4	1	5	2	3

The analysis of the S/N ratio of Gs revealed that the factors that cause Gs to be increased were the heat treatment, the cutting speed, the feed rate, the coolant and the depth of drilling (see the 'rank' row of Table 4.3). After that, the analysis was made to determine the suitability of each of the main factors which was made to determine the

suitable factors from an S/N ratio, as shown in Figure 4.14. From the S/N ratio analysis (Figure 4.14) the optimal drilling parameters were the cutting speed 50m/min (level 3), the feed rate 0.08 mm/rev (level 1) at a depth of 30 mm (level 2) with coolant, while the block was left un-heat treated (as received). However, a feed rate at the maximum level (0.15 mm/rev) was chosen as it affected only 0.02 (= 23.68-23.66 in Table 4.3) in the S/N ratio by comparison to that of the feed rate 0.08 mm/rev. Therefore, a feed rate of 0.15 mm/rev should be chosen for the sake of a higher material removal rate (more economy) with an abandoned effect in comparison to choosing a feed rate of 0.08 mm/rev.

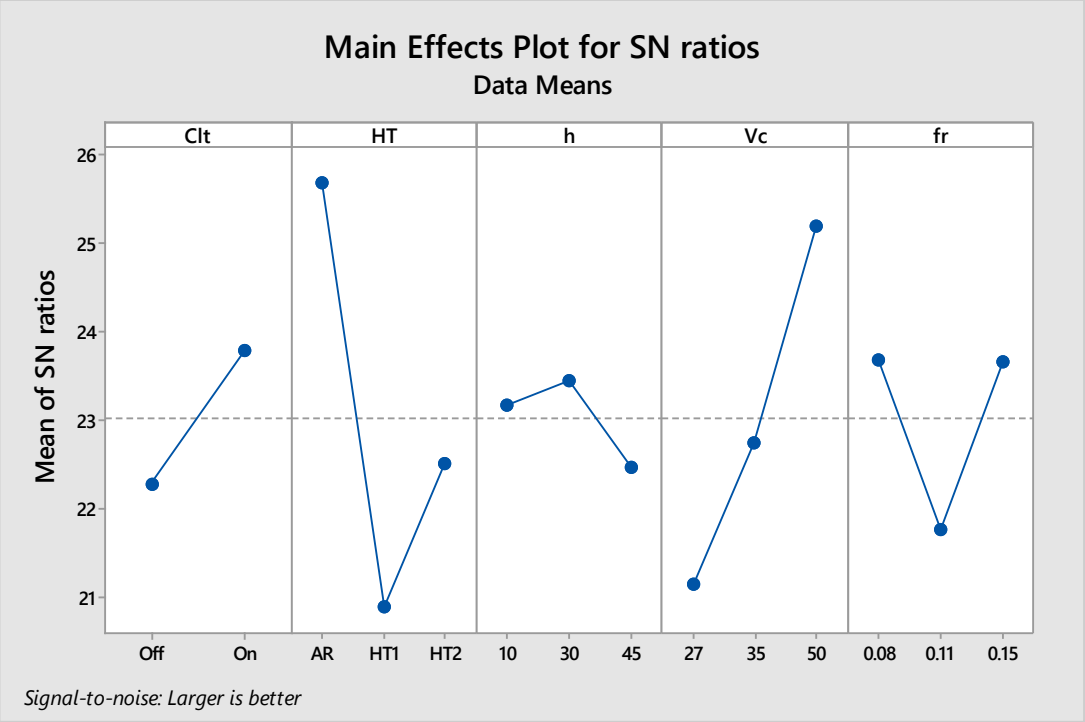

Figure 4.14. S/N ratio values for parameter Gs.

Heat treatment had the greatest effect on the value of the degree of serration. The largest value of the degree of serration would be achieved when drilling the AR material, while the smallest degree of serration was achieved when drilling a HT1 block. It may be related to the microstructure of the blocks prior to drilling. The AR material has a coarser microstructure compared to that of HT, where it may be easier for the chips to crack at their free surface. Therefore, the value of the Gs was higher.

The depth of drilling affected the degree of serration the least in comparison to other parameters. The best condition for drilling was at a depth of 30 mm, and the worst was when drilling at 45 mm. It may be related to the chips formed when drilling at a greater

depth which tended to be a zig zag, a denser form of chip and between segments close to each other and more bonded. The relative effect of the cutting speed, the feed rate and the coolant toward the serrated chip has been described in the earlier part of this sub-section.

4.6 Analysis of Variance

Analysis of variance (ANOVA) is a statistical method, as a tool for decision-making by perceiving variations in the average performance of three or more in the independently tested group. ANOVA compares relativity sizes of two sources of variation in the data. ANOVA also detects a variation between and within groups. Moreover, ANOVA assists in finding the significance of all factors involved in the experiments in a percentage form. ANOVA is also able to detect the interaction between factors by contrasting the value of the mean square to an estimation of experimental errors. It presents all the comparison data at a specific confidence level.

Some terminologies and their formulas need to be understood in using ANOVA. First, the total sum of squares is the sum of squared deviations Seq SS from the total mean Gs ratio n_m which can be calculated as:

$$Seq.SS = \sum_{i=1}^{n}(n_i - n_m)^2 \quad \text{.....(4.2)}$$

Here, n denotes the quantity of experiments in the Taguchi method and n_i represents the mean Gs for the experiment.

Second, the percentage contribution P, which is formulated as:

$$P\% = \frac{SeqSS_D}{SeqSS_T} \text{.....(4.3)}$$

Here, Seq SS_D denotes the sum of the squared deviations. Table 4.4 is presenting the ANOVA results.

To check whether a certain parameter has an important impact on the characteristic of the output, a statistical tool which is called F, then tests need to be carried out. In the analysis, the F-ratio is the comparison of variations between the sample means to the variation within the samples. Usually, it used to verify the significance of a factor. The F-ratio also means the ratio of the mean square error to the residual error. Table 4.4 consists of the P-value which states the level of importance or level of significance as

to whether a factor significantly affects the output or not. The percentage (%) is defined as the rate of significance of the process parameters on the parameter Gs. The row which is marked 'Error' refers to errors caused by uncontrollable factors, or in the Taguchi model, called 'noise'. Noise is from the parameters not included in the experiments and the experimental error. The error of 33% was quite big, however as a general guide the error should be less than 50%, otherwise, results would not be reliable [106]. The percentage number revealed that the applied heat treatment and cutting speed have significant effects on Gs up to 29.0% and 20.1% respectively. Here, the feed rate, the coolant and the depth of drilling, only affects 17.4% accumulatively of the Gs.

Table 4.4. Analysis of variance for Gs using adjusted SS for Tests

Source	DF	Adj SS	Adj MS	F-Value	P, %
Clt	1	65.56	65.56	1.38	5.8
HT	2	329.43	164.71	3.46	29.0
h	2	35.77	17.89	0.38	3.2
Vc	2	227.86	113.93	2.40	20.1
fr	2	94.93	47.47	1.00	8.4
Error	8	380.47	47.56		33.6
Total	17	1134.02			100.0

The result of the ANOVA in this analysis is in accordance with the S/N ratio (Figure 4.14). The difference is that the ANOVA presents the F-value of each of the parameters used in the experiments. So, the higher the F-value, the higher the influence of the parameters on the measured output. The heat treatment has most influence on the parameters to the serration degree, followed by the cutting speed. The depth of drilling has no significant effect on the degree of serration. However, the feed rate and coolant moderately influence the degree of serration.

4.7 Modeling of Chip Formation

Some attempts to simulate the drilling titanium-6246 with the focused aim of showing the formation of serrated chips has been carried out. The results were not good enough to be presented as a main part of this thesis. Instead, it is presented as Appendix E.

4.8 Conclusion

The following conclusions can be drawn in this chapter:

1. Both the OES and the EDS test resulted in a comparable value to the nominal composition (literatures) of Ti6246 alloy;
2. Chip forms were not affected by the heat treatments or the drilling parameters on the early stage of drilling and on deeper drilling. By contrast, they were changed with different heat treatments and drilling parameters on a depth of drilling about 3 mm to 10 mm. The changing of the chips form most likely due to increasing tool deterioration and friction as drilling deeper;
3. All experiments resulted in serrated chips with a different degree and length, but no continuous chips resulted;
4. The chips experienced strain softening; therefore the chip hardness was softer than that of the block before drilling. The chips also experienced grain elongation in all sections, not only in the shear band area;
5. The chip formed by the cyclic thermoplastic shear volatility happened inside the primary shear zone;
6. The parameters most influential to the degree of serration were the heat treatment and cutting speed with a percentage of 29.0% and 20.1%, while the depth of drilling affected only 5%;
7. The optimal result of drilling based on their chip formation was achieved by keeping the Ti-6246 in the as received condition (for this investigation) and applying a cutting speed of 50 m/min, a feed rate 0.15 mm/rev for drilling of 30 mm with a coolant. This parameter resulted in the highest segmented chips and an adequate material removal rate.

CHAPTER 5. ANALYSIS OF TOOL DETERIORATION

5.1 Introduction

In this research, a TiAlN PVD coated carbide insert drill was used for drilling titanium alloy Ti-6246. There were specific reasons in the selection of TiAlN PVD coated carbide for drilling Ti-6246 alloy. TiAlN PVD coated carbide was recommended for higher cutting speeds in turning Ti-6Al-4V [32]. Ti-6Al-4V has some similarities to Ti-6246. In drilling the titanium alloy Ti-6Al-4V, the TiAlN coated tool was superior to the uncoated tool; it increased tool life by 2416% (Is this percentage figure correct? Please check) at the same cutting speed of 25 m/min [18]. By contrast, tool delamination occurred in 5 seconds when face milling Ti-6246 using TiN coated carbide [34]. By studying TiAlN coated drill performance it will help to improve machinability of the Ti-6246 alloy.

In studying tool deterioration, tools were observed with SEM from both sides, i.e. flank and rake. An evaluation was carried out at four different sections on each side, i.e. chisel, inner blade, outer blade and the corners of both the inner and outer blades. For the sake of simplicity, the term 'corner' would sometimes be used to replace the term 'corner between inner and outer blade.' The views and the sections are presented in Figure 5.1.

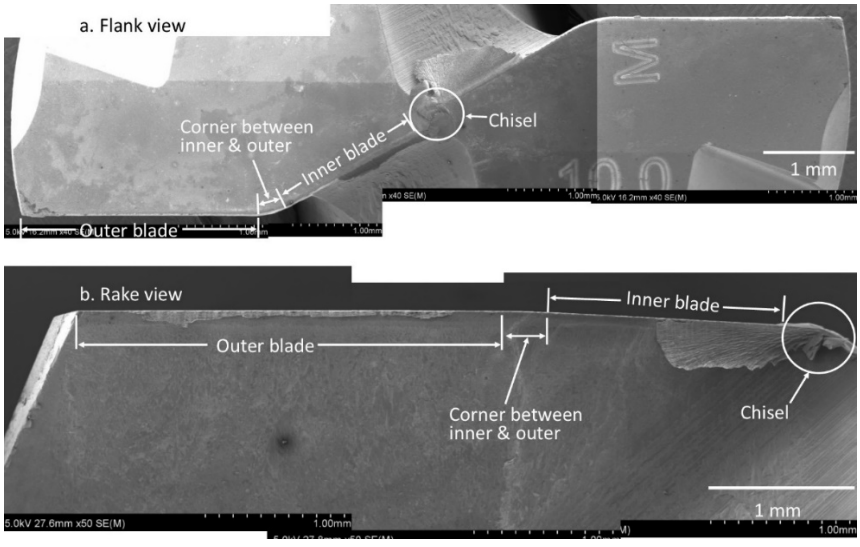

Figure 5.1. Sectioning in tool deterioration observations and the views of observation: (a) flank view, and (b) rake view.

5.2 Type of Tool Deterioration

Tool wear was not observed in all drilling conditions. Tool wear in this study referred to flank wear (VB) of more than 0.3 mm and a maximum of 0.5 mm [14]. This may be due to short drilling time or cycles of drilling in comparison to what was found by Zhang et al. [24], that the uncoated carbide tool wear was achieved after milling Ti-6Al-4V for about 77 minutes of VB 0.3 mm or 63.5 minutes of VB max 0.5 criterion respectively. Also, there was no crater wear at the rake face in this research for the same reason as that of the flank wear. According to Hatt et al. [107] though, crater wear is more susceptible when machining Ti-6246 than machining Ti-54M due to less formation of a protective TiC layer at the interface of Ti-6246 to that of Ti-54M.

Three types of deterioration were observed in this research. Two types involved reducing the tool from its original shape: delamination and chipping. The other is an addition to the original tool shape: built-up edge (Figure 5.2-a). A built-up edge is an attachment of debris or segments of chips on the tool. As mentioned in sub-chapter 2.2.7 that there are three kinds of built-up edge, i.e. built-up edge (BUE) which is stuck on the edge of the tool, built-up layer (BUL) which is on the lip of the rake-layer, and flank built-up (FBU) which is on the lip of the flank side [58]. However, in this research, we would refer to them all as a built-up edge (BUE). Attachments in the form of a built-up edge predominated in all conditions of drilling; it happened in all parameters used. Usually, BUE still exists at the vicinity of the chisel to the inner blade and is less pronounced on the edge of the outer blade. However, the leftover mark on the tool clearly shows that BUE has been pulled out at this site.

Delamination was the second common type of tool deterioration observed in this research. When the tool has been delaminated the grains of the tool base (WC-Co) are exposed, as shown in Figure 5.2-b_3. Delamination is the loss of coating adhesion to a surface or between coating layers.

The last but not least, was chipping. Even though chipping rarely happened, it is considered as one of the most severe types of tool deterioration. Chipping is a loss of a small fragment of the tool by sudden action. Consequently, pronounced base tool material can be seen clearly in Figure 5.2-c_1 – c_3.

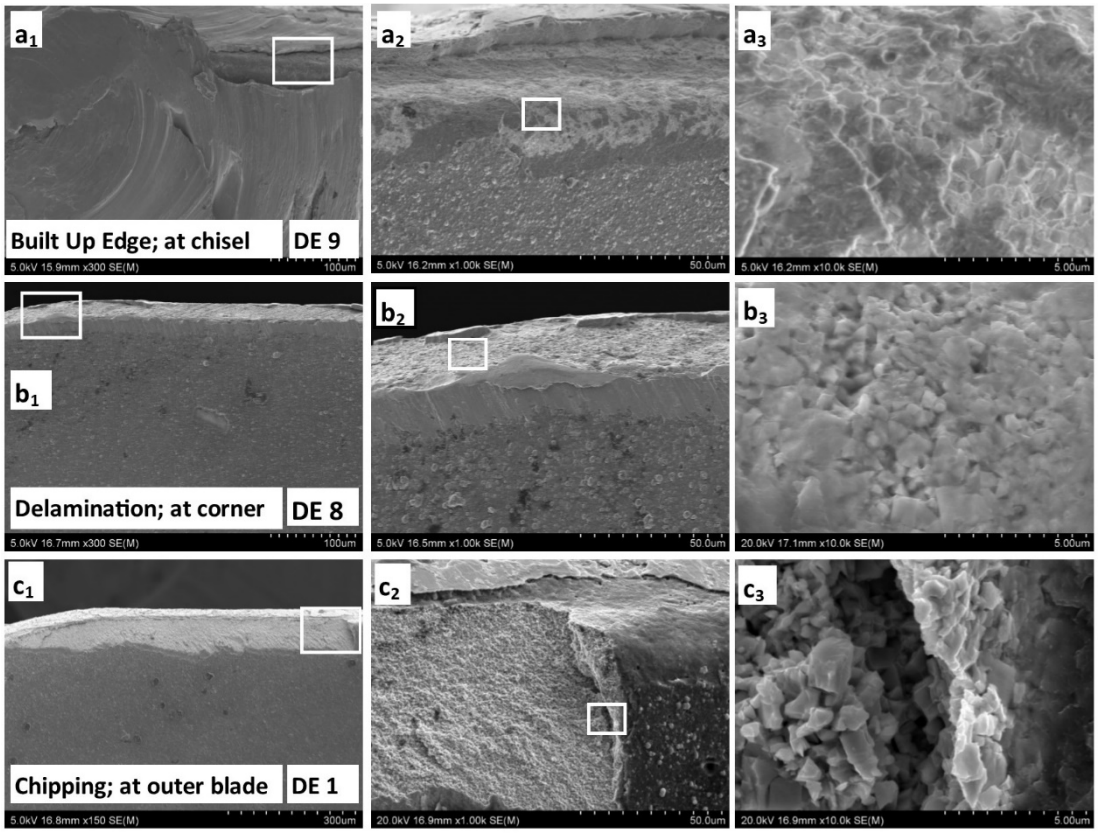

Figure 5.2. Typical of tool deterioration in drilling Ti-6246; all observations were from the flank view.

5.3 Mechanism of Tool Deterioration

A built-up edge (BUE) is a method of particles adhering to the rake face of the cutting tool being created during machining. An amount of microchips or powdered particles are produced during drilling. According to the first law of thermodynamics that total energy of an isolated system is constant. The energy emerged from the cutting process will be converted into heat; therefore the rake face experiences a high temperature. When the microchips or powdered particles are moving across the rake face of the tool, they will be exposed to a high-temperature environment and some of the particles may get adhered or welded to the rake face of the tool; this is known as a built-up edge.

Built-up edge formation is very common in machining titanium alloy due to its affinity to most of the tool material [25], [26]. A built-up edge does not occur in other material, such as steel, when high-speed machining is applied [57]. Therefore, built-up edge formation in machining titanium alloys is due to its affinity when machining at a low cutting speed. Thus, a built-up edge still exists in machining titanium alloy because it

is nearly impossible to apply a high cutting speed in its machining. In the case of drilling, the formation of BUE is inevitable, even if a high speed is applied, because the cutting speed varies from the maximum at the peripheral of the outer blade, to zero at the chisel. A thick BUE at the vicinity of the chisel and inner blade is shown in Figure 5.2-a_1. Higher magnification (in Figure 5.2-a_2 and further in Figure 5.2-a_3) indicates that carbide particles (the bright part) of the base tool material has been revealed.

Some researchers argued that BUE is not tool deterioration because underneath the BUE there is not necessarily tool loss [108]. To some extent this argument is true. It is possible that part of the BUE would still stick on the tool. It is displayed in Figure 5.3-a and Table 5.1, that under the BUE peeling off (#pt3), a percentage weight of 1.07% Zr and 1.64% Mo remained and these elements ought to be from the BUE that were formed from chips. The process of building up and breaking away may be repeated many times per second. During the peeling off process, the tool can be torn away. Titanium alloy has a high affinity to other materials. Therefore, during BUE formation, it is possible to form a strong adhesive bonding between the BUE and the tool [32], [34]. Then, at the time of peeling off, some part of the tool coating was delaminated. EDS examination proved that the peeled off surface clearly manifests the base material (tungsten), as presented in Fig 5.3-b and Table 5.2 (#pt2). That means some of the TiAlN coating has been removed during the peeling off mechanism.

Most titanium alloys are very responsive to other materials at temperatures of more than 500^{o}C; no exception to the tools. Some physical and chemical reactions may occur at the elevated-temperatures conditions, such as diffusion of the titanium particles into the carbide tool of material. The chemical reaction results in a strongly bonded interlayer of titanium carbide (TiC) on both the tool and the chip [109]. This interlayer piled up to form a BUE. When drilling continued this interlayer got weakened by the heat generated then the pulling out mechanism happened.

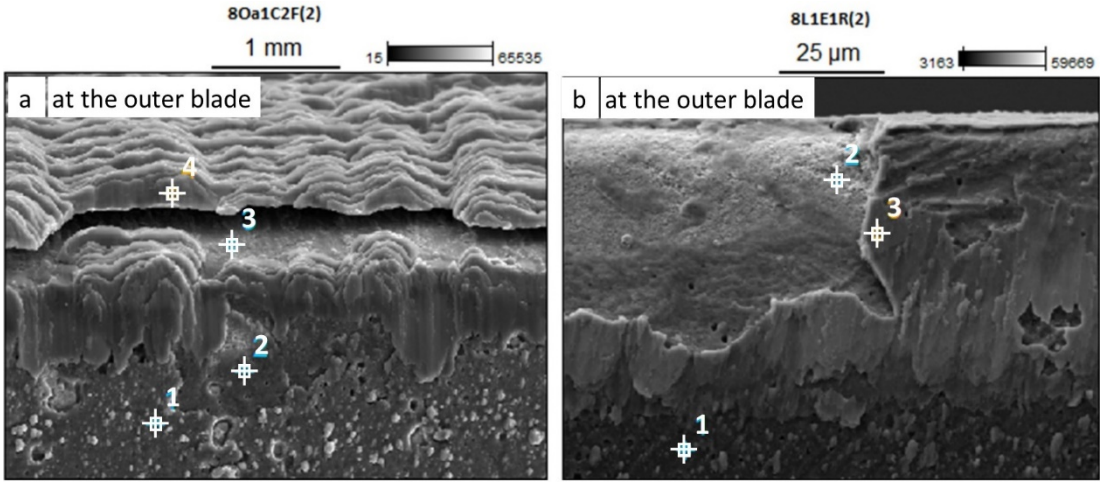

Figure 5.3. EDS of the BUE peeling off and delamination at outer blade

Table 5.1. Weight % of elements by EDS analysis corresponds to Fig 5.3a

	N-K	Al-K	Ti-K	Zr-L	Mo-L	W-L	Ir-L
8Oa1C2F(2)_pt1	25.68	21.55	52.77				
8Oa1C2F(2)_pt2	21.17	18.91	55.78			4.15	
8Oa1C2F(2)_pt3	10.12	20.97	66.20	1.07	1.64		
8Oa1C2F(2)_pt4	6.27	6.74	81.81		4.70		0.49

Table 5.2. Weight % of elements component of the EDS test of Fig 5.3b

	N-K	Al-K	Ti-K	Zr-L	Mo-L	W-L
8L1E1R(2)_pt1	17.57	25.59	56.84			
8L1E1R(2)_pt2			2.81			97.19
8L1E1R(2)_pt3	14.71	19.49	59.41	1.86	3.21	1.32

Delamination of TiAlN coating from the base tool material was also reported by previous researchers [46]. They concluded that coating delamination was the continuation of adhesion and diffusion modes in machining the Ti-6Al-4V. We are reluctant to accept their opinion that delamination is a diffusion mode. Diffusion is a physical process due to different concentrations. In our investigation, we could not recognise any different concentrations between tool surfaces and the microchips or powdered particles. According to Zhang et al. [20] and Rahim & Sharif [24] the delamination is a chemical reaction. However, there was no change to the substance at the molecular level. The BUE was formed and then after a while when a critical load is reached, the BUE breaks away from the cutting edge. The mechanism of forming and peeling off may repeat a thousand times per second [110]. During the peeling off mechanism, some parts of the tool can be torn away. In the case of the coated tool, the

coating may be delaminated, as seen in Figure 5.2-b_2 and more clearly in Figure 5.2-b_3. Actually, the initial delamination has been shown in Figure 5.2-a_3. Therefore, our results suggested that delamination is a continuation of the BUE peeling off.

Fracture or chipping at the edge corner of the drill was reported by previous researchers [24], [25], [109]. They argued that this chipping process related to a BUE peeling off mechanism. According to them, the adherent layer was formed on this site due to a high temperature. When the temperature was increased, the adhered layer became weak and could no longer withstand the high compressive stresses. The moving chips then pulled out the tool particles along with it. In this research, chipping randomly occured at different places; this not only happened at the corner edge of the drill. Figure 5.2-c_1 shows chipping at the corner between the inner and outer blade, about 600 µm long. Figure 5.2-c_2 shows the edge of the chipping area, and from Figure 5.2-c_3, grains of carbide of the base tool material was obvious. Some of the tool chipping was associated with a high feed rate (0.15 mm/min). The trial on drilling with a feed rate of 0.194 mm/rev proved that severe chipping was obvious at the corner between the inner and outer blade (Figure 5.4). There was chipping of 263 µm and 587 µm long at the corner between the inner and outer blade (Figure 5.4-a & 5.4-a1) and outer blade (Figure 5.4-b & 5.4-b1) respectively. It may relate to a high metal removal rate (MRR); a volume of the material that has to be removed in a certain time. When a higher volume of material has to be removed in a short period of time, a higher force is needed. Therefore, the tool chipping may be caused by a combination of high force and the BUE peeling off mechanism.

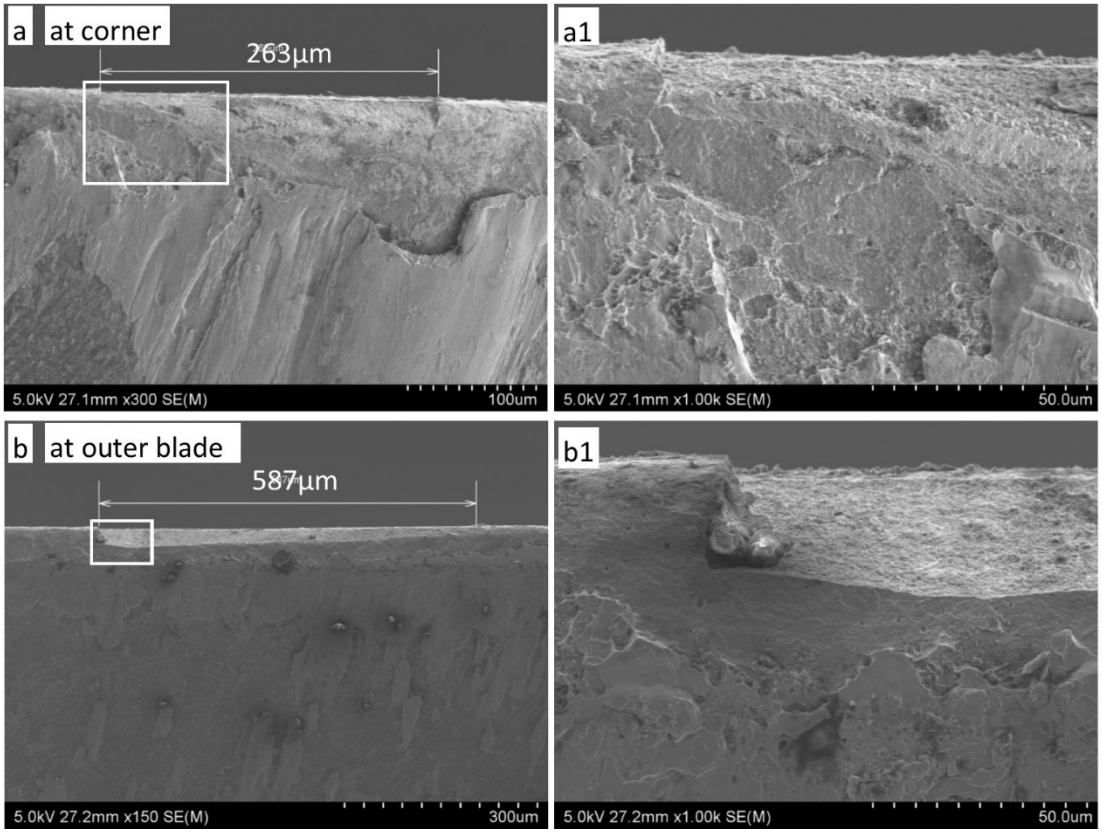

Figure 5.4. Severe chipping due to a high feed rate (0.194 mm/rev) application.

5.4 Performance of the TiAlN Tool

In regards to the mechanism of tool deterioration, the rank from light to heavy deterioration is: a BUE, delamination and then chipping. Therefore, we will quantify the degree of deterioration as 1 to 3. The note 1 was when only a BUE was observed, note 2 when a BUE and delamination had happened, and notation 3 if there was tool chipping. Observations were carried out at four main sections, viz. at the chisel, at the inner blade, at the corner of the inner and outer blade and at the outer blade (refer to Figure 3.4-c of sub Chapter 3.2 and Figure 5.1). So, total tool deterioration is the cumulative value of four areas of observation. An example of the calculation of tool deterioration of the design experiment (DE) 1 is presented in Figure 5.4. In DE1 there was a BUE, delamination, chipping and chipping at the four areas of observation. Therefore, the tool deterioration of DE1 is 1+2+3+3=9 (Figure 5.5). The tool deterioration calculation result of all of the experiments is presented in Table 5.3. The minimum value of tool deterioration was 4 in experiment 11 and the highest value of 10 was achieved in experiments 6 and 10. However, in the Taguchi method the

conclusion could not be drawn unless an analysis of signal to noise (S/N) has been carried out.

Table 5.3. Tool deterioration as machining parameters change

Experiment	Coolant	HT	h (mm)	Vc (m/min)	fr (mm/rev)	Tool Deterioration
1	No	AR	10	27	0.08	9
2	No	AR	30	35	0.11	6
3	No	AR	45	50	0.15	6
4	No	HT1	10	27	0.11	8
5	No	HT1	30	35	0.15	5
6	No	HT1	45	50	0.08	10
7	No	HT2	10	35	0.08	7
8	No	HT2	30	50	0.11	5
9	No	HT2	45	27	0.15	8
10	Yes	AR	10	50	0.15	4
11	Yes	AR	30	27	0.08	7
12	Yes	AR	45	35	0.11	8
13	Yes	HT1	10	35	0.15	5
14	Yes	HT1	30	50	0.08	7
15	Yes	HT1	45	27	0.11	7
16	Yes	HT2	10	50	0.11	7
17	Yes	HT2	30	27	0.15	10
18	Yes	HT2	45	35	0.08	8

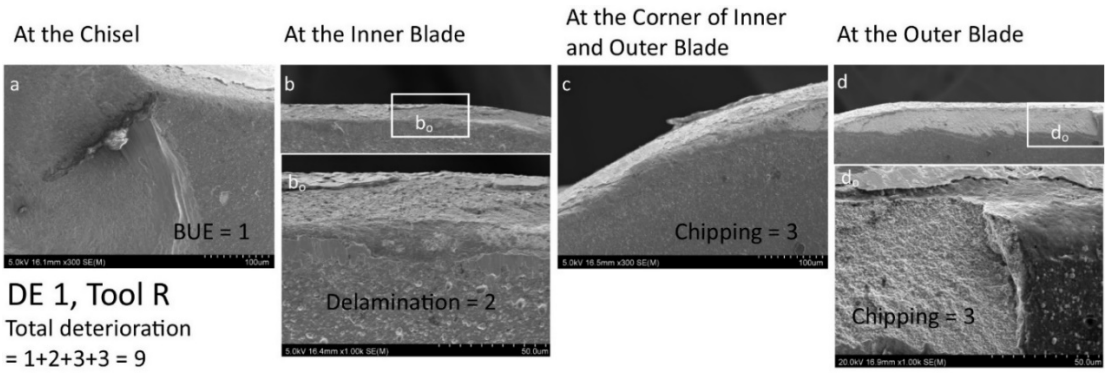

Figure 5.5. An example of calculating the value of tool deterioration.

Tool performance has the opposite meaning to tool deterioration. Therefore we use a "smaller is better" quality characteristic criteria of the main effect plot of means to find

the minimum effect of tool deterioration of each machining parameter as presented in Figure 5.6. It can be seen that varying the coolant application had the least effect on tool performance. Keeping the block as received (AR) had the least effect on deterioration. From a hardness consideration, the HT2-ed material should have been the easiest to machine and have the least effect on tool performance. However, machinability is not only influenced by the hardness of the material being cut but also by other properties such as tensile strength and thermal conductivity. A material with lower hardness and strength may increase machinability, but it is also possible to decrease the machinability when its thermal conductivity decreases, as reported by other researchers, when comparing annealed and solution + aged of Ti-6Al-4V [111]. Other researchers [39] found that mill annealing of Ti-6246 did not change the tool performance in comparison to its condition as forged due to a similarity of its microstructure. In our previous publication [112] it was stated that AR was in an annealed condition. HT2 has decreased the hardness of the block to 289 HV, compared to 318 HV in an AR condition. HT1 has slightly decreased the hardness to 311HV and also changed the grain to be smoother than AR [112]. Drilling of up to 30 mm deep results in the lower rate of tool deterioration, while drilling at 45 mm leads to rapid tool deterioration. The cutting speed and feed rate greatly influenced tool deterioration. Applying either a cutting speed of 35 or 50 m/min does not change the tool performance. In terms of economy, a higher cutting speed is preferable. Therefore, the higher the feed rate, the smaller the tool deterioration. According to the minimum value of mean value in each parameter, it should be ideal if we apply these following parameters during drilling: with coolant, AR, 30 mm deep, Vc 50 m/min and fr 0.15 mm/min.

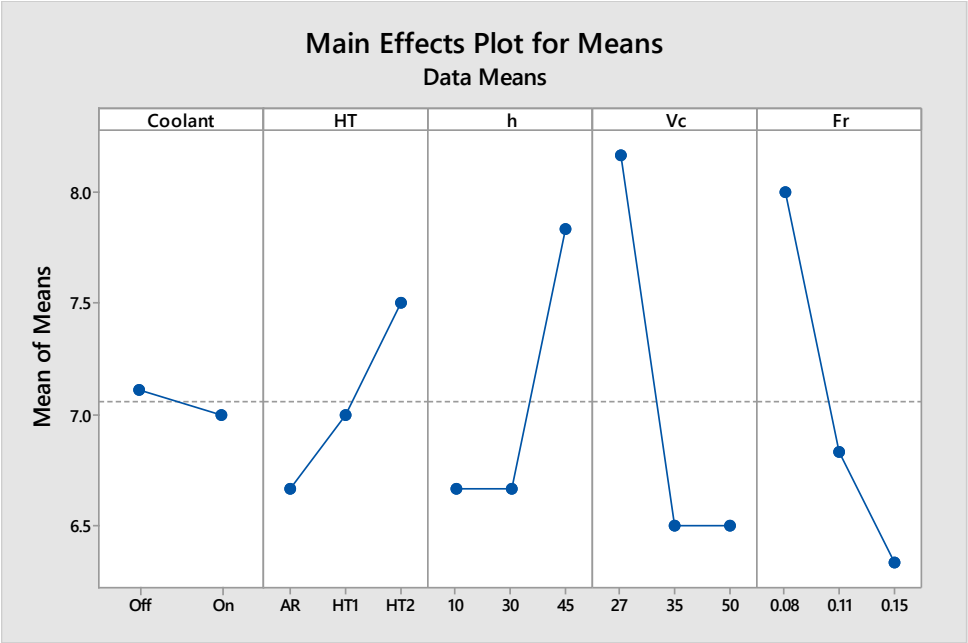

Figure 5.6. Effect of machining parameters on tool performance.

5.5 Further Discussion

In this section, we will discuss the compatibility of a TiAlN PVD coated carbide tool for drilling Ti-6246. Much of the literature stresses its advantages. TiAlN coating has a strong chemical stability, a low thermal conductivity, and a high oxidation wear resistance at 900^{o}C. The TiAlN coating increases the surface hardness to approximately 3400-3600 HV and improves the resistance to abrasive wear [46]. Other researchers [113], [114] proved that the Al element incorporated in TiAlN coating forms the superficial layer Al_2O_3 to improve the wear resistance and to enhance the chemical stability. In contrast to our findings, it is obvious, that delamination happened and is very common in all machining parameters we used for drilling which was within the range suggested by manufacturers. Applying a coolant could not help much in preventing this deterioration. According to a general consideration of conventional machining, with a hardness of TiAlN coating up to 3450 HV [115] which is much higher than the machined material (hardness of Ti-6246 is 318 HV for as received and 311 HV as HT1, while 289 HV for as HT2) together with some advantages of its wear resistance, the tool should perform well. The fast tool delamination phenomena may be caused by the high affinity of Ti-6246 towards other materials, including TiAlN.

5.6 Conclusion

Following the above discussion, we come to some conclusions. First, a built-up edge is an unavoidable effect of tool deterioration in the drilling of Ti-6246. The cycle of BUE formation through a forming and peeling off mechanism may lead to delamination of TiAlN coating from the carbide substrate tool. Effectively, tool chipping has caused the BUE peeling off mechanism. Last, the best performance of the TiAlN PVD coated WC-Co carbide drill was achieved in drilling the Ti-6246 block in the AR condition when using these parameters: with coolant, 30 mm depth maximum, a cutting speed of 50 m/min and a feed rate of 0.15 mm/min.

CHAPTER 6. ANALYSIS OF FORCES AND SURFACE INTEGRITY

6.1 Force Analysis

The cutting force is a measure of machinability. Usually, a lower cutting force is preferable. The cutting force can stimulate a vibration of the spindle axis, resulting in a poor quality of the drilled surface. It may also cause premature failure of drilling and reduce tool life. High torque, as an indication of increasing friction between the drill and the workpiece, can create a huge instance of heat, causing a higher temperature at the tool-workpiece interface [20]. It is interesting to study the forces in drilling as they directly affected the surface quality [116].

In drilling, two different motions are required: the cutting speed and the feed rate. Cutting speed makes the tool cut the workpiece only once in a full rotation and the feed rate gives continuity in the cutting. Torque is the force that makes the drill able to rotate along the vertical axis; it relates to the cutting speed. Therefore, the thrust force is the force that makes the drill move along the vertical axis (Z-axis) and also relates to the feed rate.

Some previous researchers have observed a relationship between forces that work during machining titanium alloys and the machining parameters. The cutting force (Fc) and feed force (Fk) have been discussed in the machining of three types of titanium alloys: Ti-6Al-4V, Ti-54M and Ti-10.2.3 with variations in the machining parameters. Khanna and Davim concluded that the feed rate was the most prominent parameter which influences the forces [117]. Laser assisted machining (LAM) has reduced the forces up to a maximum of 15% in comparison to conventional machining of Ti-6Cr-5Mo-5V-4Al [118]. There are also some published papers on drilling titanium which focuses on the cutting forces. The main forces that work drilling (thrust force and torque) were greatly affected by the type of coolant used [119], [120]. Thrust force declined as the cutting speed inclined, but lower torque values were attained at the higher cutting speed applied [121]. Other researchers concerns were on the effect of the drilling technique on forces, as reviewed in Sharif et al. [120]. To the extent of my knowledge there is no published paper discussing drillability of titanium alloy 6Al-2Sn-4Zr-6Mo, neither from the cutting forces nor from the drilled surface perspective.

6.1.1 Result of Experiments

In Figure 6.1, a photo is presented of the moment immediately after drilling, showing the drill and the block as well as the dynamometer. The recorded forces (Fx, Fy, Fz and Mz) were then plotted as a graph using a Microsoft Excel programme. The average of Fx and Fy were around a zero value, which may be because there was relatively no movement on the X and Y directions. Therefore, both forces were abandoned upon further analysis and only Fz (thrust force) and Mz (torque around the vertical axis) were considered. For analysis in Minitab 17, the forces were the average of the steady state, as illustrated in Figure 6.2. The steady state indicated that the tool was fully engaged in the drilling process. This result concurs with the previous work done by Neto [122].

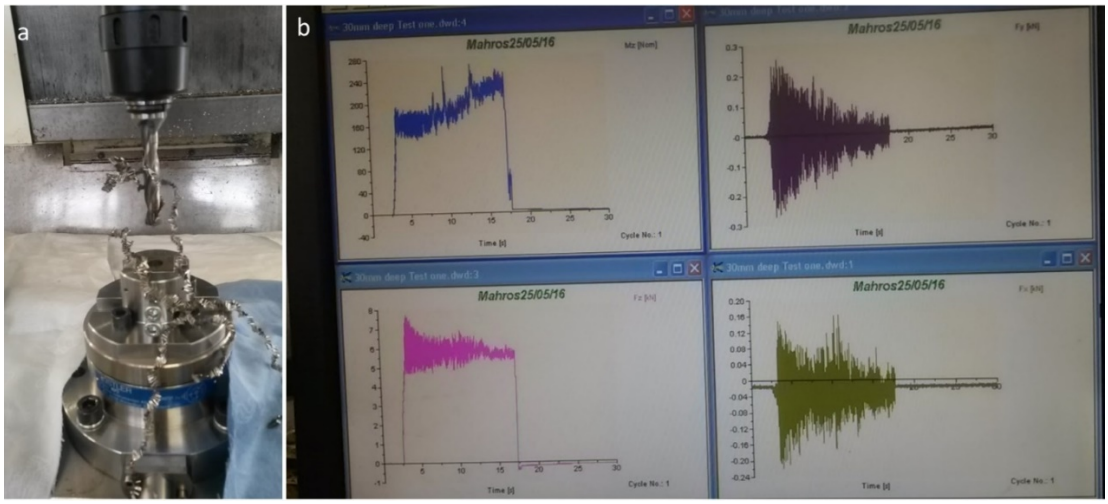

Figure 6.1. Images showing (a) a moment after a complete drilling, (b) appearance of forces measurement in a PC monitor in the CCW direction from the upper right: Fy, Fx, Fz, and Mz.

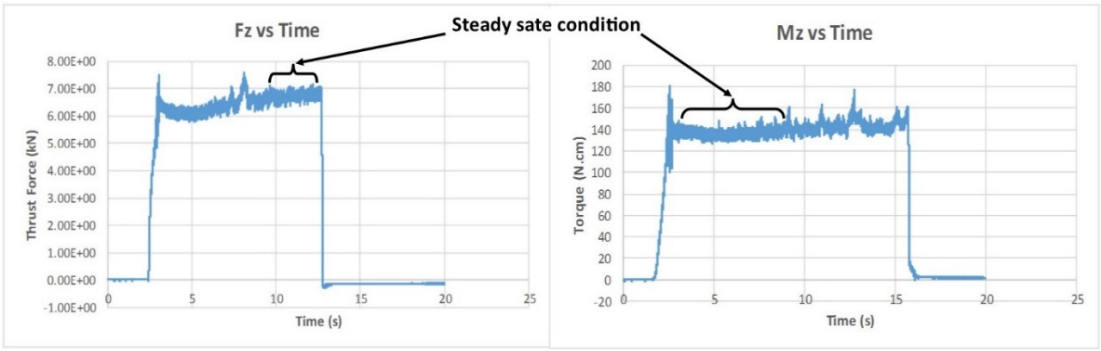

Figure 6.2. Illustration of how the average thrust force and torque were calculated from the steady state condition.

Some graphs of thrust forces and torques are not grown 'smoothly', as shown in the Figure 6.3. In the torque of DE 15 for example, the graph is smoothly flat in the first five seconds of development then harshly developed for the rest of the drilling period. For graph DE 12, the torque has increased up to about double of the steady period. It has also fluctuated severely in comparison to the steady state. However, the value of torque for analysis in both cases were still taken from the steady state period by taking the average, for reasons that will be described in the following paragraph.

The magnitude of thrust force and torque in drilling are shown in the following formulas [123]:

$$Fz \approx 0.5 \times k_c \times \frac{d}{2} \times f_n \times sin\mathrm{K}_r \quad \text{.....(6.1)}$$

Where Fz is the thrust force, kc is the specific cutting force, f_n represents the feed per revolution (in case of indexable insert drill $f_n = f_r$, the feed rate), K_r denotes the positioning angle = half of a point angle.

$$Mz = \frac{P_c \times 30 \times 10^3}{\pi \times n} \quad \text{.....(6.2)}$$

Where Mz is torque, P_c is the net power requirement, and n is the spindle speed.

According to those formulas, the magnitude of thrust force and torque that work during drilling are influenced by the drilling parameters which are keep constant. Therefore, the value of Fz and Mz should be constant during one drilling. That is why the value of Fz and Mz should be taken from the average of the steady state. However, some graphs showed fluctuation patterns along with the time taken for drilling. The increase of forces represented in the graph may relate to tool deterioration and the chip expelling process. In a twist drill, the drill is a rotating end- or side-cutting tool with two cutting edges, and one or more straight or helical grooves for the passage of chips and the admission of coolant [124]. In experiment 12 (DE 12), coolant was used and the chips were changed from discontinuous at the early stage of drilling, to long-segmented in the middle, then became a zig zag type in the deeper location, as shown in Figure 6.4. Because the drilling was with a coolant, the change was probably related to effectiveness of the coolant. When it was at the early stage the coolant caused the chips to break easily due to a sudden change of temperature. When it was deeper it was difficult for the coolant to reach the just-formed chips, therefore they became longer and zig zag chips resulted. This may also lead to an increase of the torque.

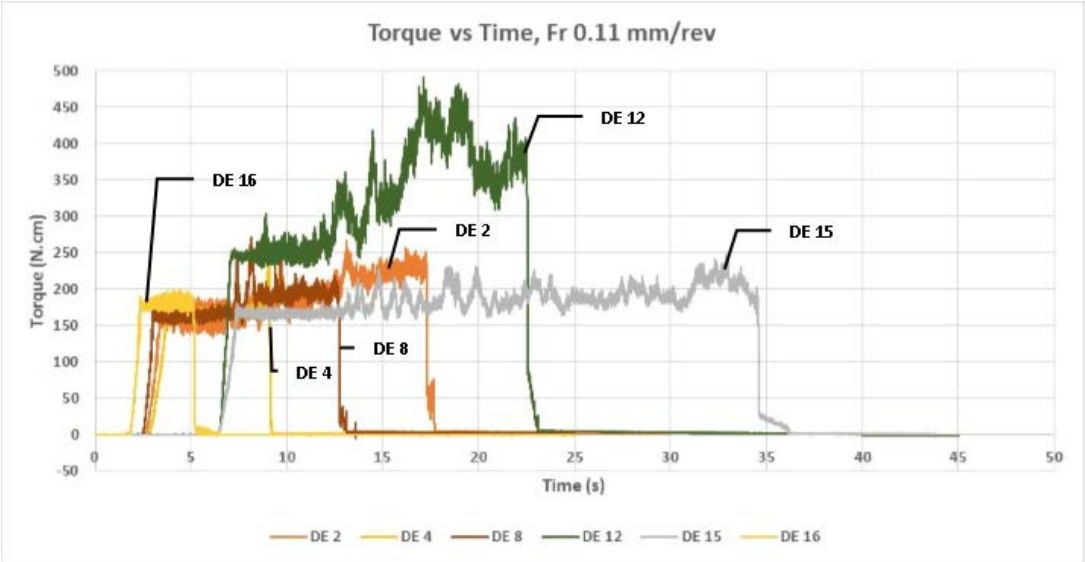

Figure 6.3. Graphs of torque which show some severely unsteady and high fluctuations.

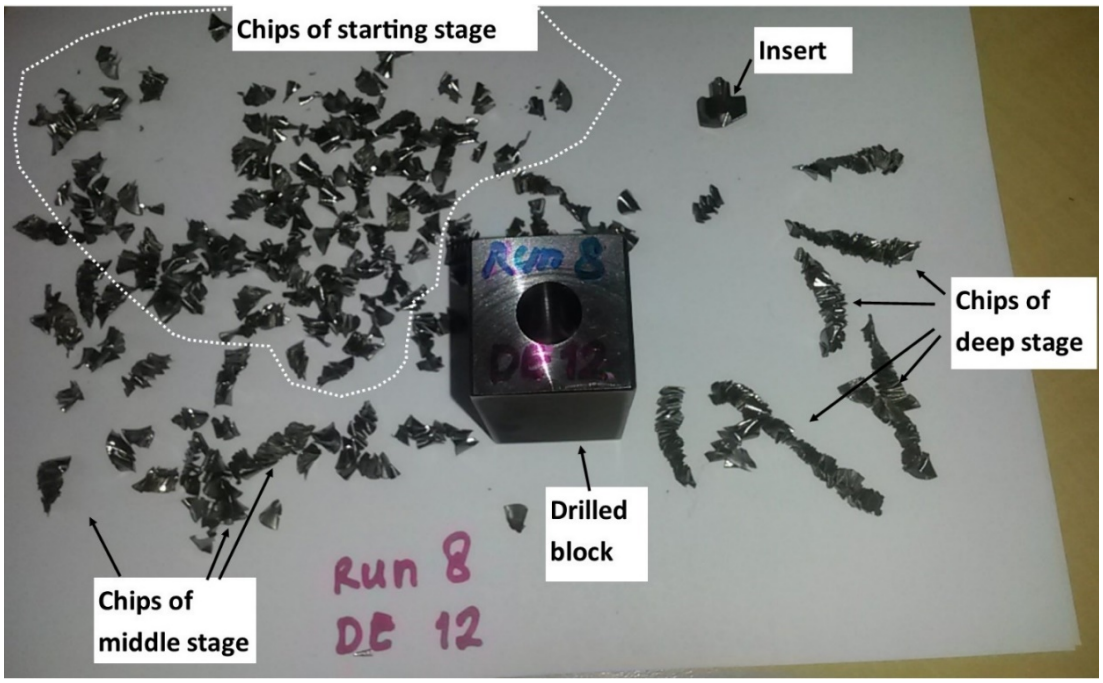

Figure 6.4. Photo of chips from experiment 12.

The completed average of thrust force (Fz) and torque (Mz) is presented in Table 6.1 along with the calculated signal to noise ratio (S/N ratio). The calculation of S/N ratio was based on minimisation because the smaller forces are preferable, as in the formula 2.2 in Chapter 2.2 [117].

Table 6.1. The Taguchi method L-18 design experiments, the forces and S/R ratio

Exp	Average of responses		S/N ratio (dB)	
	Fz (N)	Mz (N.cm)	Fz	Mz
1	2638	147	-68.43	-43.35
2	5762	165	-75.21	-44.33
3	3567	227	-71.05	-47.10
4	2679	171	-68.56	-44.66
5	6701	215	-76.52	-46.64
6	2234	135	-66.98	-42.63
7	2245	139	-67.02	-42.86
8	6761	164	-76.60	-44.31
9	2744	200	-68.77	-46.01
10	3895	235	-71.81	-47.42
11	5256	143	-74.41	-43.12
12	7231	171	-77.18	-44.67
13	3064	210	-69.73	-46.44
14	2260	137	-67.08	-42.72
15	2735	167	-68.74	-44.43
16	2761	180	-68.82	-45.11
17	2037	207	-66.18	-46.32
18	5225	128	-74.36	-42.12

6.1.2 Discussion

ANOVA analysis was used to detect which factors were affecting the forces. A significant level of $\alpha = 0.05$ (or confidence level 95%) was used the carry out the critical analysis. The ANOVA of thrust force and torque are presented in Table 6.2 and Table 6.3. A factor with P-values less than 0.05 means it was statistically significant at 95% confidence level and vice versa [117]. Consequently, the greater the F-value for a certain parameter, the higher the influence on the performance characteristic due to changes in that process parameter [117].

Each of the factors contributing to affecting the thrust force are in this order: 24% by the cutting speed, 21% by the depth of drilling, 13% by heat treatment and 11% by the feed rate. By contrast, the torque predominantly affected the feed rate by up to 94%. Other machining parameters therefore influence cumulatively about 6% toward the torque. The result is in accordance with what was found by Khanna in [125] that the feed rate contributed to 97.2% of the cutting force, and Prabukathi revealed that feed rate contributed to 82% of the torque in drilling Ti-6Al-4V [30]. Some previous researchers in drilling Al7075 using Response Surface Methodology (RSM) found that

an increased cutting speed did not result in an increase of Fz and Mz (Kyratsis et al. in Davim [125]), while an increased feed rate and tool diameter would increase both forces in drilling. The difference in results may be due to the different materials used. Another research on drilling titanium using a RSM design experiment showed that the cutting force and feed rate were both significantly affecting the thrust force and torque [126].

It is also evident that the cutting fluid does not play a role in affecting both forces. It may be due to the method of applying a coolant in these experiments, i.e. external coolant supply was not effective. The coolant could not reach the tool-chip interface; therefore there was no difference in forces whether drilling with or without a coolant application. A compressive flood coolant application might help to reduce the forces during drilling, as claimed by Rahim et al. [119]. There was a difference up to 1000 N of thrust force between MQL synthetic ester and flood coolant with a torque difference up to 11 N.m.

Table 6.2. Data from ANOVA for thrust force

Source	DF	Adj SS	Adj MS	F-Value	P-Value	Contribution, %
Coolant	1	41762	41762	0.02	0.892	0
HT	2	6829219	3414609	1.62	0.257	13
h	2	11065125	5532562	2.62	0.133	21
Vc	2	13077118	6538559	3.10	0.101	24
fr	2	5823134	2911567	1.38	0.306	11
Error	8	16896812	2112102			31
Total	17	53733170				

Table 6.3. Data from ANOVA for torque

Source	DF	Adj SS	Adj MS	F-Value	P-Value	Contribution, %
Coolant	1	13.3	13.28	0.46	0.518	0
HT	2	446.8	223.38	7.69	0.014	2
h	2	315.5	157.75	5.43	0.032	2
Vc	2	249.4	124.69	4.29	0.054	1
fr	2	18164.6	9082.29	312.82	0	94
Error	8	232.3	29.03			1
Total	17	19421.7				

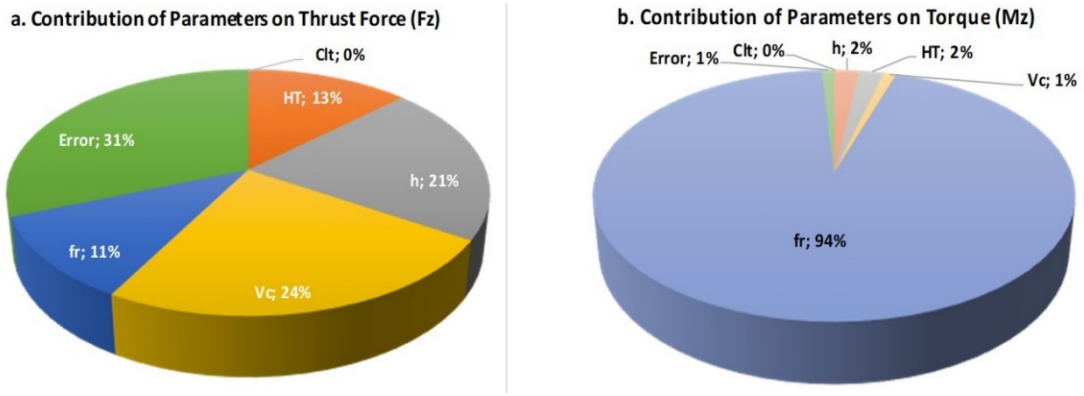

Figure 6.5. Pie chart showing contribution of each factor to thrust force (a) and torque (b).

An important note in interpreting the experimental analysis: if the percentage contributing to any error (either from unknown or uncontrolled factors) is low, then it is presumed that no essential parameters were neglected from the experiments. The threshold of being low is 15 %. By contrast, if the value is high (50% or more), then it may be because of (i) some important parameters were definitely neglected, or (ii) conditions were not precisely controlled, or (iii) there was an excessive error in measurement [127]. In the case of the ANOVA result of the thrust force, the error is 31%, which means some factors that may have influenced the thrust force were omitted from the experiments. However, an error less than 50% is still acceptable.

The S/N ratio presented in Table 6.1 shows that both thrust and torque were then plotted into a graph, as shown in Figure 6.6. The S/N ratio indicates how the controlled parameters (signal) affected the measured result in comparison to disturbance (noise or uncontrolled parameters). Therefore, a higher S/N ratio is preferable. From Figure 6.6 we can detect that the optimum thrust force would be achieved by choosing machining with a coolant and the material being HT1 would be treated at a drilling depth of 10 mm, a cutting speed of 27 m/min and a feed rate of 0.08 mm/rev. A minimum torque would therefore be achieved when drilling without coolant, the material as HT2, would be at a depth of drilling 45 mm, a cutting speed at 35 m/min and a feed rate of 0.08 mm/rev.

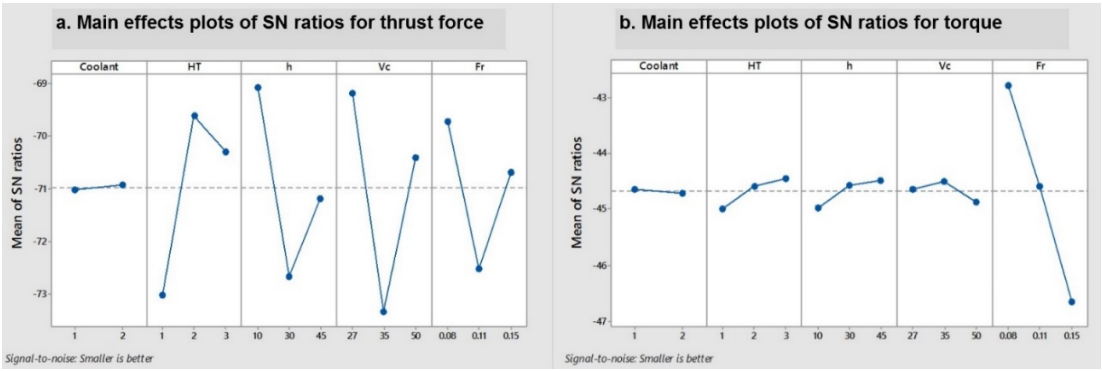

Figure 6.6. Graph showing means of forces and S/N effect for each control factor; (a) thrust force, (b) torque.

As mentioned previously that an application of coolant together with environmental considerations would not significantly affect the thrust and torque, therefore drilling without a coolant may be chosen. Furthermore, as the feed rate predominantly affects the torque we may abandon the inclusion of the low levels of three other factors and follow the ones which result in the minimum thrust force. Thus, the optimum thrust force and torque may be achieved by applying a Vc of 27 m/min, fr of 0.08 mm/rev on a depth of 10 mm on material at HT1 without a coolant.

6.2 Surface Analysis

The machined surface quality is one of the main interests in the manufacturing industries. A good surface roughness and roundness of the holes are among the qualities that should be aimed for after drilling. Surface roughness as it is frequently called, as only roughness is a part of surface texture. It measures the deviancies of the real surface to its ideally perfect model in a normal vector direction. Based on this measurement, if the deviancies are big, then the surface is rough; by contrast, a surface is called smooth if the deviancies are small. The roundness measurement determines how much a hole deviates from being an accurate circle. In other words, if there is a mathematically perfect circle, roundness is the measure of closeness of a measured shape to this perfect circle. Both specifications are important in judging the quality of drilled holes.

Some researchers have revealed the correlation between the quality of holes and the mechanical properties of their functions. Kahles et al. [128] emphasised that special attention should be given when machining titanium in order to evade loss of surface

integrity and dramatic loss of mechanical properties such as fatigue. Weiping et al. [129] studied the effect of the drilling process on fatigue life from open holes. They proved that cracks were initiated at the edge of counter holes. This crack, then, energised the fatigue crack nucleation. The crack life accounts for 80% of total fatigue from fastener holes. Castle [130] studied the drilling-induced fatigue damage in Ti-6Al-4V. The author concluded that the surface finish has an impact on fatigue life and has to be maintained below the specific threshold level.

In drilling hard-to-machine metals such as titanium alloys, it is not easy to achieve a reliable surface finish, especially with conventional drilling. The main reason is that the tool deteriorates very quickly. General advice from the industrial viewpoint of machining titanium alloy is to apply a low cutting speed and high feed rate together with abundant cutting fluids [131]. This advice may not be applicable to drilling for several reasons. First, in drilling, the cutting speed varies from zero at the chisel edge (centre) of the drill to a maximum at the heel (outer part of the drill bit). Second, applying a higher feed rate leads to increasing the torque significantly. Meanwhile, increasing both the cutting speed and the feed rate would accelerate the axial force [132]. Third, the coolant does not easily reach the interface of the tool-workpiece through the helical flutes because it collides with the chips from the opposite direction.

Kurt et al. [133] claimed that the feed rate was the most influential to the surface quality when drilling Al-2024 followed by the cutting speed and the depth of cut. Kilickap et al. [134] have tried to optimise drilling parameters (cutting speed, feed rate and cutting environment) to find the lowest surface roughness for AISI 1045 with a Response Surface Method (RSM) and Genetic algorithm (GA). They concluded that the best surface roughness was achieved under low cutting speed and feed rate together, also applying an MQL condition. Zhu et al. [135] therefore investigated the speed and feed rate to performance characteristics in drilling Ti-6Al-4V. They found that smaller roundness values of the holes were the result of higher cutting speeds.

6.2.1 Measurements of Roughness and Roundness

Some surface terms have been defined by ISO (EN ISO 4287) as mentioned in [136].

> "***The actual profile*** is the one resulting from the intersection of the workpiece surface and a plane normal to that surface and in a direction that maximises the surface roughness value, normally at right angles to the lay of the machining marks."

> "***The measured profile*** is the one resulting from scanning the actual profile with a probe which mechanically filters it due to the probe radius tip and, if fitted, by the skid of the probe system."

Surface imperfections, such as cracks, scratches and dents are not part of the profile and should not be included in the recording. If necessary, tolerances according to DIN EN ISO 8785 can be set for them.

> "***The arithmetical mean roughness value (Ra)*** is the arithmetical mean of the absolute values of the profile deviations (Z_i) from the mean line of the roughness profile."

Expression of arithmetic surface roughness is presented in Figure 6.7. The definition of Ra is formulated in the following equation:

$$Ra = \frac{1}{l}\int_0^l |Z_x| dx \quad \text{.....(6.3)}$$

According to equation 6.3, the recorded measurements were taken from their absolute values or measurement which does not differentiate between the peaks and the valleys. A discontinuity or defect can cause an extreme value. The effect of a single extreme value on the overall measurement value becomes extremely small, so a settled stable result can be obtained. Ra is a commonly-used parameter in representing the surface roughness.

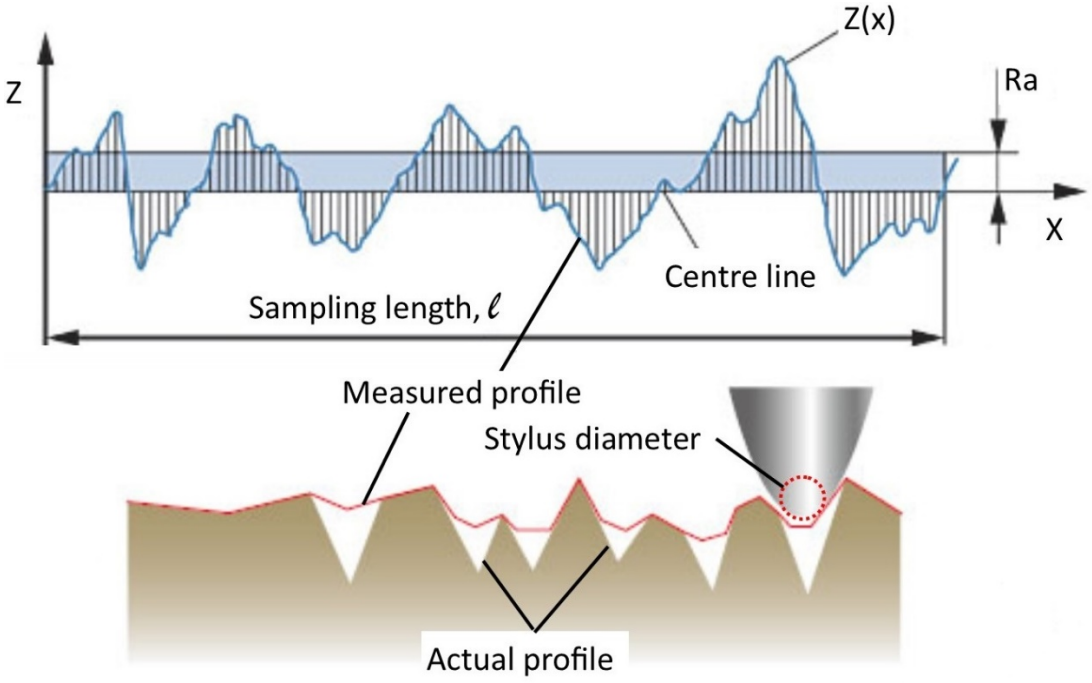

Figure 6.7. Arithmetical mean roughness value Ra and some terminology for roughness measurement.

The holes were measured for their surface roughness (shown at Figure 6.8-a) at the circumference side near the vicinity of the bottom, to ensure the surface quality. Measurements were taken at the four quadrants with three times the replication for each position. The arithmetical surface roughness (Ra) values were measured in order to characterise the surface quality with a surface roughness device with the stroke of probe 0.8 mm (cut off) and range 99.9 µm. The total average of surface roughness for one hole was used for inputting the analyses of Taguchi with Minitab 17 software. The Ra surface roughness equation for this experimental study can be written as:

$$Ra = \frac{1}{N}\sum_{i=1}^{N}\left|x_i\right| \quad \text{.....(6.4)}$$

where x_i is the measured surface value and N is the number of measurement = 12.

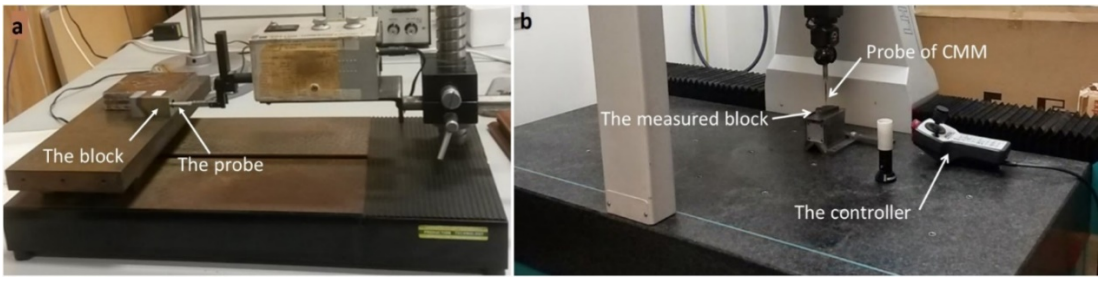

Figure 6.8. Photographs showing measurement of the block: (a) surface roughness, (b) roundness.

The roundness was measured with a CMM machine (as shown Figure 6.8-b). This is the least square error of the fitted circle to the entire set of points. The least square circle (LSC) can be defined as a reference circle that functions as a balanced separation between the sum of the total areas of the inside and outside. The error of roundness can then be projected as the disparity between the highest and lowest distance from this reference circle. Roundness (Rd) is expressed in the mathematical equation 6.5 as follows:

$$Rd = \frac{1}{N}\sum_{i=1}^{N}R_i \quad \text{.....(6.5)}$$

Here, N represents the number of the measurement. In this experiment N = 3 in regards to three positions of measurement: at the top, in the middle and at the bottom of the hole circumference; and R_i is the value of roundness.

6.2.2 Analysis of S/N Ratio

The roughness and roundness of the drilled holes are presented in Table 6.4. The least roughness resulted from experiment 1, whereas the maximum roughness was found in experiment 17. The maximum roughness is in accordance with the maximum tool deterioration [132]. The results of the optical microscopy of both experiments (1 and 17) are shown in Figure 6.9. It is evident that the surface of experiment 17 is rougher than that of experiment 1. The white lines (scratches) in Figures 6.9-c & d represent the contour surface profile. It is also obvious that there are two patterns of valleys. The right one is of the tool when it rotates forward and another one (left) is of the retreated tool which is usually faster. Therefore, the patterns are more sloping.

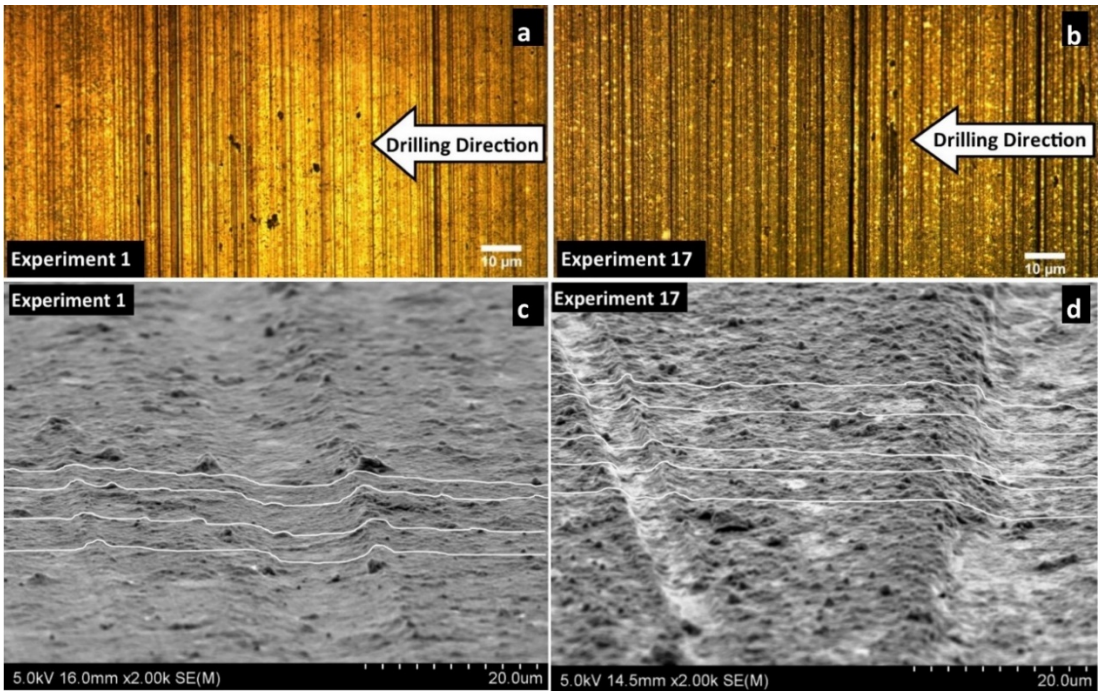

Figure 6.9. Optical micrographs of drilled surface roughness with magnification of 100X from experiments 1 & 17 (a and b) and SEM images at 2000X magnification (c and d) showing the surface roughness and the pattern of surface.

A sample of roundness measurements are presented in Figure 6.10, from experiment 16 at the top hole position, with a roundness value of 0.0196. This calculation is a result of deducing both the maximum and minimum measurements. This value was then averaged with another two, resulting in roundness measurements in the middle and at the bottom of the holes. The diameter was 10.0213 mm, a bit bigger than it should be, but it should still be acceptable or within the tolerance.

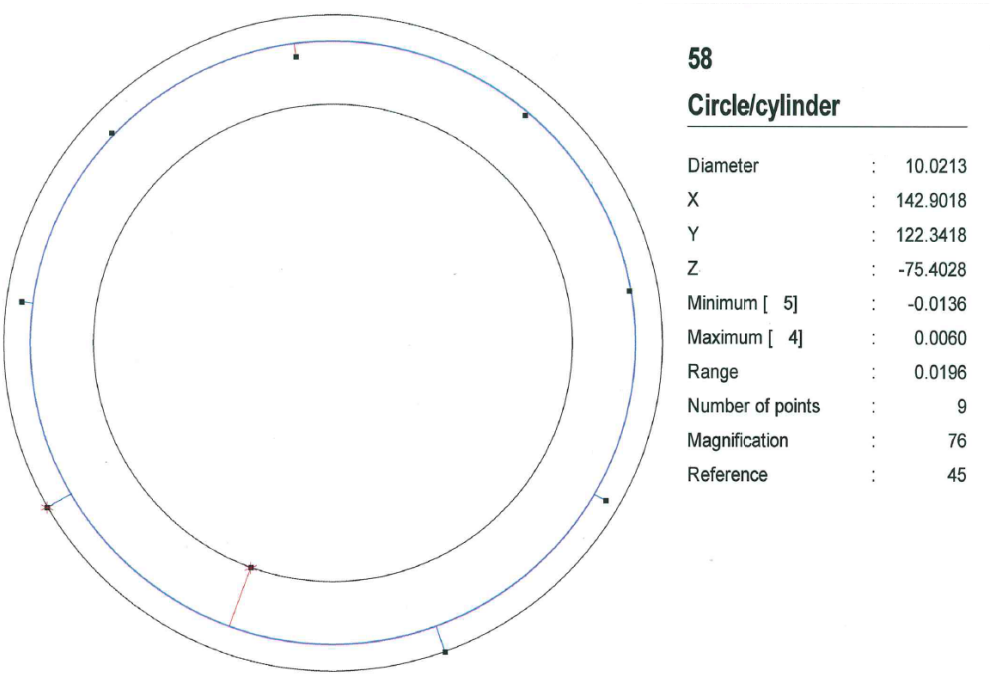

Figure 6.10. Sample measurement result using CMM on experiment 16 at the top of the hole, with a result of maximum roundness of 0.0196.

The S/N of both measured parameters was calculated using Minitab 17 and the result is presented in the last two columns of Table 6.4. The average value of Ra and Rd were calculated as 1.17 µm and 0.013 respectively. In the same way, the average of S/N ratio values for Ra and Rd were found to be -0.95686 dB and 37.8331 dB.

For the signal value, representing the actual value of the optimum levels of the control factors, the highest S/N ratio was used. Depending on the combination control factors, the S/N ratio was calculated to be 4.84871 dB for the lowest Ra value of 0.6 µm. Similarly, the S/N ratio was calculated to be 44.7815 dB for the roundness of 0.006 (Table 6.4).

The level values of the control factors for Ra and Rd according to the Taguchi method, are presented in Table 6.5-a & b. It is obvious that among the five input parameters used, that they affect the roughness in the following order as: depth of drilling (h), heat treatment (HT), cutting speed (Vc), feed rate (Fr) and coolant (Clt). This result was slightly different to that affecting the roundness; in order those parameters are – h, Vc, HT, Clt and Fr. The optimum drilling condition for the lowest Ra was determined as $Clt_{off}HT_{AR}h_{10}Vc_{35}Fr_{0.08}$, whereas for the lowest Rd values they were

$Clt_{on}HT_{AR}h_{10}Vc_{27}Fr_{0.08}$. A visualisation of the optimal drilling conditions are also clearly seen in Figure 6.11.

Table 6.4. Drilling parameters and their levels on Taguchi Design L18

Exp.	Observed values		S/N Ratio (dB)	
	Ra (μm)	Rd	Ra	Rd
1	**0.57**	0.006	**4.84871**	44.2461
2	0.86	0.023	1.30057	32.7654
3	1.28	0.016	-2.15927	23.1478
4	0.80	0.009	1.89008	41.0122
5	1.21	0.022	-1.65078	33.1253
6	1.14	0.020	-1.12539	34.0960
7	0.85	0.010	1.45145	40.2646
8	1.56	0.014	-3.87930	37.0981
9	1.79	0.009	-5.07322	40.8830
10	0.77	0.006	2.25141	**44.7815**
11	1.31	0.009	-2.31221	40.9474
12	1.13	0.008	-1.08289	42.0475
13	0.81	0.009	1.81839	41.1433
14	1.19	0.014	-1.48600	36.9542
15	1.52	0.014	-3.64322	36.9135
16	0.93	0.015	0.59926	36.3441
17	**1.95**	0.011	-5.81059	38.8619
18	1.44	0.015	-3.16055	36.3631
Tot.	21.12	0.230	-17.22354	680.9951
Ave.	1.17	0.013	-0.95686	37.8331

Table 6.5-a. The Mean Response for Roughness (Ra)

The controlled parameters	Surface Roughness (Ra)				
	Level 1	Level 2	Level 3	Delta	Rank
Clt	1.1189[a]	1.2281		0.1092	5
HT	0.9875[a]	1.1118	1.4212	0.4337	2
h	0.7898[a]	1.3462	1.3844	0.5946	1
Vc	1.3247	1.0499[a]	1.1459	0.2749	3
fr	1.0812[a]	1.1359	1.3033	0.2221	4

[a] Optimum level, Delta = difference between maximum and minimum

Table 6.5-b. The Mean Response for Roundness (Rd)

The controlled parameters	Roundness (Rd)				
	Level 1	Level 2	Level 3	Delta	Rank
Clt	0.014233	0.011300[a]		0.002933	4
HT	0.011222[a]	0.014656	0.012422	0.003433	3
h	0.009083[a]	0.015600	0.013617	0.006517	1
Vc	0.009783[a]	0.014439	0.014078	0.004656	2
fr	0.012322[a]	0.013878	0.012100	0.001778	5

[a] Optimum level, Delta = difference between maximum and minimum

To find out which process parameters are statistically important, an Analysis of variance (ANOVA) was executed. The ANOVA of the raw data (Ra and Rd) is exhibited in Table 6.6 and 6.7 respectively.

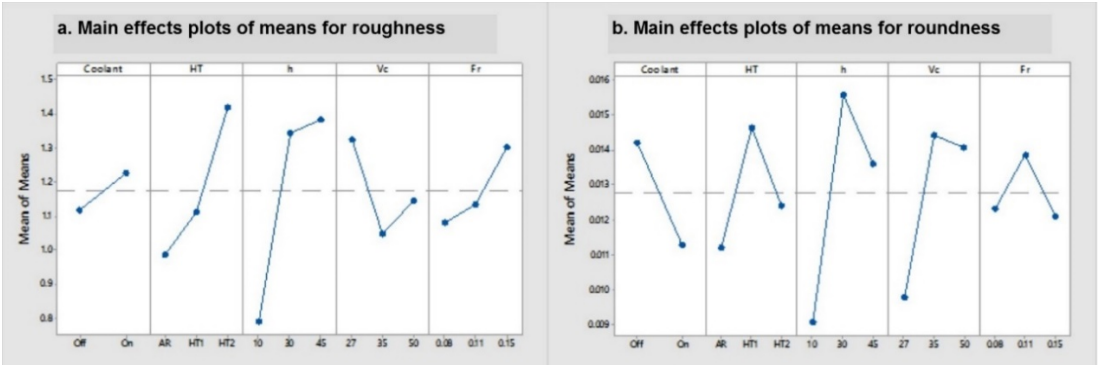

Figure 6.11. Graphs showing quality of the drilled holes as average of (a) surface roughness, and (b) roundness.

The effect of input parameters is considerably significant if its P-value is less than 0.05 (P-value < 0.05) [117]. Therefore, it is evident that all the input factors are statistically significant to the roughness (Table 6.6). On the contrary, as their P-value to the roundness is more than 0.05 the effect of all the factors on roundness are statistically insignificant (Table 6.7).

Table 6.6. Analysis of Variance ANOVA for Means of Ra

Source	DF	Seq SS	Adj SS	Adj MS	F	P	Contribution (%)
Clt	1	0.05366	0.05366	0.053657	9.62	0.015	2.22
HT	2	0.59846	0.59846	0.299229	53.63	0.000	24.73
h	2	1.32918	1.32918	0.664591	119.12	0.000	54.92
Vc	2	0.23352	0.23352	0.116759	20.93	0.001	9.65
fr	2	0.16070	0.16070	0.080349	14.40	0.002	6.64
Residual Error	8	0.04463	0.04463	0.005579			1.84
Total	17	2.42015					100
R-Sq = 98.2%							

Table 6.7. Analysis of Variance ANOVA for Means of Rd

Source	DF	Seq SS	Adj SS	Adj MS	F	P	Contribution (%)
Clt	1	0.000039	0.000039	0.000039	2.04	0.191	8.61
HT	2	0.000036	0.000036	0.000018	0.96	0.423	7.95
h	2	0.000134	0.000134	0.000067	3.53	0.080	29.58
Vc	2	0.000080	0.000080	0.000040	2.12	0.182	17.66
fr	2	0.000011	0.000011	0.000006	0.30	0.751	2.43
Residual Error	8	0.000152	0.000152	0.000019			33.55
Total	17	0.000453					100
R-Sq = 66.5%							

Accordingly, it is obvious that the most influential parameter of the control factor on the Ra is the depth of drilling, with the contribution of 55% (Table 6.6 and Figure 6.11-a). This can be attributed to a loss of surface integrity by the deeper drilling, which coarsened the drilled holes. Consequently, when measuring the surface roughness of the drilled holes, we should consider measuring at a different depth then calculate the average as it will potentially result in different values between the top and the bottom of the holes.

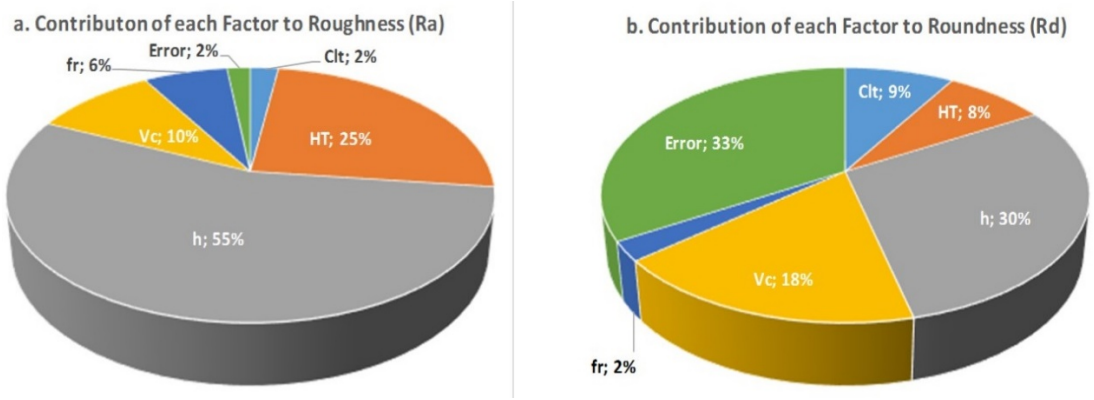

Figure 6.12. Pie charts showing the contribution of input parameters to (a) the roughness and (b) the roundness.

Heat treatment influenced 25% to the surface roughness (Figure 6.12-a). It may be related to the different hardness of the material which resulted from the different heat treatments. The HT2-ed material is softer than the AR and HT1-ed ones. It is obvious that the HT2-ed material resulted in a rougher surface, as shown in Figure 6.11., Therefore, the harder the material, then the smoother the surface roughness after drilling. It may be because the softer material is easier for the tool to cut. In drilling other materials which were softer than titanium alloys, usually a rougher surface was

achieved. Kabakli et al.[137] achieved a roughness of between 0.8 µm to 2.62 µm on drilling low alloyed medium carbon steel with a hardness of 207HB. Meanwhile Amran et al. [138] achieved a roughness of 1.06 µm and 2.59 µm upon drilling an aluminium alloy with a HSS twist drill.

By contrast, using a coolant only contributes 2% to the roughness of the drilled holes. It may be due to the nature of the method of supplying the coolant. In drilling with an external coolant supplied, it can only get in to the interface of the tool-material via helical flutes. These flutes are also the way for chips to get out from the drilling area in the opposite direction from the coolant. Therefore, the effectiveness of applying an external coolant is very low.

The result is paramount when other researchers [18], [121], [137], [139], [140], [141] only consider the cutting speed and feed rate as the main parameters to improve the drilled surface roughness of titanium alloys. The recently published papers [142], [143] have also not taken the depth of drilling into account in optimising hole quality in drilling Ti-6Al-4V. In fact, an accumulation of both parameters (cutting speed and feed rate) only contributed 16% to the roughness.

The ANOVA for roundness shows that a P value of all the factors are more than 0.05, which means the selected parameters influenced the roundness at the level of confidence of less than 95%. Or more simply, the roundness was not significantly influenced by the designated factors used in these experiments. The residual error contributes 34% to the roundness. It means that other factors, which were not chosen in these experiments, had more influence than those five factors. The depth of drilling influenced 30% of the roundness. However, the P value is 0.08 (or higher than 0.05), where the depth of the drilling influences the roundness of the hole at the confidence level of less than 95%. Moreover, as already mentioned earlier, that the maximum error for ANOVA is 50% – though it is preferable to be less than 30%, we may use this analysis result. The results are in accordance with what was found by Sultan et al. [144], that there was no substantial difference in roundness by varying the cutting speed and the feed rate. Abdelhafeez et al. [91] found that although there were some irregularities of roundness when drilling titanium and aluminium alloys, that cutting speed and feed rates (as individual factors or their interactions) did not have a statistically significant effect on hole diameter regularity.

6.2.3 Estimation of Minimum Surface Roughness

Prediction of the minimum surface roughness (Ra) was based on selection of levels of significant parameters. The optimum levels along with the significant parameters were already selected as Clt_{off}, HT_{AR}, h_{10}, Vc_{35}, $fr_{0.08}$ for roughness. In this study the interactions between factors was not a concern. The estimated mean of response characteristics and Ra can be computed by equation 6.6 [79], [117], [145]:

$$\mu_{Ra} = Clt_{off} + HT_{AR} + h_{10} + Vc_{35} + fr_{0.08} - 4T_{Ra} \quad \text{.....(6.6)}$$

where T_{Ra} is an overall mean of surface roughness = 1.17 (Table 6.4), while Clt_{off}, HT_{AR}, h_{10}, Vc_{35}, and $fr_{0.08}$ are the average roughness values with parameters at minimum levels. From Table 6.5 it is revealed that Clt_{off} = 1.189, HT_{AR} = 0.9875, h_{10} = 0.7898, Vc_{35} = 1.0499, and $fr_{0.08}$ = 1.0812. Therefore, μ_{Ra} = 1.189 + 0.9875 + 0.7898 + 1.0499 + 1.0812 - 4(1.17) = 0.4174.

A confidence interval (CI) is a prediction of mean on the confirmation runs. It can be calculated using the following formula:

$$CI = \sqrt{F_{\alpha}(1, f_e).V_{e.}\left[\frac{1}{N_{eff}} + \frac{1}{R}\right]} \quad \text{.....(6.7)}$$

Here, $F_{\alpha}(1, f_e)$ is the F ratio required for α, and α is the risk for the opposite meaning of the confidence level, f_e represents error DOF, V_e denotes error variance, and N_{eff} symbolises an effective number of replications. Table 6.6 revealed that V_e = 0.005579, f_e = 8, and $F_{0.05}(1, 8)$ = 5.3177 (from Table F in Appendix B). Therefore, an effective number of replication (N_{eff}) is formulated as:

$$N_{eff} = \frac{N}{1 + [T_{dof}]} \quad \text{.....(6.8)}$$

R represents the number of repetitions for confirming the experiment and N stand for the total number of measurements = 4 quadrants X 3 repetition X 18 (experiments) = 216 times. Consequently, T_{dof} denotes the total degree of freedom correlated with the mean minimum = 9. Thus, N_{eff} = 21.6.

Therefore,

$$CI = \sqrt{(5.3177)(0.005579)\left[\frac{1}{21.6}+\frac{1}{3}\right]} = \pm 0.1061$$

Thus, an interval predicted the surface roughness with a confidence level of 95% to be 0.4174 ± 0.1061 µm. It means the confirmation result should be between 0.3113 µm < µRa < 0.5235 µm.

The roughness resulted from this investigation was comparable with the results of some previous research. It was between 0.7 µm to 1.8 µm for titanium alloy materials with different drilling parameters [143], [146]. All the results of the experiments were also within the general standard of surface roughness of the drilled surface for common applications, i.e. between 1.6 µm (min) to 6.3 µm (max) [147].

6.3 Surface Damage and Integrity of Drilled Surfaces

Hardness tests were carried out using a micro Vickers machine with a load of 100 grams and a dwelling time of 10 s. The first indentation was carried out at the top-left corner of the block about 10 microns from the top and the edge of the drilled side. The first array was five dots to the right side of the first indentation at about the same distance of 60 microns each. The three down the vertical array were made at a distance of 70 microns. The measurements were made about every 5 mm down to the bottom. Therefore, there were 3, 7, and 10 sets of measurements for the depth of drilling of 10, 30 and 45 mm respectively. The position of indentations is illustrated in Figure 6.13. The mirror polishing was carried out prior to the hardness tests.

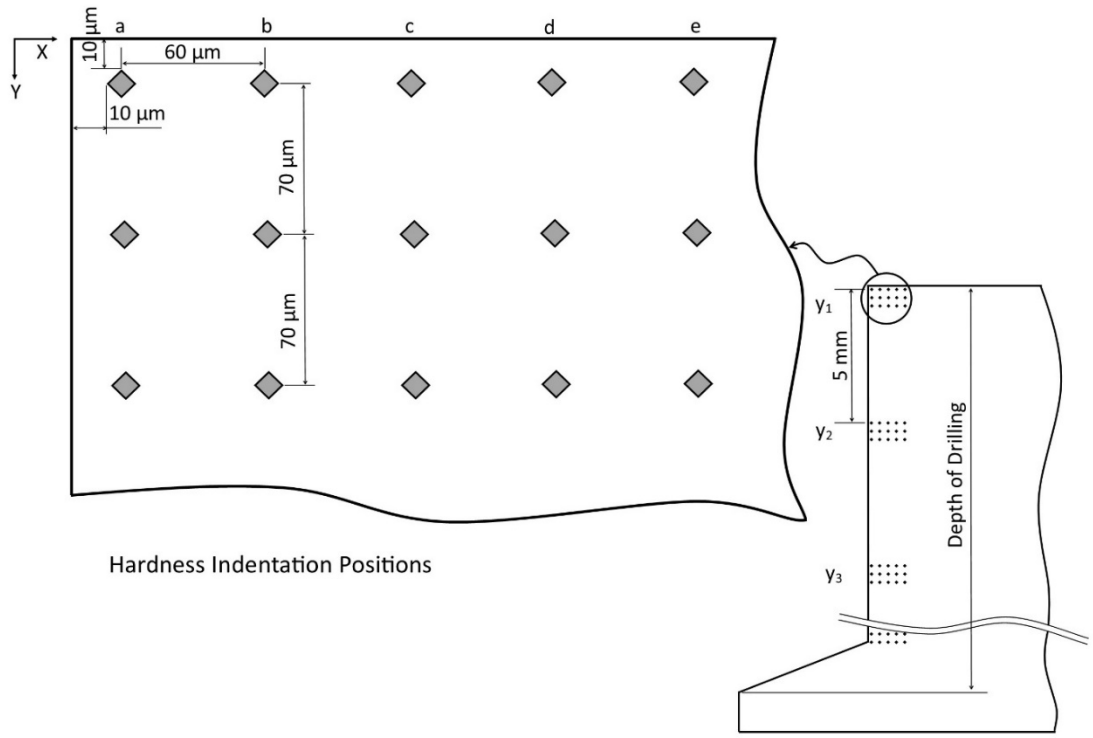

Figure 6.13. Hardness indentation positions

The distribution of hardness for the three different treatments is presented in Figures 6.14-6.16. The hardness is invariably with the distance both from the top surface and from the drilled holes in the case of blocks from the as received (AR) material. As for HT 1 and HT 2, it is obvious that at the top position, the hardness is greater than in the rest of any other positions. Therefore, the increase of hardness is because of the impact of the heat treatment, not because of the drilling. The nonexistence of noticeable micro-hardness changes after the drilling of Ti-6246 indicates the nonexistence of plastic deformation in the microstructure below the drilled surfaces. It is in accordance to the finding of Da Silva et al. [148] that there is no confirmation of surface hardening of the machined surface following the turning of Ti-6Al-4V with PCD tools. This fact is in contrast with the results of Cantero et al. [26], that there is an increase in hardness as an effect of drilling Ti-6Al-4V until the distance of 300 microns from the drilled surface. Rahim & Sharif [27] also detect the hardness changes under the drilled surface of up to 0.5 mm (500 microns).

a

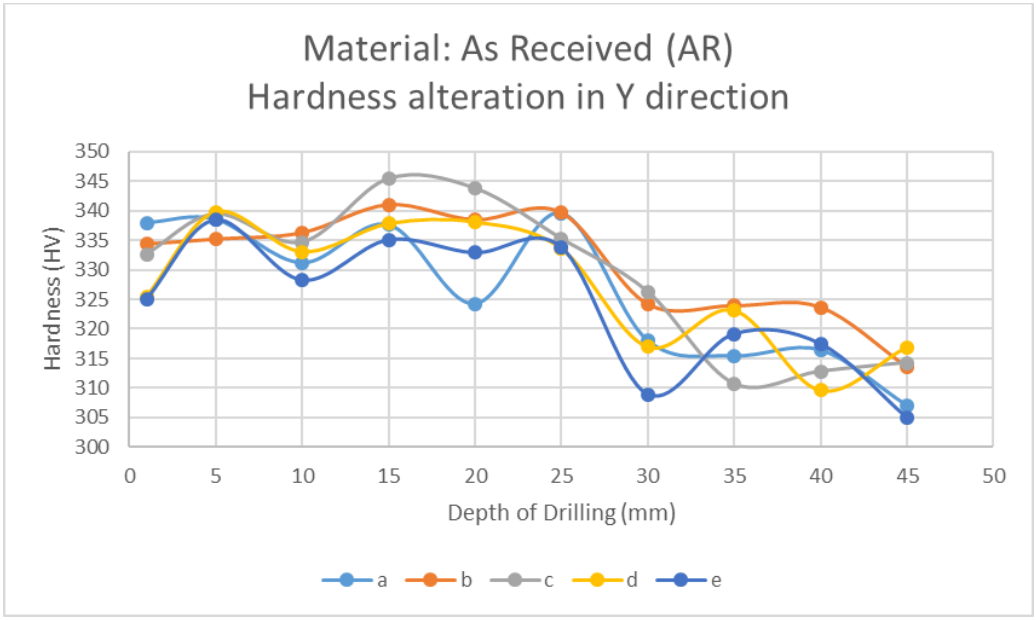

b

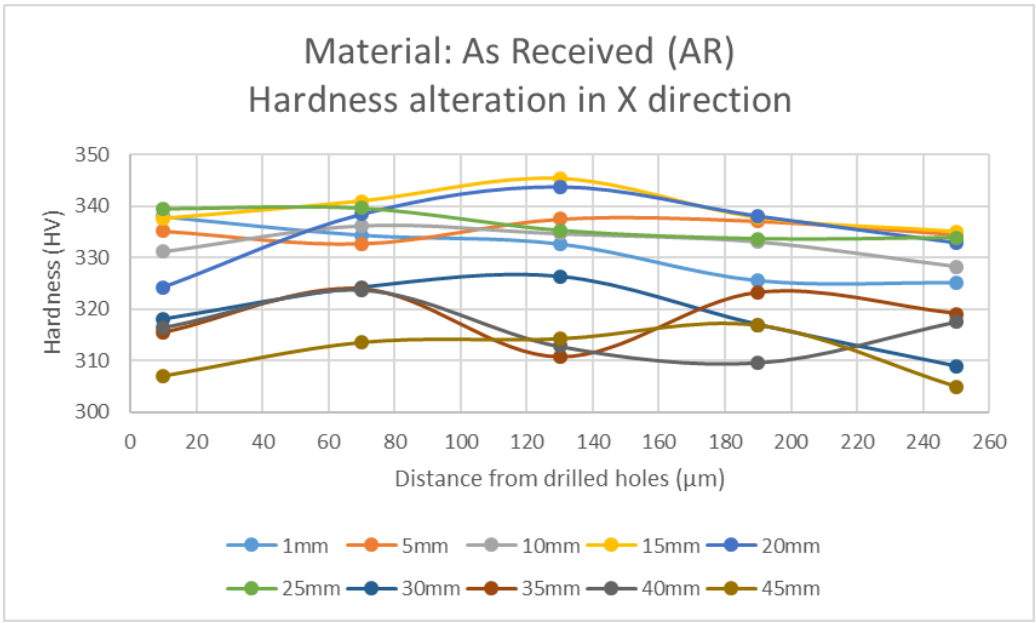

Figure 6.14. Hardness distribution at different positions in X direction (a) and in Y direction (b) for the material As Received (AR).

a

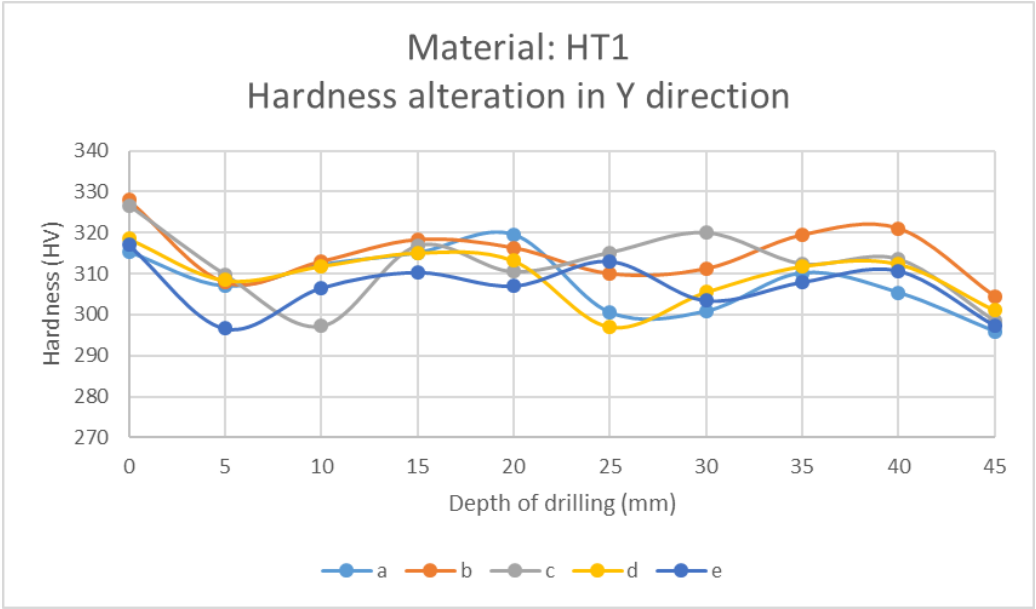

b

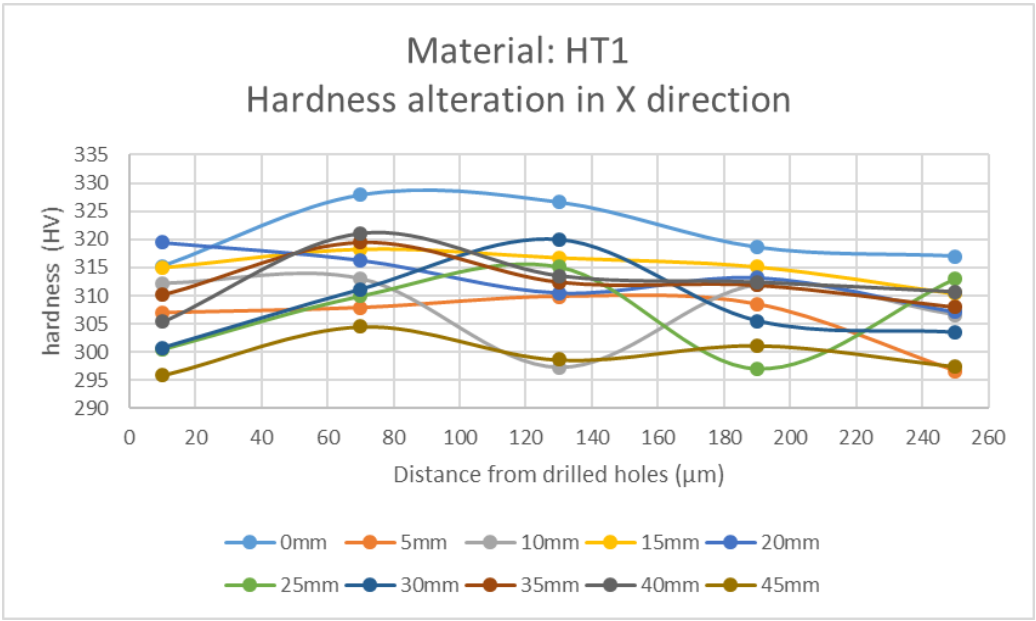

Figure 6.15. Hardness distribution at different positions in X direction (a) and in Y direction (b) for the material as HT1.

a

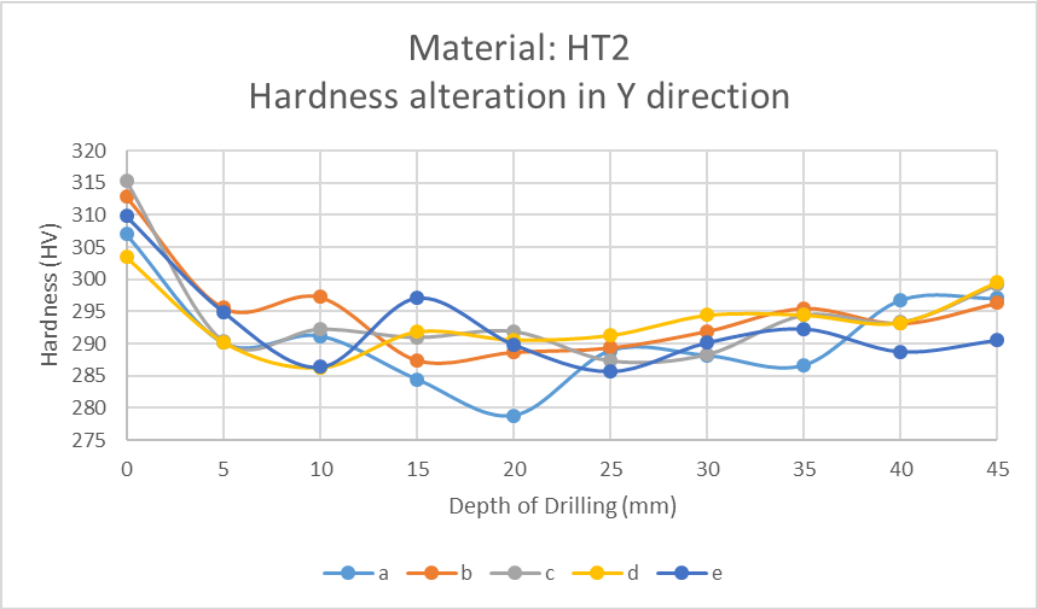

b

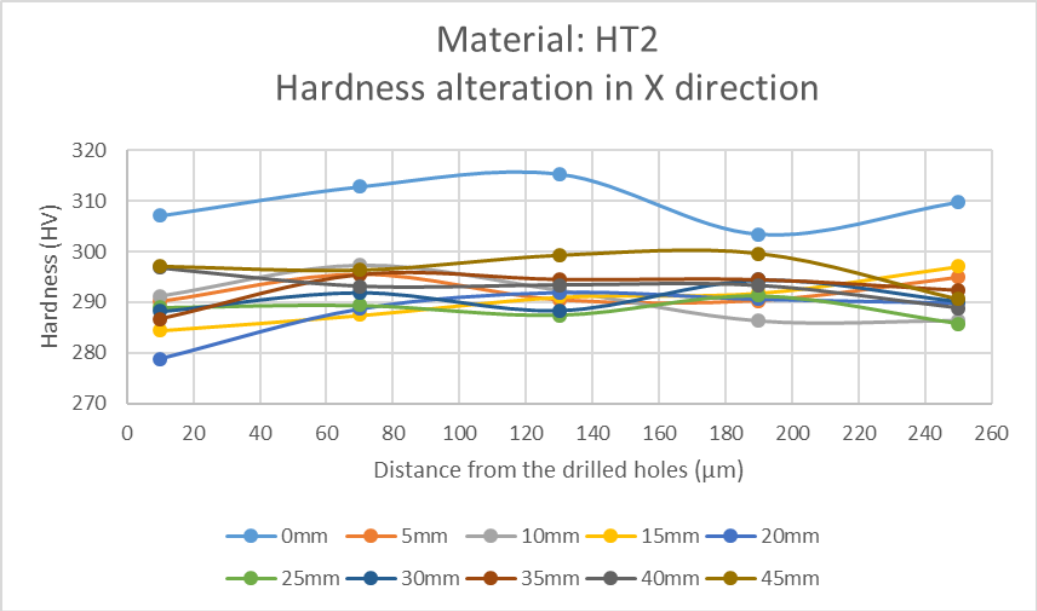

Figure 6.16. Hardness distribution at different positions in the X direction (a) and in the Y direction (b) for the material as HT2.

In regards the microstructure of the blocks after drilling, this is discussed together with the subject of changes in hardness in these coming paragraphs. Figure 6.17 shows the microstructure of the blocks as received (AR) after drilling at the different positions. Microstructure changes due to drilling were not observed in the AR material. As can be seen in Figures 6.17-6.19, either the AR or the heat treated ones, the microstructure of the drilled blocks was relatively stable from the left (drilled side) to the right. The hardness also did not change consistently.

The alpha prime phase (the transformed beta) was stimulated by rapid cooling. Therefore, the lattice parameter of alpha prime may be different from a 'normal' alpha, which is a transformation from beta to alpha under diffusion control, if the alloying elements are present. Alpha prime might then be supersaturated with beta stabilising elements. In general the hardness of the water quenched samples (HT2) are harder than the as received ones, as well as slow cooling ones [10]. It may be why the hardness of HT2 at the top side is greater than the AR as well as the HT1-ed.

The microstructure of the blocks adjacent to the drilled surfaces from HT1 and HT2 also did not clearly change after drilling. It may be because during drilling the highest temperature is much lower than the beta transus temperature. In our preliminary experiments, with Vc of 60 m/min, fr of 0.05 mm/rev without a coolant, the maximum temperature detected at the vicinity of the drilled wall is 270^{o}C, as shown in Figure 6.20. This temperature is considered to be too low for the Ms temperature (662^{o}C see section 3.1.2). Though the size of the grains at the vicinity of the wall at HT2 were smaller, we cannot see this effect on the hardness.

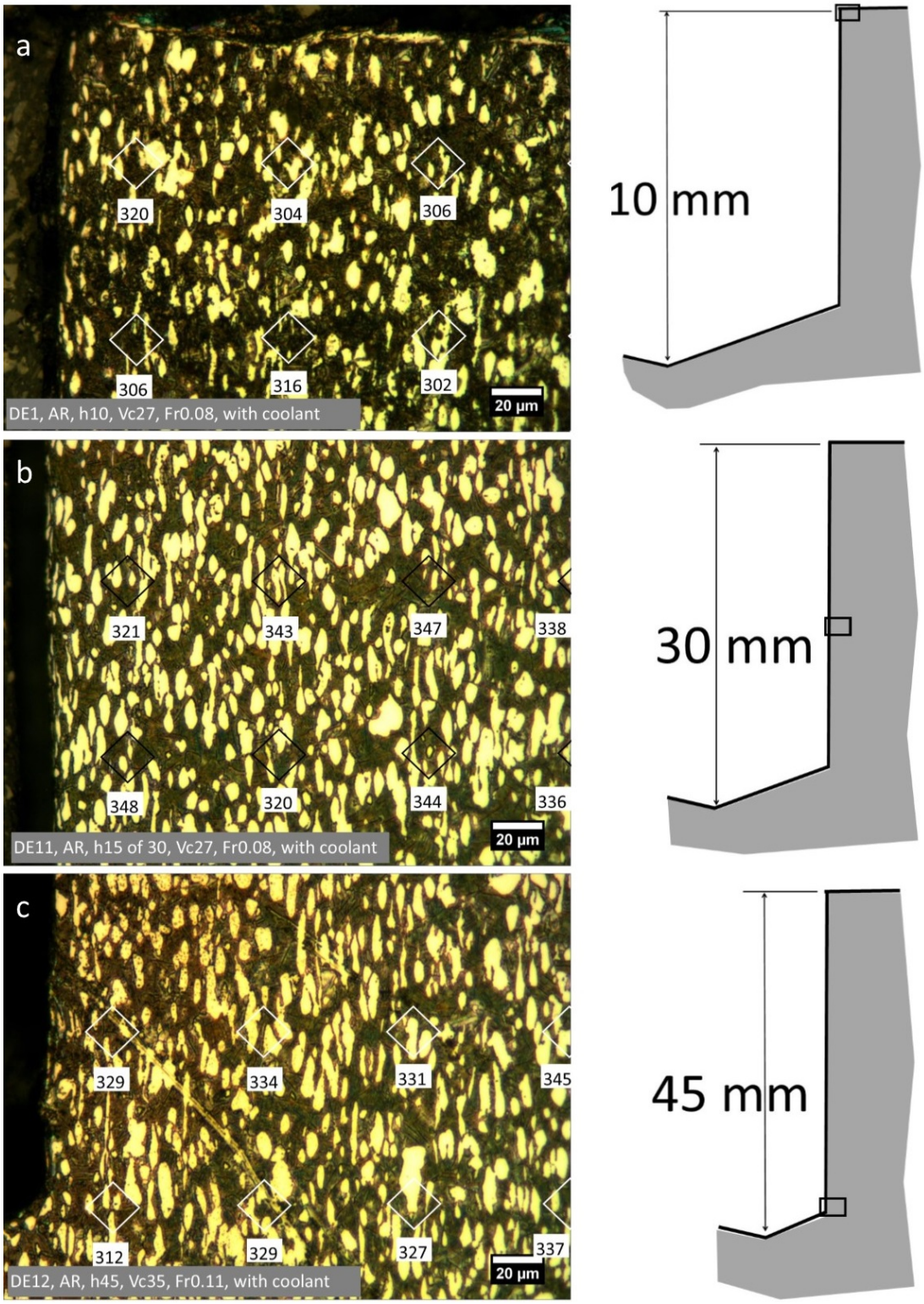

Figure 6.17. Microstructure of the blocks as received at different depths of drilling. Hardness values at various positions are also shown.

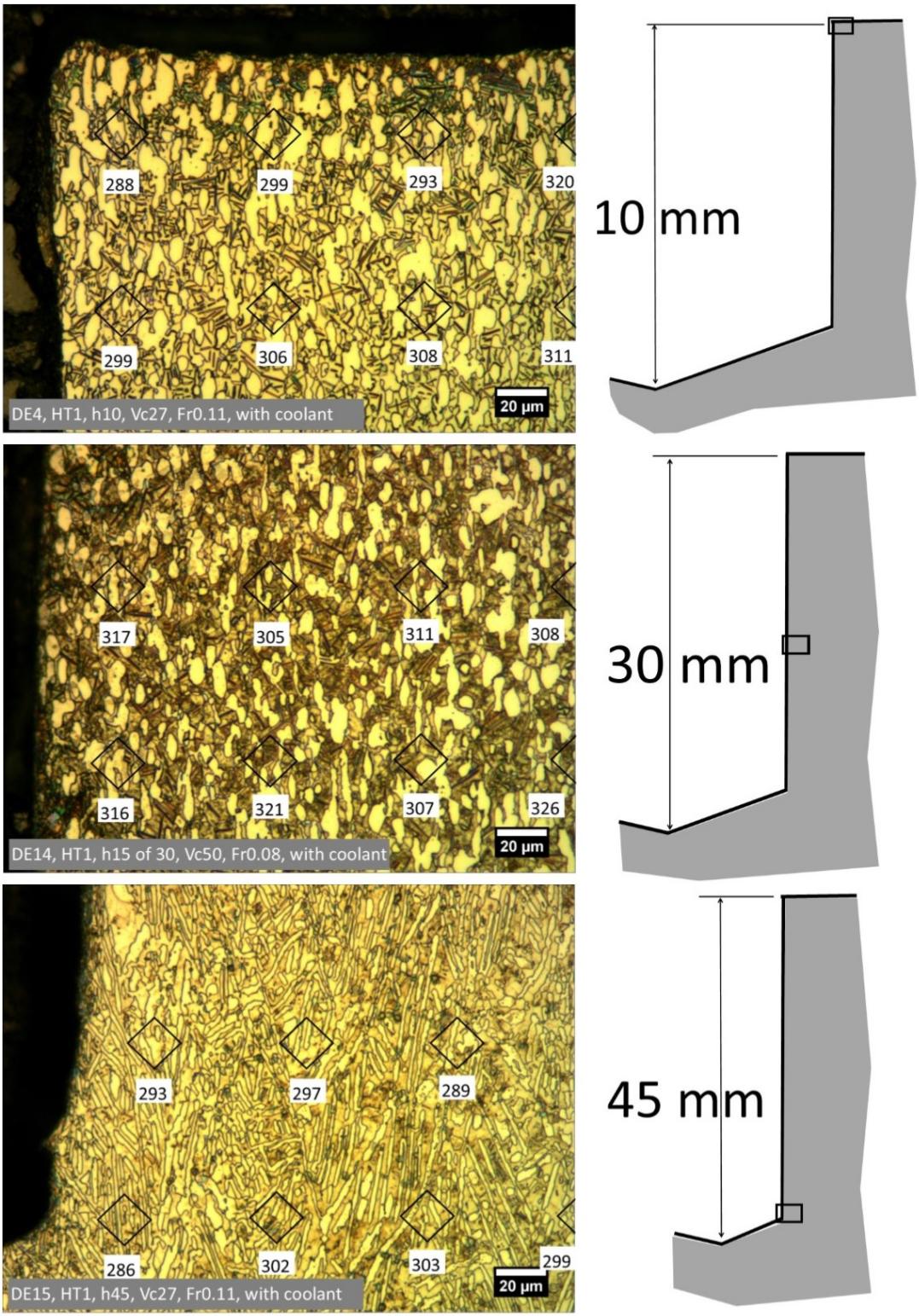

Figure 6.18. Microstructure of the blocks HT1 at different depths of drilling. Hardness values at various positions are also shown.

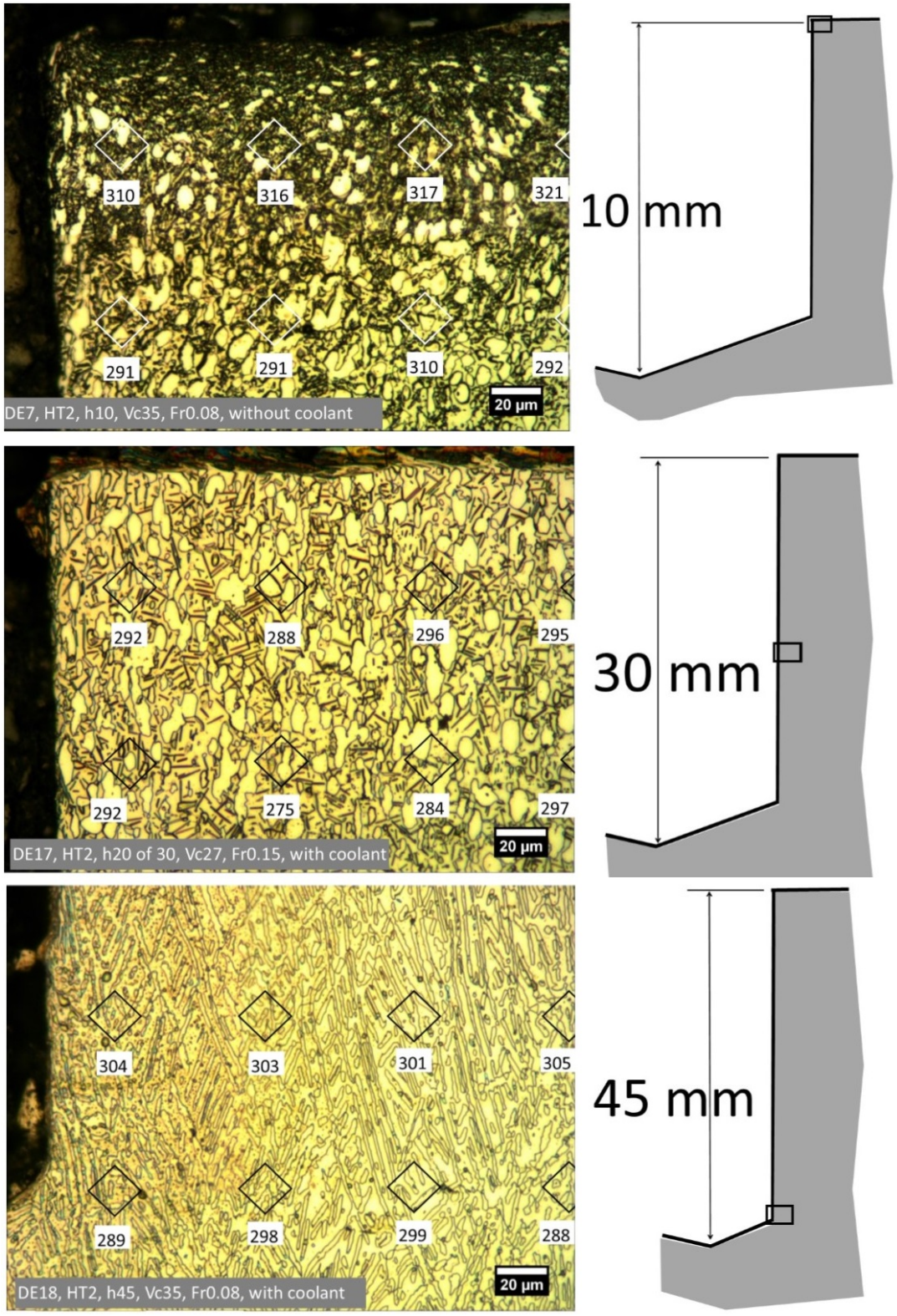

Figure 6.19. Microstructure of the blocks of HT2 at different depths of drilling. Hardness values at various positions are also shown.

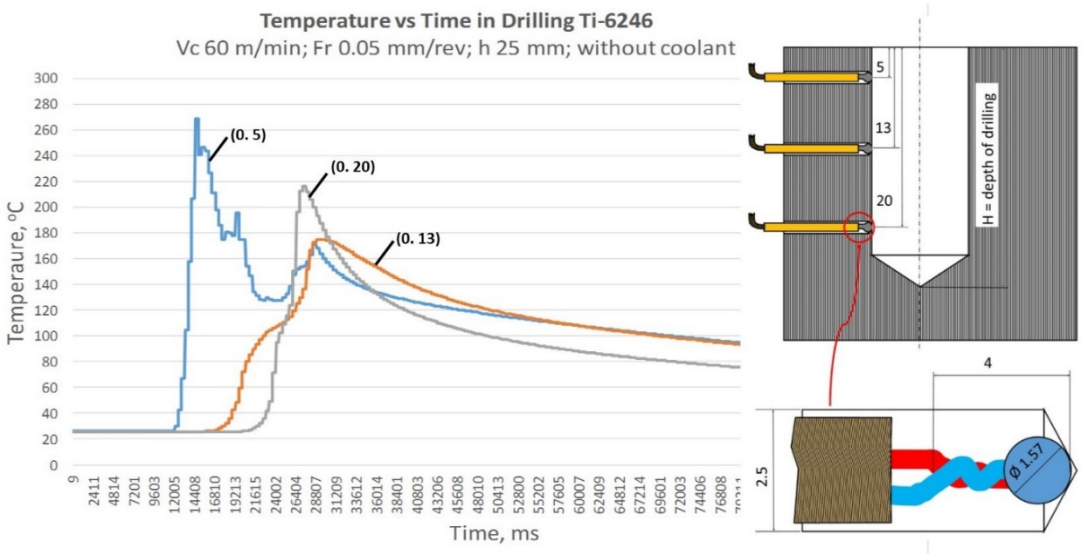

Figure 6.20. Temperature measurement on the block during drilling. The position of the thermocouple is designed to be touched by the drill head at the consequent position.

6.4 Conclusion

Some conclusions may be taken from the previous analysis.

A. Based on force analysis:

a. Among five parameters that varied, the cutting speed, depth of drilling, heat treatment and feed rate influenced the thrust force by order of percentage as 24, 21, 13, and 11 respectively. While torque was significantly affected by the feed rate of up to 94%. The use of a coolant did not contribute to reducing the drilling forces.

b. The minimum drilling force conditions would be achieved when drilling with a cutting speed of 27 m/min, a feed rate of 0.08 m/rev on a depth of only 10 mm without coolant, while material should be HT1 treated.

A further reduction in forces may be gained either by applying flood coolant or using a through coolant tool design.

B. Based on surface quality:

a. Depth of drilling employed the paramount effect on the surface roughness by 55%, followed by heat treatment (25%), cutting speed (10%), feed rate (6%) and coolant application (2%).

b. All of the above parameters affected the roundness of the holes at a level of significance of less than 95%.

c. The minimum surface roughness between 0.3113 µm to 0.5235 µm was achieved when drilling with these parameters: Clt_{off}, HT_{AR}, h_{10}, Vc_{35}, and $fr_{0.08}$.

For future research, the depth of drilling should be considered the main parameter when the surface roughness is the focus of investigation.

C. Based on surface damage and surface integrity:

There was no hardness and microstructure change under the drilled surface. The heat generated during drilling was far below the beta transus temperature to change the microstructure and subsequently its hardness. Change of hardness on the surface of the HT2 material was an effect of water quenching.

CHAPTER 7. GENERAL DISCUSSION & CONCLUSION AND FUTURE RESEARCH

This chapter is a broad discussion and wrap up on drillability of Ti-6246 with TiAlN PVD coated drills. Future research has also been suggested at the end of the chapter.

7.1 General Discussion & Conclusions

7.1.1 Effectiveness of the Taguchi Method

The Taguchi method proved in this research to be an effective design for experiments that would achieve the optimum condition of machining with the smallest number of experiments needed. A combination of four parameters and three levels of variation and a single parameter with two levels of variation only needed 18 experiments. Indeed it is very highly efficient in comparison to that of a full factorial design which would need 162 experiments. Its effectiveness was also supported by the available software to process the data, such as Minitab. The online support of this software enabled even the new user to become familiar with the menu fairly quickly.

The effectiveness of the Taguchi method becomes more powerful when combined with an analysis of variance (ANOVA). ANOVA provides the impact of each variable on the drillability criteria by percentage. Therefore, it is easier for the user or decision-maker to judge which level of parameters are to be used in machining from the available alternatives. For example, in case of drillability from a roundness perspective, the feed rate only gave an effect to the roundness of 2% (Table 6.5-b) and the optimum feed rate would be at a level 1, or fr 0.08 mm/rev (with a mean data value of 0.012322). When it is compared to that of fr 0.15 mm/rev, the mean data value is 0.012100; the difference was as small as 0.000222. Therefore, it is advised to choose the feed rate of 0.15 mm/rev instead of 0.08 mm/rev, because a higher feed rate means a higher metal removal rate (MRR), which is preferable with a smaller risk of achieving inferior roundness.

Another example has already been discussed in section 6.1.2 regarding choosing parameters for the optimum torque. The torque was influenced by 94% by the feed rate, and the other 6% influencer was from the four other factors. As the optimum thrust force and torque would be achieved at a feed rate of 0.08 mm/rev, therefore the

rest of the parameters chosen for the optimum torque followed the parameters to achieve an optimum thrust force [see also Table 8.1 row of "Torque (compromised)"].

The next example is regarding surface roughness, which was influenced by 55% by the depth of drilling in this study. To my knowledge, the depth has never been considered by previous researchers as the factor which would affect the roughness of the drilled holes. In conventional machining, such as turning and milling, the length of machining does not have much effect on the machined surface roughness unless the tool has deteriorated, as long as the chips could be kept away from the machined surface, such as by a chip breaker mechanism/design. In drilling, the case is different. Although the chips are already broken, they will scratch the drilled surface on the way out from the drilling area. The deeper the depth of drilling, the more possible there will be scratching made by the chips. Therefore, the rougher the surface will be.

Those three examples should be adequate evidence that the ANOVA data and its analysis would be a good source for decision making, whether such a level of parameters should be used or should be ignored. It is also possible to ignore a certain parameter in the next experiment if its effect on the drillability is not significant.

7.1.2 Evaluation on Drillability of Ti-6246

Analysis following the Taguchi method design experiments showing different suggestions relating to the parameters should be used for achieving the optimum conditions for drillability. Drillability was observed from four points of view: (i) chip formations, (ii) tool deterioration, (iii) forces (thrust and torque), and (iv) the quality of the drilled hole, such as the hole's surface roughness and roundness. Table 8.1 shows the parameters should be used to aim for optimum drillability for different criterions.

Drillability is a term derived from machinability. The machinability of a material is how easily it can be machined using a cutting tool. A material is said to have good machinability if after machining it is proved that the tool wear is low and the surface finish produced is good. Furthermore, poor machinability is also associated with the high chemical reactivity of the material with the many tool materials and the low elastic modulus [149]. Therefore, it is possible that a material having a reputable machinability grading in one point of view can have an undesirable ranking when examined from another perspective [32]. In this research, the drillability of the Ti-6246

also suggested different combinations of five parameters to choose from for different criteria.

Table 7.1. Summary of parameters to be used for achieving optimum drillability from various perspectives

No	Point of view	S/N criterion	Machining parameters					Distinguished Parameter(s)
			Clt	HT	h	Vc	fr	
1	Chips formation – serrated degree	HB	on	AR	30	50	0.15	HT 29%, Vc 20%
2	Tool deterioration	SB	on	AR	30	50	0.15	
3								
	a. Thrust force	SB	on	HT1	10	27	0.08	Vc 24%, h 21%
	b. Torque	SB	on	HT2	45	35	0.08	fr 94%
	Torque (compromised)	SB	on	HT1	10	27	0.08	
4								
	a. Roughness	SB	off	AR	10	35	0.08	h 55%, HT 25%, Clt 2%
	b. Roundness	SB	on	AR	10	27	0.15	h 30%, Vc 18%

In general, there are some similarities of suggestions that a coolant should be used during drilling except for the surface roughness criteria. It is due to an ineffective coolant method application, i.e. an external method. The effect of applying a coolant by the external method contributed only 2% toward the roughness. Therefore, if the main concern of drillabilty is the surface roughness (whether using a coolant or not), it will not affect it much. Unless however, a through coolant is used, this may make the application much more effective. However, to be able to apply the through coolant, the tooling system or the whole system of the machine tool needs to be changed or replaced. Alternatively, if an external cooling method is to be used, it has to be performed with high pressure.

In regards which condition the material should be drilled, most of the criteria for drillability suggests to use the as received (AR) condition, except for the forces-based point of view. For the thrust force-based perspective, the HT1 was optimal, while on the torque-based criteria, the HT2 was the optimum. However, as already discussed in section 6.1.2 and re-emphasised on section 8.1.1, the HT1 may be chosen considering

that 94% of the torque was influenced by the feed rate. Therefore, the optimum torque may be achieved by using the parameters that have made the thrust force optimal.

For other parameters, which level should be chosen to achieve the optimum drillability depends on the focus of the manufacturers. It they are customer-oriented, the quality of the holes will be a focus. If they are profit-oriented, tool deterioration will be the focus.

Another attention related to drillability is conformity of the TiAlN PVD coated carbide insert which was used in these experiments. As already discussed in section 5.5, this tool may not be the right choice for drilling Ti-6246. A BUE was unavoidable in all drilling parameters, especially at the vicinity of the chisel, then on the inner blades. The tool delamination very commonly happened in all parameters used in these observations. Additionally, chipping was also observed, even though only drilling to a depth of 10 mm. In our previous plan two alternatives of tools were proposed: (i) IC907 – the uncoated carbide insert, and (ii) IC908 – the TiAlN coated one. Unfortunately, during the experimental stage, the manufacturer did not produce the IC907 as uncoated anymore.

7.1.3 Surface Integrity of the Drilled Holes

The drilled holes did not experience a mechanical properties change. The hardness at the vicinity of the drilled material did not change. The change in hardness was at the top of the surface of the heat treated materials (HT1 & HT2). That means the change of hardness was associated with the heat treatment instead of as an effect of the drilling. Further observation with an optical microscope and SEM also did not show that the drilled surface experienced microstructural change.

7.1.4 Drilling Simulation

It cannot be denied that simulation has been a new trend in the research, and this is no exception in machining. Simulation of machining has helped to resolve the machining problems with lower cost. However, in order to be able to do a simulation of drilling, especially with 3D visualisation, three conditions should be fulfilled. First, there needs to be a deep understanding of the mechanics of the material. Second, the researcher should be familiar with computer programming which is compatible with the simulation software used. Without this ability, a complex simulation would not be able

to be carried out. Third, a high grade computer specification such as a high speed processor, high random access memory, complete with video card is essential. Lack of these three requirements would not have a high hope for being able to gain a good result from a simulation of drilling.

7.2 Future Research

From these studies some further investigations are required, including:

a. Using different parameters and levels for studying the drillability of this material. Attempts to drill deeper as it has the most influencing factor on the surface roughness.
b. Develop a drilling simulation on a well-established programme which has already worked for other machining simulations, such as DEFORM, ABAQUS, and ADVANTEDGE. Furthermore, availability of high speed computing (HSC) is a must to achieve the simulation results faster and better.
c. Comparing the experimental result and the simulation.

REFERENCES

[1] D. Fischer, “The Story of Titanium - a Historical Perspective.” International Titanium Association, 2017.

[2] G. Lutjering and J. C. Williams, *Titanium*, 2nd ed. Springer-Verlag BerlinHeidelberg, 2007.

[3] R. R. Boyer, “Attributes, characteristics, and applications of titanium and its alloys,” *JOM*, vol. 62, no. 5, pp. 35–43, 2010.

[4] N. E. Prasad and R. J. H. Wanhill, *Aerospace Materials and Material Technologies*, vol. 1. Springer, 2017.

[5] K. M. Youssef, A. J. Zaddach, C. Niu, D. L. Irving, and C. C. Koch, “A novel low-density, high-hardness, high-entropy alloy with close-packed single-phase nanocrystalline structures,” *Mater. Res. Lett.*, vol. 3, no. 2, pp. 95–99, 2014.

[6] M. Donachie, *Titanium, a Technical Guide*, 2nd ed. ASM International, 2000.

[7] Titanium Engineers, “Titanium 6Al-2Sn-4Zr-6Mo Ti 6246 (UNS R56260).” Titanium Engineers, pp. 5–6, 2015.

[8] R. Boyer, G. Welsch, and E. W. Collings, *Materials Properties Handbook: Titanium Alloys*. 1994.

[9] W. Sha and S. Malinov, *Titanium alloys: Modelling of microstructure, properties and applications*. Boca Raton: Woodhead Publishing, 2009.

[10] C. Siemers, “Researchgate Question & Answer,” *Researchgate.net*, 2014. [Online]. Available: https://www.researchgate.net/post/Hello_everyone_my_question_is_why_martensite_in_Titanium_alloys_is_softer_than_B_phase. [Accessed: 01-Nov-2017].

[11] S. W. Raza, S. Pervaiz, and I. Deiab, “Tool wear patterns when turning of titanium alloy using sustainable lubrication strategies,” *Int. J. Precis. Eng. Manuf.*, vol. 15, no. 9, 2014.

[12] R. Pederson, “The microstructures of Ti-6Al-4V and Ti-6Al-2Sn-4Zr-6Mo and their relationship to processing and properties,” Luleå University of

Technology, 2004.

[13] C. Leyens and M. Peters, *Titanium and Titanium Alloys*. Weinheim: WILEY-VCH Verlag GmbH & Co., 2003.

[14] J. Stráský, “Lecture 3: Technological Aspecs of Titanium Alloys.” Department of Physics, Charles University, Praha, pp. 1–24, 2017.

[15] M. P. Groover, *Fundamentals of Modern Manufacturing: Materials, Processes, and Systems.*, 4th ed. John Wiley & Sons, Inc., 2010.

[16] R. Singh, *Introduction to Basic Manufacturing Processes and Workshop Technology*. New Delhi: New Age International Publishers, 2006.

[17] H. a. Youssef and H. El-Hofy, *Machining technology: Machine tools and operations*. CRC Press Taylor & Francis Group, 2008.

[18] S. Sharif and E. A. Rahim, “Performance of coated- and uncoated-carbide tools when drilling titanium alloy-Ti-6Al4V,” *J. Mater. Process. Technol.*, vol. 185, no. 1–3, pp. 72–76, 2007.

[19] J. G. Bralla, *Handbook of Manufacturing Processes: How Products, Components and Materials are Made*, 1st ed. New York: Industrial Press, Inc., 2007.

[20] P. F. Zhang, N. J. Churi, Z. J. Pei, and C. Treadwell, “Mechanical drilling processes for titanium alloys: A literature review,” *Machining Science and Technology*, vol. 12, no. 4. pp. 417–444, 2008.

[21] S. F. Krar, A. R. Gill, and P. Smid, *Technology of Machine Tools*, 7th ed. New York: McGraw-Hill, 2011.

[22] J. W. Sutherland, “Manufacturing Education Page,” 1998. [Online]. Available: http://www.mfg.mtu.edu/marc/primers/drilling/nomen.html.

[23] J. S. Strenkowski, C. C. Hsieh, and A. J. Shih, “An analytical finite element technique for predicting thrust force and torque in drilling,” *Int. J. Mach. Tools Manuf.*, vol. 44, no. 12–13, pp. 1413–1421, 2004.

[24] E. A. Rahim and S. Sharif, “Evaluation of tool wear mechanism of TiAlN coated tools when drilling Ti-6Al-4V,” *Int. J. Manuf. Technol. Manag.*, vol. 17, no. 4, p. 327, 2009.

[25] A. Pramanik, “Problems and solutions in machining of titanium alloys,” *Int. J. Adv. Manuf. Technol.*, vol. 70, no. 5–8, pp. 919–928, 2014.

[26] J. L. Cantero, M. M. Tardío, J. A. Canteli, M. Marcos, and M. H. Miguélez, “Dry drilling of alloy Ti-6Al-4V,” *Int. J. Mach. Tools Manuf.*, vol. 45, no. 11, pp. 1246–1255, 2005.

[27] E. A. Rahim, S. Sharif, Z. A. Ahmad, A. S. Mohruni, and I. A. Syed, “Machinability investigation when drilling titanium alloys,” *LEM 2005 - 3rd Int. Conf. Lead. Edge Manuf. 21st Century*, pp. 553–557, 2005.

[28] Y. Kosaka, J. C. Fanning, and S. P. Fox, “Development of low cost high strength alpha/beta alloy with superior machinability,” in *Proceedings of the 10th World Conference on Titanium*, 2004, pp. 3028–3034.

[29] M. N. Murad, S. Sharif, E. A. Rahim, and Rival, “Effect of Drill Point Angle on Surface Integrity when Drilling Titanium Alloy,” *Adv. Mater. Res.*, vol. 845, pp. 966–970, 2013.

[30] A. Prabukarthi, V. Krishnaraj, M. Santhosh, and M. Senthilkumar, “Optimisation and tool life study in drilling of titanium (Ti-6Al-4V) alloy,” *Int. J. Mach. Mach. Mater.*, vol. 13, no. 2004, pp. 138–157, 2013.

[31] MatWeb Material Property Data, “Titanium Ti-6Al-2Sn-4Zr-6Mo (Ti-6-2-4-6) BSTA,” 2017. [Online]. Available: http://www.matweb.com/search/datasheet.aspx?MatGUID=47cc69e4926f4177a13288cfc693bc99. [Accessed: 03-Jul-2017].

[32] S. Pervaiz, A. Rashid, I. Deiab, and M. Nicolescu, “Influence of tool materials on machinability of titanium- and nickel-based alloys: A review,” *Mater. Manuf. Process.*, vol. 29, no. 3, pp. 219–252, 2014.

[33] Z. Rihova, K. Saksl, C. Siemers, and D. Ostroushko, “Analyses of Wear Mechanisms Occurring During Machining of the Titanium Alloy Ti-,” *Word Acad. Sci. Eng. Technol.*, vol. 68, pp. 1515–1518, 2012.

[34] S. Sharif, E. A. Rahim, A. S. Mohruni, and A. Jawaid, “Effect of edge geometry on PVD-TiN coated carbide tools when face milling titanium alloy Ti-6246,” in *Intl. Conf. on Leading Edge Manufacturing in 21st Century*, 2005.

[35] S. L. Soo *et al.*, "The effect of wire electrical discharge machining on the fatigue life of Ti-6Al-2Sn-4Zr-6Mo aerospace alloy," *Procedia CIRP*, vol. 6, pp. 215–219, 2013.

[36] R. Muhammad, A. Maurotto, A. Roy, and V. V. Silberschmidt, "Ultrasonically assisted turning of Ti-6Al-2Sn-4Zr-6Mo," *J. Phys. Conf. Ser.*, vol. 382, p. 012016, 2012.

[37] R. Muhammad, M. S. Hussain, A. Maurotto, C. Siemers, A. Roy, and V. V. Silberschmidt, "Analysis of a free machining alpha + beta titanium alloy using conventional and ultrasonically assisted turning," *J. Mater. Process. Technol.*, vol. 214, no. 4, pp. 906–915, 2014.

[38] P. Stella, I. Giovanetti, G. Masi, M. Leoni, and A. Molinari, "Microstructure and microhardness of heat-treated Ti-6Al-2Sn-4Zr-6Mo alloy," *J. Alloys Compd.*, vol. 567, pp. 134–140, 2013.

[39] M. Armendia, P. Osborne, A. Garay, J. Belloso, S. Turner, and P. J. Arrazola, "Influence of heat treatment on the machinability of titanium alloys," *Mater. Manuf. Process.*, vol. 27, no. 4, pp. 457–461, 2012.

[40] S. S. Gill and J. Singh, "Effect of deep cryogenic treatment on machinability of titanium alloy (Ti-6246) in electric discharge drilling," *Mater. Manuf. Process.*, vol. 25, no. 6, pp. 378–385, 2010.

[41] F. Brunke, E. Meyer-Kornblum, and C. Siemers, "Influence of iron on the size and distribution of metallic lanthanum particles in free-machining titanium alloys Ti 6Al 7Nb xFe 0.9La," *Mater. Sci. Forum*, vol. 765, pp. 42–46, 2013.

[42] M. S. Hussain, C. Siemers, and J. Rösler, "Development of a free-machining (α+β) titanium alloy based on Ti 6Al 2Sn 4Zr 6Mo," in *Proceedings of the 37th International MATADOR Conference*, 2012, vol. I, pp. 197–200.

[43] D. Ostroushko, K. Saksl, C. Siemers, and Z. Rihova, "Chips of Ti-6Al-2Sn-4Zr-6Mo Alloy – A Detailed Geometry Study," *Word Acad. Sci. Eng. Technol.*, vol. 6, pp. 942–945, 2012.

[44] P. Rokicki, Z. Spotz, L. Fusova, K. Saksl, C. Siemers, and B. Zhara, "Chip formation process of Ti-15V-3Al-3Sn-3Cr alloy," in *Metal 2010*, 2010.

[45] S. Joshi, P. Pawar, a. Tewari, and S. S. Joshi, “Tool wear mechanisms in machining of three titanium alloys with increasing b-phase fraction,” *Proc. Inst. Mech. Eng. Part B J. Eng. Manuf.*, 2014.

[46] M. Nouari and H. Makich, “On the physics of machining titanium alloys: interactions between cutting parameters, microstructure and tool wear,” *Metals (Basel).*, vol. 4, no. 3, pp. 335–358, 2014.

[47] C. Siemers, B. Zahra, T. Leemet, and J. Rösler, “Development of advanced beta-titanium alloys,” in *Proceeding of the 8th AMMT ’09 Conference*, 2009, pp. 1–7.

[48] R. Komanduri, “Some clarifications on the mechanics of chip formation when machining titanium alloys,” *Wear*, vol. 76, no. 1, pp. 15–34, 1982.

[49] H. Zhen-Bin and R. Komanduri, “On a thermomechanical model of shear instability in machining,” *Ann. CIPR*, vol. 44, no. 1, pp. 69–73, 1995.

[50] J. Barry, G. Byrne, and D. Lennon, “Observations on chip formation and acoustic emission in machining Ti-6Al-4V alloy,” *Int. J. Mach. Tools Manuf.*, vol. 41, no. 7, pp. 1055–1070, 2001.

[51] B. Wang and Z. Liu, “Serrated chip formation mechanism based on mixed mode of ductile fracture and adiabatic shear,” *Proc. Inst. Mech. Eng. Part B J. Eng. Manuf.*, vol. 228, no. 2, pp. 181–190, 2014.

[52] M. Bäker, J. Rösler, and C. Siemers, “The influence of thermal conductivity on segmented chip formation,” *Comput. Mater. Sci.*, vol. 26, no. SUPPL., pp. 175–182, 2003.

[53] M. D. Morehead and Y. Huang, “Chip morphology characterization and modeling in machining hardened 52100 steels,” *Mach. Sci. Technol. Sci.*, vol. 11, pp. 335–354, 2007.

[54] S. Zhang, J. Li, X. Zhu, and H. Lv, “Saw-tooth chip formation and its effect on cutting force fluctuation in turning of Inconel 718,” *Int. J. Precis. Eng. Manuf.*, vol. 14, no. 6, pp. 957–963, 2013.

[55] A. Antic *et al.*, “Influence of tool wear on the mechanism of chips segmentation,” *Tech. Gaz.*, vol. 10, pp. 105–112, 2013.

[56] K. Nakayama, M. Arai, and T. Kanda, “Machining characteristics of hard materials,” in *Annals of the CIRP*, 1988, vol. 37, no. l, pp. 89–92.

[57] J. Kümmel, J. Gibmeier, E. Müller, R. Schneider, V. Schulze, and A. Wanner, “Detailed analysis of microstructure of intentionally formed built-up edges for improving wear behaviour in dry metal cutting process of steel,” *Wear*, vol. 311, no. 1–2, pp. 21–30, 2014.

[58] N. Tomac, K. Tonnessen, F. O. Rasch, and T. Mikac, “A study of factors that affect the build-up material formation,” *Adv. Manuf. Syst. Technol.*, no. 486, 2005.

[59] J. P. Davim, Ed., *Machining Fundamentals and Recent Advances*, 1st ed. Aveiro: Springer-Verlag London Limited, 2008.

[60] J. Zang, J. Zhao, A. Li, and J. Pang, “Serrated chip formation mechanism analysis for machining of titanium alloy Ti-6Al-4V based on thermal property,” *Int. J. Adv. Manuf. Technol.*, 2017.

[61] P. C. Jindal, A. T. Santhanam, U. Schleinkofer, and A. F. Shuster, “Performance of PVD TiN, TiCN, and TiAlN coated cemented carbide tools in turning,” *Int. J. Refract. Met. Hard Mater.*, vol. 17, no. 1, pp. 163–170, 1999.

[62] A. Liu, J. Deng, H. Cui, Y. Chen, and J. Zhao, “Friction and wear properties of TiN, TiAlN, AlTiN and CrAlN PVD nitride coatings,” *Int. J. Refract. Met. Hard Mater.*, vol. 31, pp. 82–88, 2012.

[63] Z. Hao, D. Gao, Y. Fan, and R. Han, “New observations on tool wear mechanism in dry machining Inconel718,” *Int. J. Mach. Tools Manuf.*, vol. 51, no. 12, pp. 973–979, 2011.

[64] S. K. Khrais and Y. J. Lin, “Wear mechanisms and tool performance of TiAlN PVD coated inserts during machining of AISI 4140 steel,” *Wear*, vol. 262, no. 1–2, pp. 64–69, 2007.

[65] C. R. K. Kumar, P. K. Nair, and B. Ramamoorthy, “Performance of TiCN and TiAlN tools in machining hardened steel under dry, wet and minimum fluid application,” *Int. J. Mach. Mach. Mater.*, vol. 3, no. 1–2, pp. 133–142, 2008.

[66] R. Vinayagamoorthy and M. A. Xavior, “Dry machining of Ti-6AL-4V using

PVD coated tools," *Int. J. Appl. Eng. Res.*, vol. 8, no. 12, pp. 1373–1381, 2013.

[67] S. Pervaiz, I. Deiab, B. Darras, A. Rashid, and M. Nicolescu, "Performance evaluation of TiAlN-PVD coated inserts for machining Ti-6Al-4V under different cooling strategies," *Adv. Mater. Res.*, vol. 685, pp. 68–75, 2013.

[68] V. Czitrom, "One-factor-at-a-time versus designed experiments," *Am. Stat.*, vol. 53, no. 2, pp. 126–131, 1999.

[69] L. Zongming, "Using Taguchi designed experiment to reduce tire leakage rates," *Qual. Dig.*, 2009.

[70] B. Singh, B. S. Pabla, and M. Saroha, "Investigating the effects of process parameters on MRR in WEDM using molybdenum wire," *Int. J. Eng. , Bus. Enterp. Appl.*, pp. 1–5, 2014.

[71] "Taguchi Designs," *Minitab Support*. [Online]. Available: https://support.minitab.com/en-us/minitab/18/help-and-how-to/modeling-statistics/doe/supporting-topics/taguchi-designs/taguchi-designs/. [Accessed: 07-Mar-2017].

[72] NIST/SEMATECH, "e-Handbook of Statistical Methods," 2012. [Online]. Available: http://www.itl.nist.gov/div898/handbook/index.htm. [Accessed: 22-Mar-2017].

[73] Y. A. Youssef, Y. Beauchamp, and M. Thomas, "Comparison of a full factorial experiment to fractional and taguchi designs in a lathe dry turning operation," *Comput. Ind. Eng.*, vol. 27, no. 1–4, pp. 59–62, 1994.

[74] M. N. Islam and A. Pramanik, "Comparison of design of experiments via traditional and Taguchi method," *J. Adv. Manuf. Syst.*, vol. 15, no. 03, pp. 151–160, 2016.

[75] J. S. Pang, M. N. M. Ansari, O. S. Zaroog, M. H. Ali, and S. M. Sapuan, "Taguchi design optimization of machining parameters on the CNC end milling process of halloysite nanotube with aluminium reinforced epoxy matrix (HNT/Al/Ep) hybrid composite," *HBRC J.*, vol. 10/, no. 2, pp. 138–144, 2014.

[76] J. A. Ghani, I. A. Choudhury, and H. H. Hassan, "Application of Taguchi method in the optimization of end milling parameters," *J. Mater. Process.*

Technol., vol. 145, no. 1, pp. 84–92, 2004.

[77] L. B. Abhang and M. Hameedullah, "Optimization of machining parameters in steel turning operation by Taguchi method," *Procedia Eng.*, vol. 38, pp. 40–48, 2012.

[78] K. N. Kasdekar, V. Parashar, J. Singh, and M. K. Gour, "Taguchi method and ANOVA: an approach for selection of process parameters of EDM of EN-353 steel," *Int. J. Emerg. Technol. Adv. Eng.*, vol. 4, no. 6, pp. 313–321, 2014.

[79] N. Khanna, "Design of Experiments in Titanium Metal Cutting Research," in *Design of Experiments in Production Engineering*, 1st ed., no. November, J. P. Davim, Ed. Aviero, Portugal: Springer, 2016, pp. 165–182.

[80] M. Kowalczyk, "Application of Taguchi and Anova methods in selection of process parameters for surface roughness in precision turning of titanium," *Gruyter Open Adv. Manuf. Sci. Technol.*, vol. 38, no. 2, pp. 21–35, 2014.

[81] M. Nalbant, H. Gökkaya, and G. Sur, "Application of Taguchi method in the optimization of cutting parameters for surface roughness in turning," *Mater. Des.*, vol. 28, no. 4, pp. 1379–1385, 2007.

[82] T. Schermann, J. Marsolek, C. Schmidt, and J. Fleischer, "Aspects of the simulation of a cutting process with ABAQUS/explicit including the interaction between the cutting process and the dynamic behavior of the machine tool," *9th CIRP Int. Work. Model. Mach. Oper. Bled, Slowenia*, vol. 11, p. 12, 2006.

[83] Y. Zhang, J. C. Outeiro, and T. Mabrouki, "On the selection of Johnson-Cook constitutive model parameters for Ti-6Al-4V using three types of numerical models of orthogonal cutting," *Procedia CIRP*, vol. 31, pp. 112–117, 2015.

[84] S. Imbrogno, S. Sartori, A. Bordin, S. Bruschi, and D. Umbrello, "Machining simulation of Ti6Al4V under dry and cryogenic conditions," *Procedia CIRP*, vol. 58, pp. 475–480, 2017.

[85] A. Attanasio, F. Faini, and J. C. Outeiro, "FEM simulation of tool wear in drilling," *Procedia CIRP*, vol. 58, pp. 440–444, 2017.

[86] T. Ozel, I. Llanos, J. Soriano, and P. J. Arrazola, "3D finite element modelling of chip formation process for machining Inconel 718: Comparison of FE

software predictions," *Mach. Sci. Technol.*, vol. 15, no. 1, pp. 21–46, 2011.

[87] M. Zetterberg, "A critical overview of machining simulations in ABAQUS," KTH Royal Institute of Technology, 2014.

[88] M. Calamaz, D. Coupard, and F. Girot, "A new material model for 2D numerical simulation of serrated chip formation when machining titanium alloy Ti-6Al-4V," *Int. J. Mach. Tools Manuf.*, vol. 48, no. 3–4, pp. 275–288, 2008.

[89] D. Yameogo, B. Haddag, H. Makich, and M. Nouari, "Prediction of the cutting forces and chip morphology when machining the Ti6Al4V alloy using a microstructural coupled model," *Procedia CIRP*, vol. 58, pp. 335–340, 2017.

[90] F. Ducobu, E. Riviere-Lorphevre, and E. Filippi, "Material constitutive model and chip separtion criterion influence on modeling of Ti6Al4V machining with experimental validation in strictly orthogonal cutting condition," *Int. J. Mech. Sci.*, vol. 107, pp. 136–149, 2016.

[91] A. M. Abdelhafeez, S. L. Soo, D. K. Aspinwall, A. Dowson, and D. Arnold, "A coupled Eulerian Lagrangian finite element model of drilling titanium and aluminium alloys," *SAE Int. J. Aerosp.*, vol. 9, no. 1, pp. 198–207, 2016.

[92] P. Kožmín, "FEM method in chip shape and cutting force prediction when drilling difficult to cut materials," in *3rd International Scientific Conference with Expert Participation - Manufacturing 2010*, 2010, pp. 1–14.

[93] H. Chandler, Ed., *Heat Treater's Guide: Practices and Procedures for Nonferrous Alloys*. ASM International, 1996.

[94] P. J. Bania, "Beta titanium alloys and their role in the titanium industry," *Jom*, vol. 46, no. 7, pp. 16–19, 1994.

[95] F. H. Froes, *Titanium: Physical Metallurgy Processing and Application*, 1st ed., vol. 53. Ohio: ASM International, 1989.

[96] ISCAR, "Hole Making Tools Catalog, Metric Version." ISCAR, 2012.

[97] A. Alomary, S. Belhadj, S. Obeidat, I. Al-Momani, and A. Attiyat, "A comparison of SEM-EDS with ICP-OES for the Quantitative Elemental Determination of Algerian Mediterranean Sea Sediments," *Jordan J. Chem.*, vol. 7, no. 4, pp. 383–391, 2012.

[98] I. Michalak, K. Marycz, K. Basińska, and K. Chojnacka, "Using SEM-EDX and ICP-OES to investigate the elemental composition of green macroalga vaucheria sessilis," *Sci. World J.*, vol. 2014, 2014.

[99] A. Z. Sultan, S. Sharif, and D. Kurniawan, "Chip Formation When Drilling AISI 316L Stainless Steel using Carbide Twist Drill," *Procedia Manuf.*, vol. 2, 2015.

[100] F. Ke, J. Ni, and D. A. Stephenson, "Continuous chip formation in drilling," *Int. J. Mach. Tools Manuf.*, vol. 45, no. 15, pp. 1652–1658, 2005.

[101] D. Ostroushko, K. Saksl, C. Siemers, and Z. Rihova, "Chips of Ti-6Al-2Sn-4Zr-6Mo alloy – a detailed geometry study," *Word Acad. Sci. Eng. Technol.*, vol. 6, no. 8, pp. 942–945, 2012.

[102] G. F. Vander Voort, *Metallography and Microstructures Handbook*, vol. 9. 2004.

[103] C. Jian, "Development & innovation in geotechnical research: A few examples." Nanyang University of Technology, Nanjing, pp. 1–11, 2010.

[104] M. Hokka, D. Gomon, A. Shrot, T. Leemet, M. Bäker, and V. T. Kuokkala, "Dynamic behavior and high speed Machining of Ti-6246 and alloy 625 superalloys: experimental and modeling approaches," *Exp. Mech.*, vol. 54, no. 2, pp. 199–210, 2014.

[105] H. Liu, J. Zhang, Y. Jiang, Y. He, X. Xu, and W. Zhao, "Investigation on morphological evolution of chips for Ti6Al4V alloys with the increasing milling speed," *Procedia CIRP*, vol. 46, pp. 408–411, 2016.

[106] M. H. Shahavi, M. Hosseini, M. Jahanshahi, R. L. Meyer, and G. N. Darzi, "Clove oil nanoemulsion as an effective antibacterial agent: Taguchi optimization method," *Desalin. Water Treat.*, vol. 57, no. 39, pp. 18379–18390, 2016.

[107] O. Hatt, P. Crawforth, and M. Jackson, "On the mechanism of tool crater wear during titanium alloy machining," *Wear*, vol. 374–375, pp. 15–20, 2017.

[108] N. H. Razak, Z. W. Chen, and T. Pasang, "Modes of tool deterioration during milling of 718Plus superalloy using cemented tungsten carbide tools," *Wear*, vol. 316, no. 1–2, pp. 92–100, 2014.

[109] P. D. Hartung, B. M. Kramer, and B. F. von Turkovich, “Tool wear in titanium machining,” *CIRP Ann. - Manuf. Technol.*, vol. 31, no. 1, pp. 75–80, 1982.

[110] M.-A. Dittrich, “How does the built-up edge lead to surface damage?” researchgate.net, p. 1, 2014.

[111] C. Veiga, J. P. Davim, and A. J. R. Loureiro, “Review on machinability of titanium alloys: The process perspective,” *Reviews on Advanced Materials Science*, vol. 34, no. 2. 2013.

[112] M. Darsin, T. Pasang, and Z. Chen, “Drillability of titanium 6246 alloy,” in *Processing and Fabrication of Advanced Materials-XXV*, 2017, pp. 856–863.

[113] S. S. Gill, J. Singh, H. Singh, and R. Singh, “Investigation on wear behaviour of cryogenically treated TiAlN coated tungsten carbide inserts in turning,” *Int. J. Mach. Tools Manuf.*, vol. 51, no. 1, pp. 25–33, 2011.

[114] J. M. Castanho and M. T. Vieira, “Effect of ductile layers in mechanical behaviour of TiAlN thin coatings,” *J. Mater. Process. Technol.*, vol. 143–144, no. 1, pp. 352–357, 2003.

[115] D. Arulkirubakaran and V. Senthilkumar, “Performance of TiN and TiAlN coated micro-grooved tools during machining of Ti-6Al-4V alloy,” *Int. J. Refract. Met. Hard Mater.*, vol. 62, pp. 47–57, 2017.

[116] M. Pirtini and I. Lazoglu, “Forces and hole quality in drilling,” *Int. J. Mach. Tools Manuf.*, vol. 45, no. 11, pp. 1271–1281, 2005.

[117] N. Khanna and J. P. Davim, “Design-of-experiments application in machining titanium alloys for aerospace structural components,” *Measurement*, vol. 61, pp. 280–290, 2015.

[118] R. A. Rahman Rashid, S. Sun, G. Wang, and M. S. Dargusch, “An investigation of cutting forces and cutting temperatures during laser-assisted machining of the Ti-6Cr-5Mo-5V-4Al beta titanium alloy,” *Int. J. Mach. Tools Manuf.*, vol. 63, pp. 58–69, 2012.

[119] E. A. Rahim and H. Sasahara, “A study of the effect of palm oil as MQL lubricant on high speed drilling of titanium alloys,” *Tribol. Int.*, vol. 44, no. 3, pp. 309–317, 2011.

[120] S. Sharif, E. A. Rahim, and H. Sasahara, “Machinability of Titanium Alloys in Drilling,” in *Intech*, vol. 3, no. c, 1994.

[121] E. A. Rahim, K. Kamdani, and S. Sharif, “Performance evaluation of uncoated carbide tool in high speed drilling of Ti6Al4V,” *J. Adv. Mech. Des. Syst. Manuf.*, vol. 2, no. 4, pp. 522–531, 2008.

[122] N. F. M. Neto, “Orbital drilling of titanium alloys for aeronautics applications. Experimental studies,” Universidade do Porto, 2017.

[123] S. Kalpakjian and S. Schmid, *Manufacturing Engineering & Technology*, 7th ed. Boston: Pearson, 2012.

[124] G. Kirchoff, “A tale of two cutting tools: solid and indexable-insert drills,” *Cutting Tool Engineer Engineering*, Norhtfield, Sep-2016.

[125] J. P. Davim, *Design of Experiments in Production Engineering*. Springer International Publishing Switzerland, 2016.

[126] S. Chatterjee, S. S. Mahapatra, and K. Abhishek, “Simulation and optimization of machining parameters in drilling of titanium alloys,” *Simul. Model. Pract. Theory*, vol. 62, pp. 31–48, 2016.

[127] P. J. Ross, *Taguchi Method for Quality Engineering*. New York: McGraw-Hill, 1988.

[128] J. F. Kahles, M. Field, D. Eylon, and F. H. Froes, “Machining of titanium alloys,” *J. Met.*, vol. 37, no. 4, pp. 27–35, 1985.

[129] G. Weiping, X. Honglu, L. Jun, and Y. Zhufeng, “Effect of drilling process on fatigue life of open holes,” *Tsinghua Sci. Technol.*, vol. 14, no. Supplement 2, pp. 54–57, 2009.

[130] J. Castle, “Drilling Induced Fatigue Damage in Ti-6Al-4V,” Washington University in St. Louis, 2010.

[131] Milacron, “Machining Titanium,” *Cimcool Technical Report*, pp. 1–3, 2007.

[132] M. Darsin, T. Pasang, and Z. Chen, “Performance of TiAlN PVD coated carbide drill when drilling titanium 6246 alloy,” in *MATEC Web of Conferences*, 2017, vol. 109.

[133] M. Kurt, E. Bagci, and Y. Kaynak, “Application of Taguchi methods in the

optimization of cutting parameters for surface finish and hole diameter accuracy in dry drilling processes," *Int. J. Adv. Manuf. Technol.*, vol. 40, no. 5–6, pp. 458–469, 2009.

[134] E. Kilickap, M. Huseyinoglu, and A. Yardimeden, "Optimization of drilling parameters on surface roughness in drilling of AISI 1045 using response surface methodology and genetic algorithm," *Int. J. Adv. Manuf. Technol.*, vol. 52, no. 1–4, pp. 79–88, 2011.

[135] Z. Zhu, S. Sui, J. Sun, J. Li, and Y. Li, "Investigation on performance characteristics in drilling of Ti6Al4V alloy," *Int. J. Adv. Manuf. Technol.*, 2017.

[136] "Quick guide to surface roughness measurement," *Mitutoyo America Corporation*, Illinois, 2016.

[137] E. Kabakli, M. Bayramo, and N. Geren, "Evaluation of the surface roughness and geometric accuracies in a drilling process using the Taguchi analysis," *Mater. Technol.*, vol. 48, no. 1, pp. 91–98, 2014.

[138] M. A. Amran *et al.*, "Effects of machine parameters on surface roughness using response surface method in drilling process," *Procedia Eng.*, vol. 68, 2013.

[139] B. S. Kumar and N. Baskar, "Integration of fuzzy logic with response surface methodology for thrust force and surface roughness modeling of drilling on titanium alloy," *Int. J. Adv. Manuf. Technol.*, vol. 65, no. 9–12, pp. 1501–1514, 2013.

[140] M. Ramulu, T. Branson, and D. Kim, "A study on the drilling of composite and titanium stacks," *Compos. Struct.*, vol. 54, no. 1, pp. 67–77, 2001.

[141] D. Kim, M. Ramulu, and J. Garbini, "Hole quality in drilling of graphite/bismalemide-titanium stacks," in *33rd International SAMPE Technical Conference -Advancing Affordable Materials Technology*, 2001, pp. 1315–1326.

[142] Y. H. Çelik, H. Yildiz, and C. Özek, "Effect of cutting parameters on workpiece and tool properties during drilling of Ti-6AI-4V," vol. 58, no. 6, pp. 519–525, 2016.

[143] S. Waqar, S. Asad, S. Ahmad, C. A. Abbas, and H. Elahi, "Effect of drilling

parameters on hole quality of Ti-6Al-4V titanium alloy in dry drilling," *Mater. Sci. Forum*, vol. 880, no. December, pp. 33–36, 2016.

[144] A. Z. Sultan, S. Sharif, and D. Kurniawan, "Effect of machining parameters on tool wear and hole quality of AISI 316L stainless steel in conventional drilling," *Procedia Manuf.*, vol. 2, no. February, pp. 202–207, 2015.

[145] H. Singh and P. Kumar, "Tool wear optimization in turning operation by Taguchi method," *Indian J. Eng. Mater. Sci.*, vol. 11, no. 1, pp. 19–24, 2004.

[146] E. A. Rahim, K. Kamdani, and S. Sharif, "Performance evaluation of uncoated carbide tool in high speed drilling of Ti6Al4V," *J. Adv. Mech. Des. Syst. Manuf.*, vol. 2, no. 4, pp. 522–531, 2008.

[147] Amiss and J. Milton, *Machinery's Handbook. 25th edition*, 25th ed. New York: Industrial Press, 1996.

[148] R. B. da Silva, M. B. da Silva, W. F. Sales, E. O. Ezugwu, and Á. R. Machado, "Advances in the turning of titanium alloys with carbide and superabrasive cutting tools," *Adv. Mater. Res.*, vol. 1135, pp. 234–254, 2016.

[149] Collins English Dictionary, "Definition of 'machinability,'" *HarperCollins Publishers*. [Online]. Available: https://www.collinsdictionary.com/dictionary/english/machinability. [Accessed: 30-Jan-2018].

[150] V. A. Joshi, *Titanium Alloys: an Atlas of Structures and Fracture Features*. Boca Raton: Taylor & Francis, 2006.

[151] D. H. Herring, "Grain Size and Its Influence on Material Properties," *Heat Treat Dr.*, no. August, pp. 1–2, 2005.

[152] C. Danila, "Tutorial 28: Explicit Dynamics FEA of the Milling of a Copper Slab with a Rigid Tool," in *Hands-on ANSYS Workbench, Nothing Else*, 2nd ed., expertsfea, Ed. expertfea.com, 2017, pp. 1–36.

[153] Wikipedia, "Parasolid," *The Free Encyclopedia*, 2018. [Online]. Available: https://en.wikipedia.org/wiki/Parasolid. [Accessed: 01-Feb-2018].

[154] T. Fisher, "What is an X_T file?," *lifewire.com*, 2018. [Online]. Available: https://www.lifewire.com/x-t-file-2622427. [Accessed: 22-Jan-2018].

[155] H.-H. Lee, *Finite Element Simualtions with ANSYS Workbench 16*, 1st ed. Mission, Kansas: Stephen Schroff, 2015.

[156] AZoM, “Tungsten Carbide - An Overview,” *AZoM*, 2002. [Online]. Available: https://www.azom.com/properties.aspx?ArticleID=1203. [Accessed: 22-Dec-2017].

[157] E. Corona and B. Reedlunn, “A Review of Macroscopic Ductile Failure Criteria,” California, 2013.

[158] M. Slais, I. Dohnal, and M. Forejt, “Determination of Johnson-Cook equation parameters,” *Acta Metall. Slovaca*, vol. 18, no. 2, pp. 125–132, 2012.

[159] F. Li, X. Qi, and D. Xiang, “Finite element modeling of crack generation in laser shock peening processed airfoils,” *Adv. Mater. Sci. Eng.*, vol. 2014, 2014.

[160] J. F. Moxnes, J. A. Teland, S. Skriudalen, S. M. Bergsrud, L. Sundem-Eriksen, and H. Fykse, “Development of material models for semi-brittle materials like tungsten carbide,” Oslo, 2010.

[161] K. Prakash Marimuthu, H. P. Thirtha Prasada, and C. S. Chethan Kumar, “Force, stress prediction in drilling of AISI 1045 steel using finite element modelling,” *IOP Conf. Ser. Mater. Sci. Eng.*, vol. 225, 2017.

[162] P. Roud and P. Kožmín, “Numerical simulation of stress in elements for load transmission in multipurpose drilling tool,” Pilsen, Czech Republic, 2009.

[163] E. Akca, “Validation of stresses with numerical method and analytical method,” *Period. Eng. Nat. Sci.*, vol. 4, no. 1, pp. 17–28, 2016.

[164] ANSYS, “ANSYS Meshing Advanced Techniques.” ANSYS Confidental, 2017.

APPENDICES

A. Another Heat Treatment and Its Results

We also have tried the heat treatment at 985ºC for three hours then followed it by furnace cooling. This treatment resulted in a similar hardness to the as received one. The microstructure that resulted was completely different from other previous heat treatments. It was transformed beta with prior beta boundaries (Figure 4.7a). A slim incessant alpha film is existent at the grain boundaries [150]. The microstructure is similar to other titanium alpha + beta (Ti-6Al-4V and Ti-5Al-4V) when they were beta annealed [39].

The grain boundary was extremely big (more than 500 micron) not like the result of other heat treatments. Change of grain size may affect the yield strength because the movement of dislocation interacts with the grain boundary. The grain boundaries hinder the sliding of dislocation along the slip planes. The succeeding dislocations that slide along the same slip plane will be accumulated at the grain boundary. When the grain boundaries are extremely big then the number of boundaries are reduced. Consequently the cutting force would be reduced. Machinability is also affected by grain size (and grain boundary). In the case of steel, the coarse grain size preferable for rough machining is favoured while fine grain size is a better machining finish [151].

The cutting of grain boundary was revealed in some chips as shown in Figure A.1.

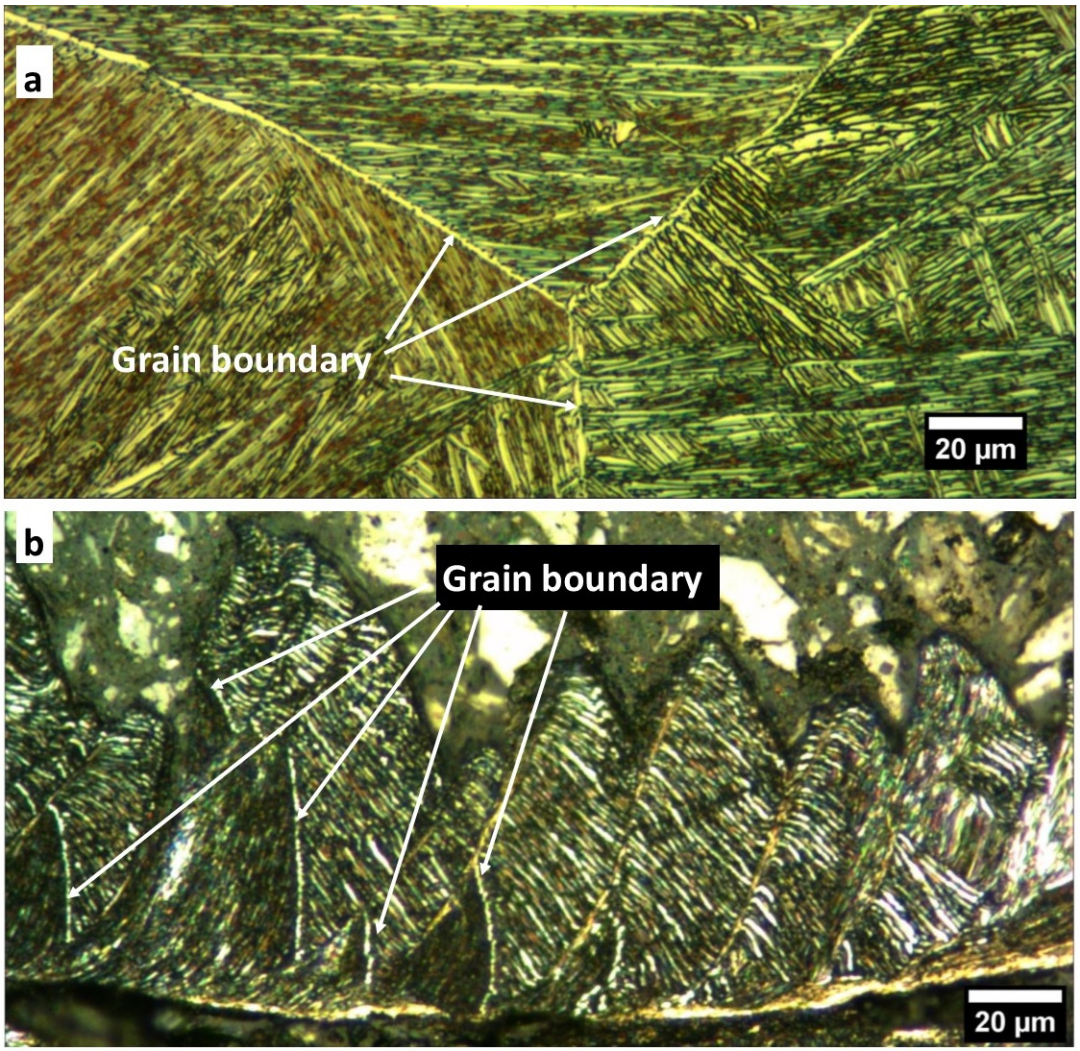

Figure A.1. Microstructure of Ti-6246 after heat treatment of 985°C for three hours then furnace cooled (a). The chips and a clear grain boundary that were cut along with chips formation (b).

B. Table F

F Table for alpha=.05

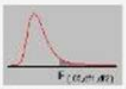

df2/df1	1	2	3	4	5	6	7	8	9	10	12	15	20	24	30	40	60	120	INF
1	161.4476	199.5000	215.7073	224.5832	230.1619	233.9860	236.7684	238.8827	240.5433	241.8817	243.9060	245.9499	248.0131	249.0518	250.0951	251.1432	252.1957	253.2529	254.3144
2	18.5128	19.0000	19.1643	19.2468	19.2964	19.3295	19.3532	19.3710	19.3848	19.3959	19.4125	19.4291	19.4458	19.4541	19.4624	19.4707	19.4791	19.4874	19.4957
3	10.1280	9.5521	9.2766	9.1172	9.0135	8.9406	8.8867	8.8452	8.8123	8.7855	8.7446	8.7029	8.6602	8.6385	8.6166	8.5944	8.5720	8.5494	8.5264
4	7.7086	6.9443	6.5914	6.3882	6.2561	6.1631	6.0942	6.0410	5.9988	5.9644	5.9117	5.8578	5.8025	5.7744	5.7459	5.7170	5.6877	5.6581	5.6281
5	6.6079	5.7861	5.4095	5.1922	5.0503	4.9503	4.8759	4.8183	4.7725	4.7351	4.6777	4.6188	4.5581	4.5272	4.4957	4.4638	4.4314	4.3985	4.3650
6	5.9874	5.1433	4.7571	4.5337	4.3874	4.2839	4.2067	4.1468	4.0990	4.0600	3.9999	3.9381	3.8742	3.8415	3.8082	3.7743	3.7398	3.7047	3.6689
7	5.5914	4.7374	4.3468	4.1203	3.9715	3.8660	3.7870	3.7257	3.6767	3.6365	3.5747	3.5107	3.4445	3.4105	3.3758	3.3404	3.3043	3.2674	3.2298
8	5.3177	4.4590	4.0662	3.8379	3.6875	3.5806	3.5005	3.4381	3.3881	3.3472	3.2839	3.2184	3.1503	3.1152	3.0794	3.0428	3.0053	2.9669	2.9276
9	5.1174	4.2565	3.8625	3.6331	3.4817	3.3738	3.2927	3.2296	3.1789	3.1373	3.0729	3.0061	2.9365	2.9005	2.8637	2.8259	2.7872	2.7475	2.7067
10	4.9646	4.1028	3.7083	3.4780	3.3258	3.2172	3.1355	3.0717	3.0204	2.9782	2.9130	2.8450	2.7740	2.7372	2.6996	2.6609	2.6211	2.5801	2.5379
11	4.8443	3.9823	3.5874	3.3567	3.2039	3.0946	3.0123	2.9480	2.8962	2.8535	2.7876	2.7186	2.6464	2.6090	2.5705	2.5309	2.4901	2.4480	2.4045
12	4.7472	3.8853	3.4903	3.2592	3.1059	2.9961	2.9134	2.8486	2.7964	2.7534	2.6866	2.6169	2.5436	2.5055	2.4663	2.4259	2.3842	2.3410	2.2962
13	4.6672	3.8056	3.4105	3.1791	3.0254	2.9153	2.8321	2.7669	2.7144	2.6710	2.6037	2.5331	2.4589	2.4202	2.3803	2.3392	2.2966	2.2524	2.2064
14	4.6001	3.7389	3.3439	3.1122	2.9582	2.8477	2.7642	2.6987	2.6458	2.6022	2.5342	2.4630	2.3879	2.3487	2.3082	2.2664	2.2229	2.1778	2.1307
15	4.5431	3.6823	3.2874	3.0556	2.9013	2.7905	2.7066	2.6408	2.5876	2.5437	2.4753	2.4034	2.3275	2.2878	2.2468	2.2043	2.1601	2.1141	2.0658
16	4.4940	3.6337	3.2389	3.0069	2.8524	2.7413	2.6572	2.5911	2.5377	2.4935	2.4247	2.3522	2.2756	2.2354	2.1938	2.1507	2.1058	2.0589	2.0096
17	4.4513	3.5915	3.1968	2.9647	2.8100	2.6987	2.6143	2.5480	2.4943	2.4499	2.3807	2.3077	2.2304	2.1898	2.1477	2.1040	2.0584	2.0107	1.9604
18	4.4139	3.5546	3.1599	2.9277	2.7729	2.6613	2.5767	2.5102	2.4563	2.4117	2.3421	2.2686	2.1906	2.1497	2.1071	2.0629	2.0166	1.9681	1.9168
19	4.3807	3.5219	3.1274	2.8951	2.7401	2.6283	2.5435	2.4768	2.4227	2.3779	2.3080	2.2341	2.1555	2.1141	2.0712	2.0264	1.9795	1.9302	1.8780
20	4.3512	3.4928	3.0984	2.8661	2.7109	2.5990	2.5140	2.4471	2.3928	2.3479	2.2776	2.2033	2.1242	2.0825	2.0391	1.9938	1.9464	1.8963	1.8432
21	4.3248	3.4668	3.0725	2.8401	2.6848	2.5727	2.4876	2.4205	2.3660	2.3210	2.2504	2.1757	2.0960	2.0540	2.0102	1.9645	1.9165	1.8657	1.8117
22	4.3009	3.4434	3.0491	2.8167	2.6613	2.5491	2.4638	2.3965	2.3419	2.2967	2.2258	2.1508	2.0707	2.0283	1.9842	1.9380	1.8894	1.8380	1.7831
23	4.2793	3.4221	3.0280	2.7955	2.6400	2.5277	2.4422	2.3748	2.3201	2.2747	2.2036	2.1282	2.0476	2.0050	1.9605	1.9139	1.8649	1.8128	1.7570
24	4.2597	3.4028	3.0088	2.7763	2.6207	2.5082	2.4226	2.3551	2.3002	2.2547	2.1834	2.1077	2.0267	1.9838	1.9390	1.8920	1.8424	1.7896	1.7330
25	4.2417	3.3852	2.9912	2.7587	2.6030	2.4904	2.4047	2.3371	2.2821	2.2365	2.1649	2.0889	2.0075	1.9643	1.9192	1.8718	1.8217	1.7684	1.7110
26	4.2252	3.3690	2.9752	2.7426	2.5868	2.4741	2.3883	2.3205	2.2655	2.2197	2.1479	2.0716	1.9898	1.9464	1.9010	1.8533	1.8027	1.7488	1.6906
27	4.2100	3.3541	2.9604	2.7278	2.5719	2.4591	2.3732	2.3053	2.2501	2.2043	2.1323	2.0558	1.9736	1.9299	1.8842	1.8361	1.7851	1.7306	1.6717
28	4.1960	3.3404	2.9467	2.7141	2.5581	2.4453	2.3593	2.2913	2.2360	2.1900	2.1179	2.0411	1.9586	1.9147	1.8687	1.8203	1.7689	1.7138	1.6541
29	4.1830	3.3277	2.9340	2.7014	2.5454	2.4324	2.3463	2.2783	2.2229	2.1768	2.1045	2.0275	1.9446	1.9005	1.8543	1.8055	1.7537	1.6981	1.6376
30	4.1709	3.3158	2.9223	2.6896	2.5336	2.4205	2.3343	2.2662	2.2107	2.1645	2.0921	2.0148	1.9317	1.8874	1.8409	1.7918	1.7396	1.6835	1.6223
40	4.0847	3.2317	2.8387	2.6060	2.4495	2.3359	2.2490	2.1802	2.1240	2.0772	2.0035	1.9245	1.8389	1.7929	1.7444	1.6928	1.6373	1.5766	1.5089
60	4.0012	3.1504	2.7581	2.5252	2.3683	2.2541	2.1665	2.0970	2.0401	1.9926	1.9174	1.8364	1.7480	1.7001	1.6491	1.5943	1.5343	1.4673	1.3893
120	3.9201	3.0718	2.6802	2.4472	2.2899	2.1750	2.0868	2.0164	1.9588	1.9105	1.8337	1.7505	1.6587	1.6084	1.5543	1.4952	1.4290	1.3519	1.2539
inf	3.8415	2.9957	2.6049	2.3719	2.2141	2.0986	2.0096	1.9384	1.8799	1.8307	1.7522	1.6664	1.5705	1.5173	1.4591	1.3940	1.3180	1.2214	1.0000

C. Energy Dispersive X-ray Spectrometry (EDS) Test Result

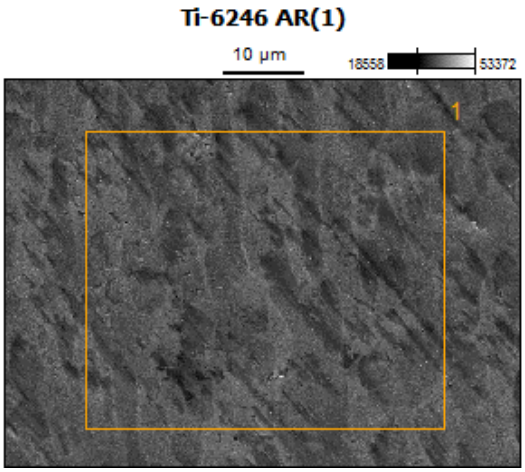

Image Name:	Ti-6246 AR(1)
Image Resolution:	512 by 384
Image Pixel Size:	0.12 µm
Acc. Voltage:	20.0 kV
Magnification:	2000

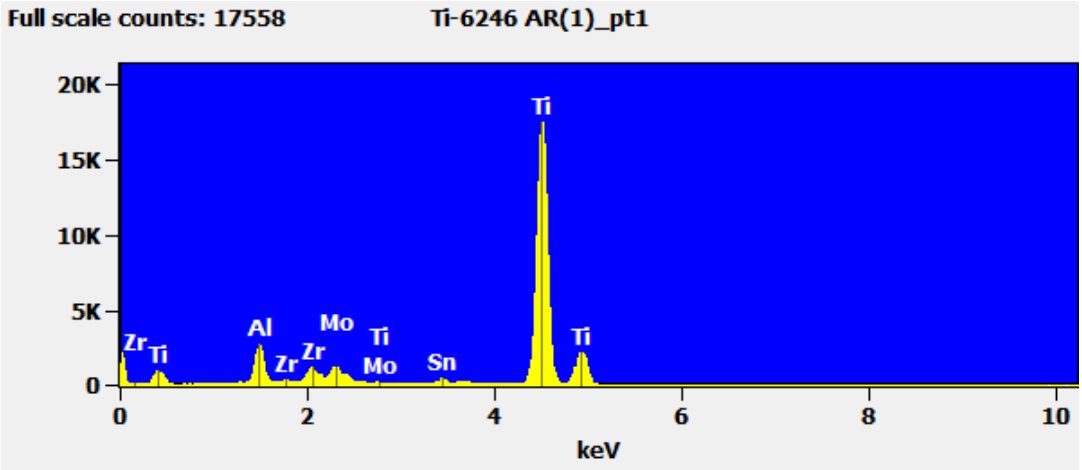

Net Counts

	Al	Ti	Zr	Mo	Sn
Ti-6246 AR(1)_pt1	24246	259323	13245	18267	5248

Weight %

	Al	Ti	Zr	Mo	Sn
Ti-6246 AR(1)_pt1	6.14	82.15	4.34	5.39	1.99

Atom %

	Al	Ti	Zr	Mo	Sn
Ti-6246 AR(1)_pt1	11.02	83.13	2.30	2.73	0.81

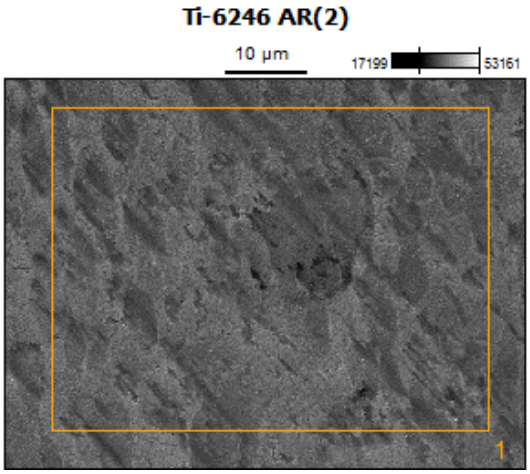

Image Name:	Ti-6246 AR(2)
Image Resolution:	512 by 384
Image Pixel Size:	0.12 µm
Acc. Voltage:	20.0 kV
Magnification:	2000

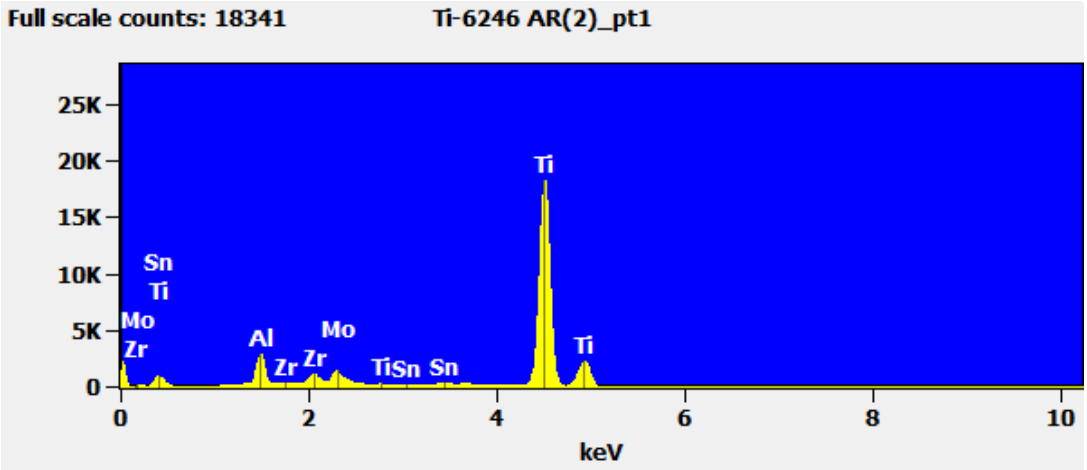

Net Counts

	Al	Ti	Zr	Mo	Sn
Ti-6246 AR(2)_pt1	25137	266582	13377	19826	5077

Weight %

	Al	Ti	Zr	Mo	Sn
Ti-6246 AR(2)_pt1	6.17	82.02	4.25	5.68	1.87

Atom %

	Al	Ti	Zr	Mo	Sn
Ti-6246 AR(2)_pt1	11.09	83.01	2.26	2.87	0.76

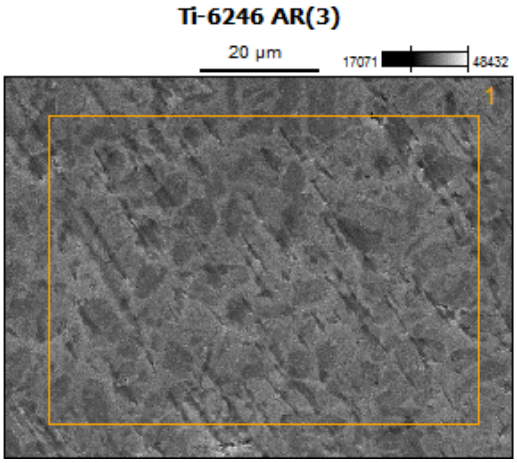

Image Name:	Ti-6246 AR(3)
Image Resolution:	512 by 384
Image Pixel Size:	0.17 µm
Acc. Voltage:	20.0 kV
Magnification:	1500

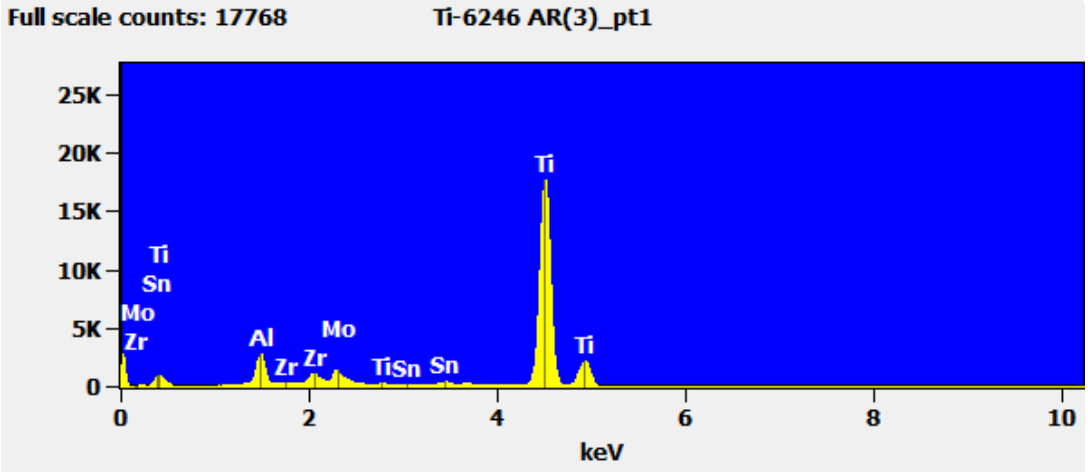

Net Counts

	Al	Ti	Zr	Mo	Sn
Ti-6246 AR(3)_pt1	24639	261888	13422	19303	5445

Weight %

	Al	Ti	Zr	Mo	Sn
Ti-6246 AR(3)_pt1	6.15	81.85	4.33	5.62	2.04

Atom %

	Al	Ti	Zr	Mo	Sn
Ti-6246 AR(3)_pt1	11.07	82.95	2.31	2.84	0.83

D. Result of Optic Emission Spectroscopy (OES)

South Auckland Forgings Engineering Ltd
116 Waihoehoe Road, Drury 2113
P.O. Box 44, Drury 2247, Auckland, New Zealand
Tel: 64 9 2948437 Fax: 64 9 2948431
info@SafeGroup.co.nz
www.SafeGroup.co.nz

MATERIAL INVESTIGATION REPORT

DATE: 17 Oct 2017
CLIENT: Mahros Darsin, AUT
SUBJECT: OES Analysis Titanium 6Al-2Sn-4Zr-6Mo
ORDER No. Timotius Pasang
REPORT / JOB No. 11584

EQUIPMENT:
Oxford FMX Optical Emission Spectrometer, calibrated with 4 supplied Ti-base calibration standards.

RESULTS:

Chemical Analysis (w/w %) Sample ground for sub-surface chemical composition.

Ti	Al	V	Cr	Cu	Fe	Mn	Mo	Sn	Ni	Si	Zr	C	Ta
81.0	6.69	0.034	0.007	0.016	0.062	0.005	5.85	2.18	0.008	0.05	4.09	0.012	0.018

TECHNICIAN:

Barry Robinson NZCE(mech)

E. Modeling of Drilling

This chapter briefly outlines the preliminary results from the modeling of the drilling process conducted in this investigation. Note that the modeling was not completed due to some technical problems relating to the computer's capability. There were some steps in modeling drilling with ANSYS. Prior to using ANSYS a model of the drill tip was developed with Solidworks software. The model was then imported to ANSYS. The first step in developing the modeling was to set the material properties. If by default the material properties are available in the software, we do not need to input it manually. The second step was setting interactions between the tool and the workpiece, followed by setting the mesh control. Before rendering – as the last step – the initial conditions and analysis should be set. We could set the velocity (linear and angular), fixed support(s) end time of simulation, mass scaling, etc. to obtain a specific behaviour and the certainty that the finite elements problem is correctly set-up. The output of the simulation should also be set-up at this stage, such as stress, strain, directional deformation, etc. Details of the steps described are in the following sections.

E.1 Tool and Workpiece Model

The tool and workpiece model was made using Solidworks. To be able to import the model into ANSYS the model was saved as an x_t format [152]. An x_t file format is a file part in a parasolid model, or is also famous as a modeler transmit file, which makes it able to be exported to or imported from different CAD programs. Parasolid is a geometric modeling kernel initially created by Shape Data Limited, now possessed by Siemens PLM Software (previously UGS Corp.), that can be licensed by other parties for use in their 3D computer graphics software products [153]. As a text-based file, the x_t format is basically comprised of numbers. The CAD programmes, then, will be able to read and identify all aspect of the 3D characteristics, such as geometry, colour, and other features [154]. The tool was modeled as a drill tip with some simplification, but the main dimensions of the tool were kept as the real dimension. Due to some limitations on modeling a coated tool, the tool material was set as tungsten carbide without coating. The workpiece of Ti-6246 alloy was modeled as a block with the same dimensions as the real one, 15 (length) x 15 (width) x 15 mm (height). Two other sizes of height were not tried for the sake of simplicity.

After opening the ANSYS programme the explicit dynamic option was then chosen from the toolbox tree. The explicit method is useful for high-speed impact problems and highly nonlinear problems [155]. The x_t file that was made in Solidworks was then imported. The next step was setting the material properties, and as there were none available for both titanium alloy 6246 or tungsten carbide in the programme ANSYS, the manual input was carried out based on some existing literature. The tungsten carbide mechanical properties were available online from AZO Materials [156], therefore most of the input source for this came from this website, unless it is stated differently. In case the properties are in a certain range of values, we intentionally chose one specific value from within it. Subsequently, the mechanical properties of the titanium alloy 6246 was taken from Boyer et al. [8] and other literature [7], [31]. Material properties of tungsten carbide and Ti-6246 are presented in Table E.1.

Table E.1 Physical, mechanical and thermal properties of Ti-6246 and tungsten carbide available from the literature

Physical/Mechanical/ Thermal Properties	**Ti-6246**		**Tungsten Carbide**	
		Chosen		Chosen
C_p [J/kgK]	508			
Density [kg/m^3]	4650		14770	
Young's Modulus [MPa]	114,000		620,000	
Shear Modulus [MPa]	42,900		255,000	
Bulk Modulus [MPa]			362,000	
Poisson's Ratio	0.33		0.215	
Yield Strength [MPa]	930 - 1137	1130		
Tensile Strength [MPa]	1000 - 1206	1200	370-530	500
Elongation [%]	6 - 20			
Reduction in Area [%]	10 - 35			
Hardness [Rc Max]	45			
Melt Temperature [^{o}C]	1595 - 1675	1615	1768	
Specific Heat [J/kg.K]	500		250	
Thermal Conductivity [W/m.K]	7.70		95	
Volumetric Thermal Expansion [K^{-1}]			0.000015	

Relating to material properties we have set the Johnson-Cook damage for failure criteria. The Johnson-Cook is a plasticity and failure model that accounts for factors that are important when materials are loaded to fail at a high rate [157]. These factors include large strains, a large strain rate, high pressure and high temperatures. There are

five parameters needed for inputting the J-C damaged failure criteria: A, B, n, C, and m. A refers to the yield stress, B denotes the hardening modulus, n symbolises the hardening coefficient, C designates the strain rate sensitivity coefficient and m represents the thermal softening coefficient [158].

Procedurally, the parameters A, B, and n should be determined by inserting the data from the isothermal stress-strain curve which is a nonlinear least square to Ludvik equation. [104]. Ludvik equation is the first section in the Johnson-Cook model. However, the parameter C was determined by directly contrasting the stress-strain curves from computation with the experimentations [104]. As we did not do our own experiments in finding the relevant parameters for input of this criteria, the parameters for Ti-6246 were taken from the literatures, such as Hokka et al. [104] and Muhammad et al. [36]. In addition, the parameters for the J-C damage initiation model d_1 to d_5 was chosen from Li et al. [159]. The tungsten carbide J-C parameters and constant were taken from Moxnes et al. [160]. The overall parameters of J-C and constants of J-C damage are presented in Table E.2.

Table E.2. J-C Model parameters value and J-C damage initiation model constants for tool and workpiece material.

	Ti-6246 [104], [159]		**Tungsten Carbide [160]**
J-C Model parameters values	**Initial**	**Optimized**	
A [MPa]	1866	1657	3000
B [Mpa]	901	402	89000
n	0.7392	0.2180	0.65
C	0.01	0.0054	0.0
m	0.6962	0.8034	1.0
T_r [ºC]	23	23	
T_m [ºC]	1625	1625	
J-C damage initiation model			
d_1		-0.09	0.0
d_2		0.14	0.0019
d_3		0.5	-3.0
d_4		0.014	0.0
d_5		3.87	0.0

By completing the properties of the materials to the database of ANSYS, the model was then ready for the next steps.

E.2 System Model

In the mechanical windows in the 1st body from the tree, we appointed Ti-6246 for the workpiece (WP) and tungsten carbide for the tool. Then, we chose a tool that was rigid while the WP was flexible. The alternative option was also tried in studying tool deterioration but it did not work and the tool blasted into dust.

In a coordinate system, instead of the global coordinate system being used as the default, we added another two: (i) cylindrical coordinate system at the tool and (ii) a Cartesian coordinate system at the workpiece, as shown in Figure 7.1. These additional coordinates would help in directing the tool when setting linear and angular velocity in applying the initial steps of the condition.

Body interactions were added in the connections branch and the type of interactions were set as frictional with a frictional coefficient of 0.25 and dynamic coefficient of 0.1. Both these values were normally used in machining simulations. Prior to this setting, we should ensure that there were no contacts defined.

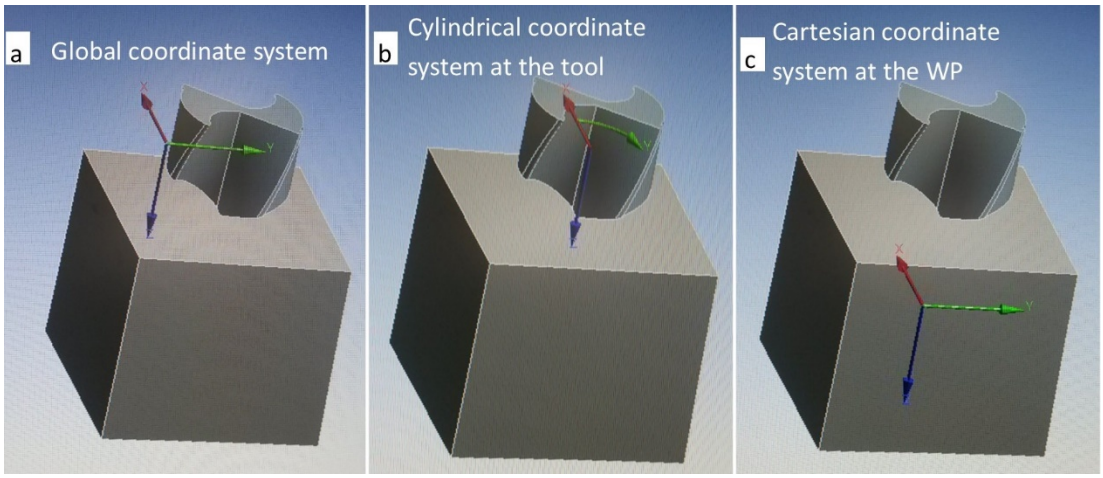

Figure E.1. Three coordinate systems: (a) Global coordinate system as default, (b) Cylindrical coordinate system on the tool, (c) Cartesian coordinate system on the workpiece.

There are three element types that can build a body in ANSYS: (i) tetrahedral (tet), (ii) hexahedral (hex) and (iii) polyhedral (poly). For ANSYS Workbench mechanical explicit dynamics, tet and hex elements are usually applied, whereas poly elements are usually for simulation in fluids. The hex method produced fewer elements, and consequently a faster solution time with better accuracy than that of the tet elements. Therefore, the hex dominant method was chosen in this simulation for the tool only

and all quads for the free face mesh type. The hex dominant was used as this option is recommended for bodies that cannot be swept. The body sizing of the tool was set as 1.00 mm and 0.2 mm for the workpiece, which means the average element edge length was 1.00 mm and 0.2 mm on the tool and workpiece correspondingly. This setting of the workpiece element size was $1/5^{th}$ smaller than that of the tool because we were after the chip formations. With this setting, it would generate total nodes of 173,370 and total elements of 163,360, as shown in Figure 7.2. Before achieving these settings, some trials with coarser elements were carried out, just to be sure that the comportment of finite element problems were correctly set-up within the short rendering time.

Prior to rendering, some initial conditions needed to be set up. First, velocities of the tool; it is impossible to set the real linear or angular velocity because it would take a long time for the rendering. Moreover, in explicit dynamic methods, the time of integration needs to be very little to ensure stability and accuracy of the solution. It is related to typical integration time set up, which is between nanoseconds to microseconds; a typical simulation time is about 1 milisecond to 1 second, which will need many thousands or millions of cycles [155]. In analysis settings, we set 'end time' as 7.0e-6s. With this very small time, we set the linear velocity of the tool at 1.0e+6 mm/s to Z component of the Cartesian coordinate system, and angular velocity of 3.0e+6 rad/s to the Z component of the Cartesian coordinate system. This angular velocity was equivalent to a feed rate of 2.09 mm/revolution.

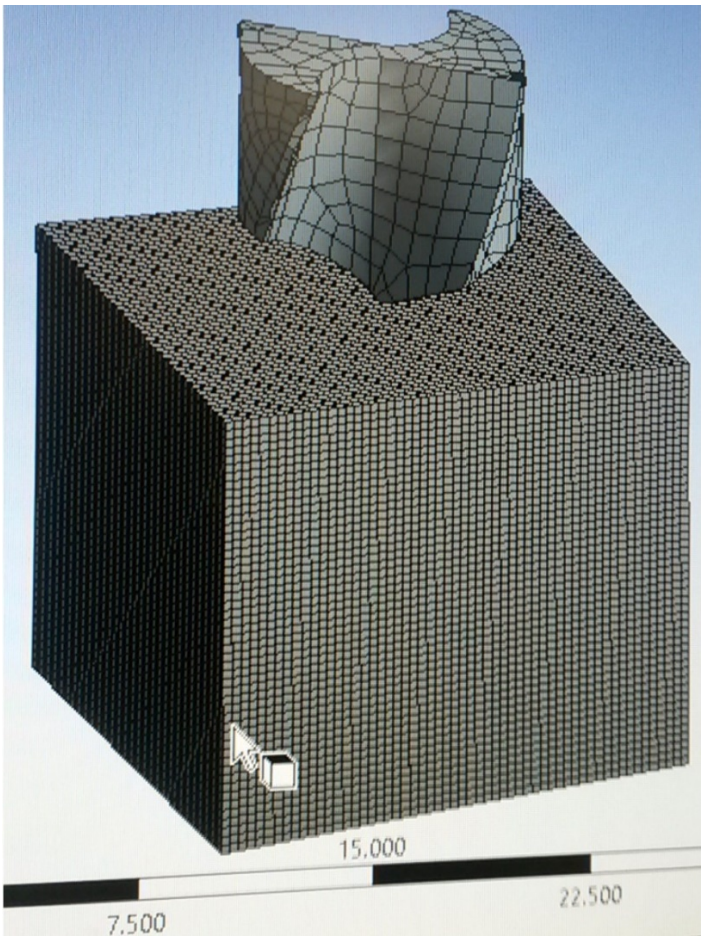

Figure E.2 Meshing result of the tool-workpiece system.

A mass scaling was used to synthetically enlarge the mass of tiny elements, so the stability time step could be raised. Only to those elements which have a calculated stability time step less than a specified value a mass scaling is applied. This specified value by default is 1.e-20s, which is to ensure that no mass scaling takes place [155]. In this simulation the minimum time value was set as 1.e-13 s. Consequently, a minimum CFL (Courant-Friedrichs-Levy) time step was 1.e-8 s. Using mass scaling, the system would automatically add artificial mass to individual elements to ensure that their CFL time step is at least equal to 1.e-8 s.

The five faces of the workpiece were set as fixed support. All of the workpiece faces were set as fixed support, except for the face which has a direct contact with the tool. This support was fixed to ensure that the workpiece would not move. To be specific, these five faces would not move as chips in the simulation.

E.3 Result and Discussion

The simulation result is presented in Figure 7.3. Creating chips could not be performed as hoped as they were shattered into pieces like dust. The rotation and forward movement of the tool deviated from where it should have to go; the circumference of the hole was not circular. This result is identical with the result of Marimuthu et al. [161] with their effort to make a drilling simulation for AISI1045. On the colour scale at the left side of Figure 7.3-a, it is clear that the red-dusted-chips experienced the maximum stress of up to 1.4284e5 MPa. This value is much higher than the maximum stress of 339.921 MPa on the tool design part which was the result gained by Roud and Kožmín [162]. The remainder of the workpiece was still both blue and light blue in colour, which means the remaining workpiece stayed in low stress. The main cause was probably from the very high speed. They used Vc = 120 m/min and fr = 0.25mm/rev [162].

Several attempts were made to achieve the chip formations better. One of the attempts was by reducing the mesh size of the workpiece from 0.3 mm to 0.2 mm. The result showed that the chip blasting was more severe and the maximum stress to 1.5861e11 Pa (=1.5862e5 MPa), or increased to 0.1577 MPa, is presented in Figure 7.3-b. On the contrary, the minimum stress was decreased from -70,887 MPa to -160,490 MPa. That means the range between maximum and minimum stress was increased. It may be because the smoother the mesh the more detail that was in the analysis. Consequently, calculation of the stress experienced by each of the elements was more detailed and made the possibility of recording with more precision. It is important to note that the minus sign of the stress means the part or element experiences compression, while the plus value means the element(s) are under tension [163].

A simulation with a smoother mesh on the workpiece has also been tried, but it took a significant amount of time to complete. Then, after several days the simulation was held up, so consequently it had to be abandoned. The result of the uncompleted simulation is presented in Figure E.3-c. Retrials of this plan resulted in the same conditions. It may be related to the capacity of the memory of the computer used for running the simulation. The more complex the parameters used and the smoother the mesh, the higher the memory of the computer needed. For the purpose of this research, the existing mesh of workpiece of 0.2 mm should be adequate.

The maximum and minimum stresses which are shown in Figure E.3 were at the last position of simulation according to the setting for linear and angular speed of the tool. The maximum and minimum stresses fluctuated along the drilling simulation, as shown in Figure E.4. The maximum stress was at a time step of 2e-6s at a value of 1.9521e5 MPa and the minimum stress was at a time step of about 3.8e-6s at a level value of -5.3451e5 MPa.

The fluctuation of stresses may be correlated to the percentage of engagement of the tool on the workpiece. At the early stage of engagement where only a tip of the drill was ploughed into the workpiece (Figure E.4-a), the maximum stress was small, it then reached its maximum when all the blades of the tool were just submerged into the workpiece (Figure E.4-b).

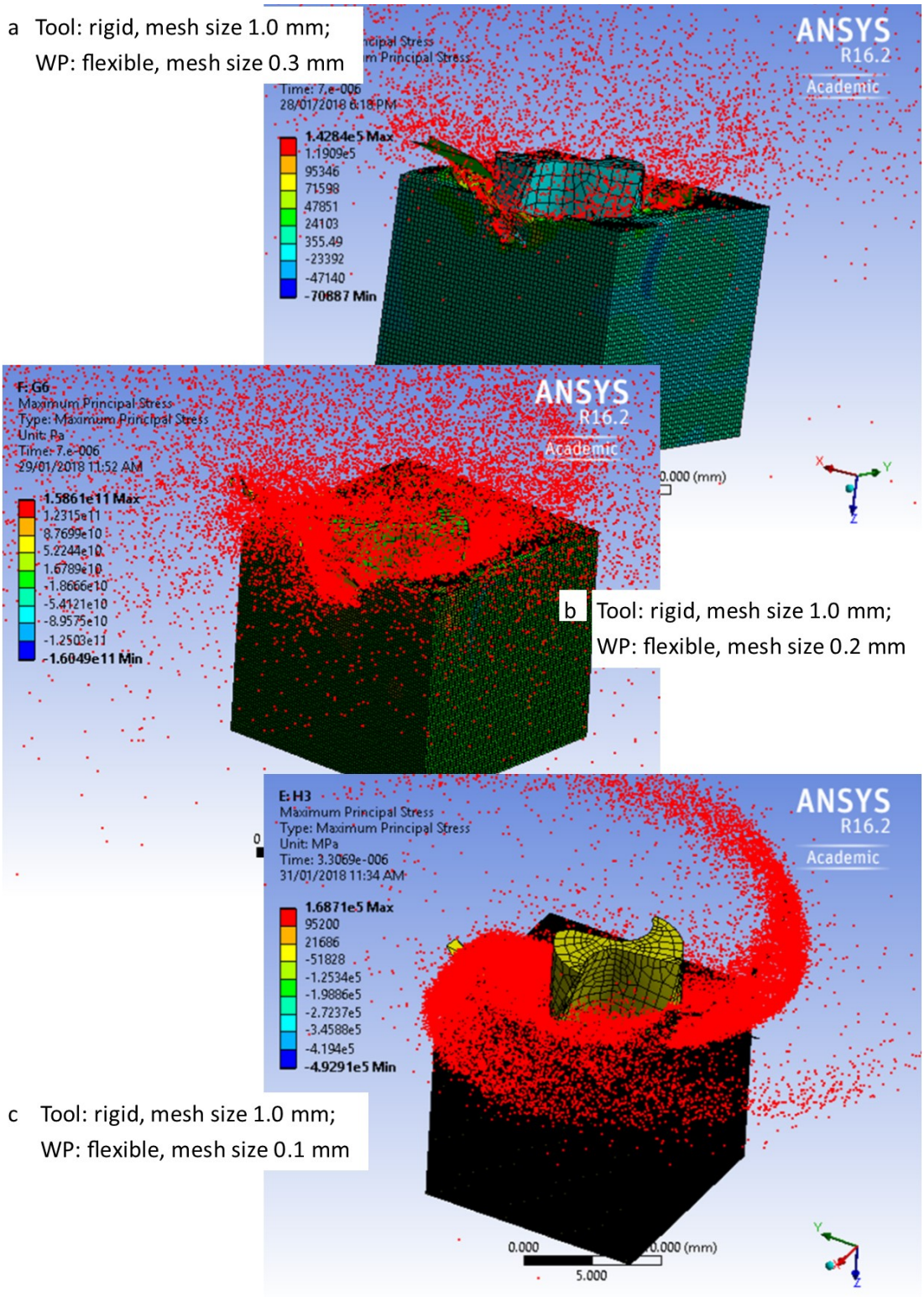

Figure E.3 Appearance of the last states of drilling; chips were shattered into pieces. Reducing the mesh size of the workpiece from 0.3 (a) to 0.2 (b) made the blasting more severe and increased the range between maximum and minimum stress. Further reduction of mesh to become (c) 0.1 made the simulation stop.

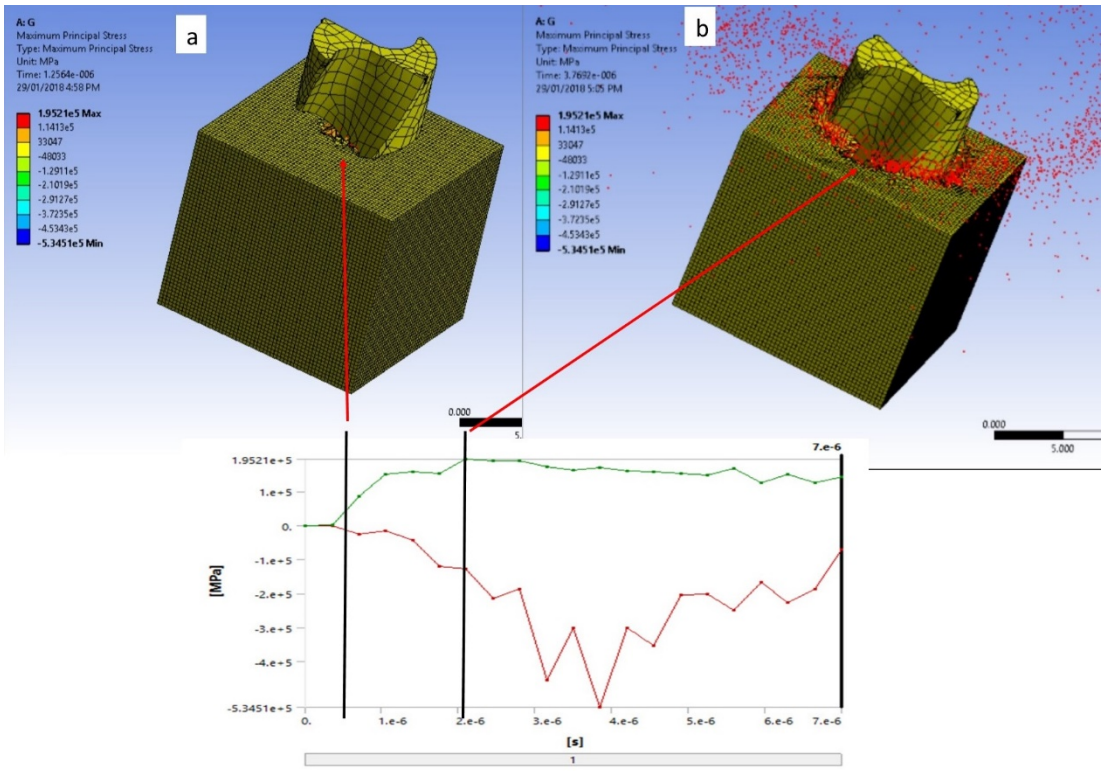

Figure E.4. Maximum stress changing over the engagement position between the tool and workpiece: (a) early stage of drilling, maximum stress relatively low, (b) fully engaged resulting in highest maximum stress.

Another attempt to reduce the equaivalent feed rate was done by increasing the angular speed of the tool ten times (from 3.0e+6 rad/s to become 3.0e+7 rad/s). Simulation results show the tool slipped on the workpiece after a little drilling, as presented in Figure E.5. It may be due to an unbalanced setting between the linear and angular settings in regard to time taken for completing the simulation. When the angular speed of the tool was increased more than 100 times (aiming to reduce the feed rate closer to the real drilling situation) the tool did not touch the workpiece, but it slid on it then bounced while rotating, avoiding the workpiece. Therefore, balancing among the three parameters, i.e. linear speed & rotational speed of the tool and 'end time' of the simulation is a critical part in the simulation of drilling using ANSYS.

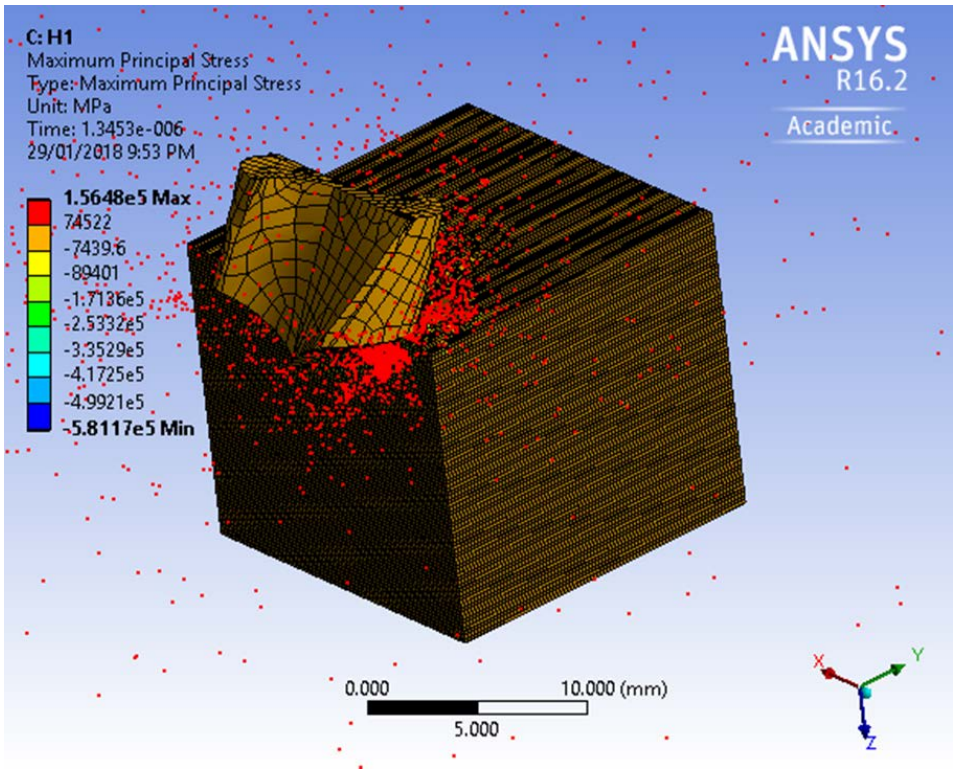

Figure E.5 Appearance of the last state of simulation when angular speed of the tool is 3e+7 rad/s, the tool slid on the workpiece with only little drilling done.

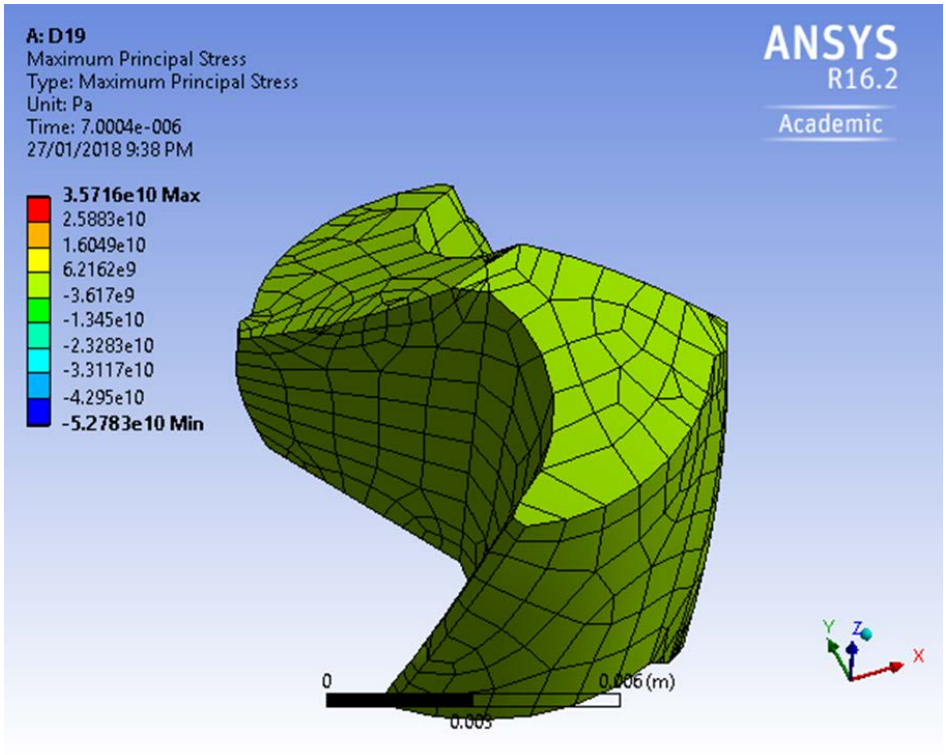

Figure E.6. The tool appearance after completion of drilling. Note: there was no analysis done on it when it was set as a rigid material.

In all the above studies there was no tool deterioration because the tool was set as a rigid material (Figure E.6). Therefore, the iteration was carried out by ANSYS within the workpiece only. In order to see the tool deterioration, the tool should be set as flexible. The first trial was made by setting the tool as flexible and the workpiece as rigid. The simulation shows that the tool was blasted into dust, as shown on Figure E.7-a. Changing the setting to both the tool and the workpiece as flexible did not improve the simulation result, as shown in Figure E.7-b. The setting of both the tool and workpiece as rigid bodies was not tried because there would not be analysis if any body was set as a rigid one. Erosion controls in the analysis setting had been determined as the condition that an element would be removed. Recommended values are in the range from 0.75 to 3.0 [164]. Several trials using different values within the recommended range exibits that there was no considerable difference on the simulation results. It was set by a default of 1.5, which means an element would be removed when its geometric strain or effective strain exceeded a limit of 150% [155]. This value is large enough to ensure that no elements are removed by default. All elements of the tool exploded because these elements exceeded its effective strain; that may be due to a very high linear and rotational speed of the tool.

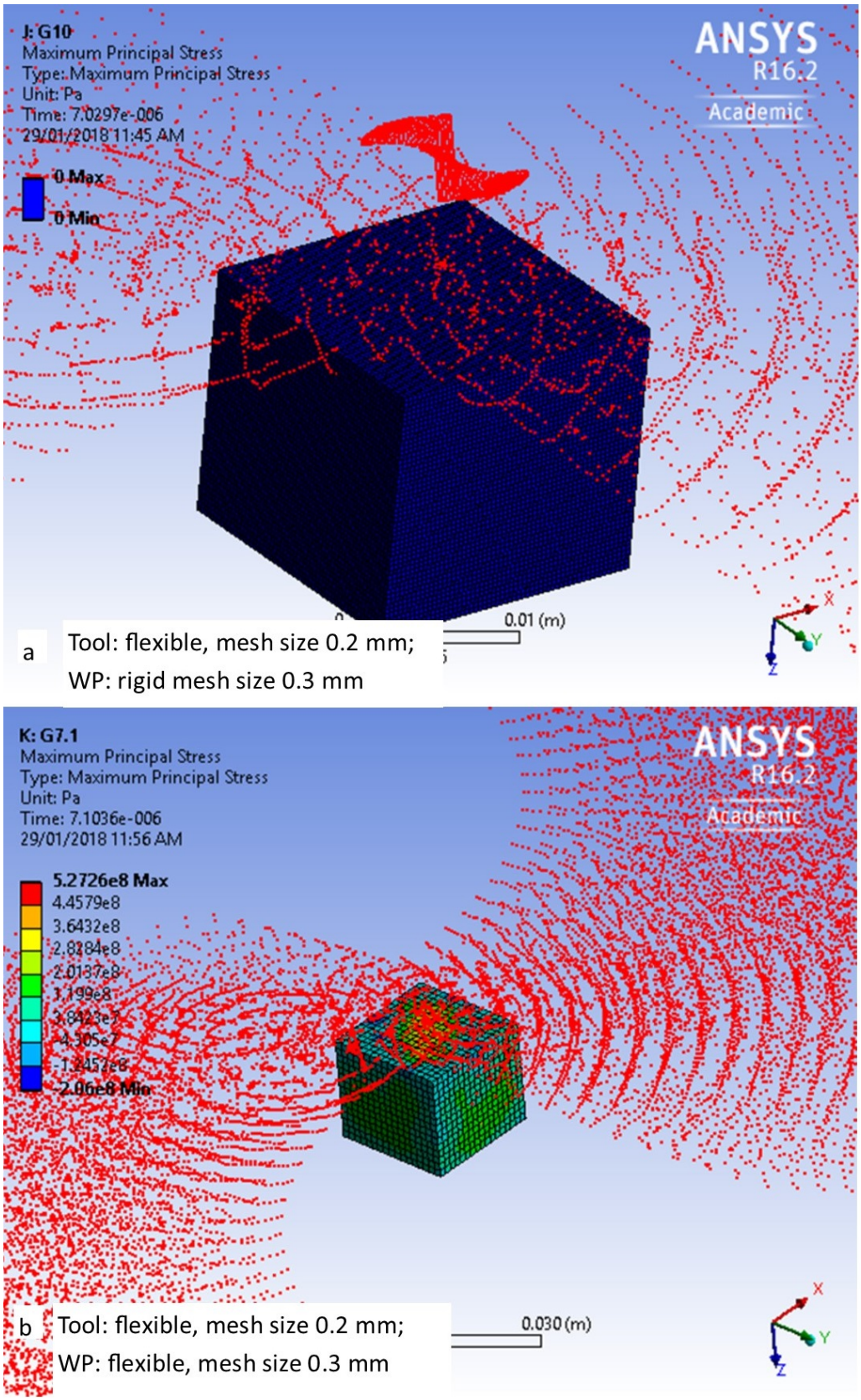

Figure E.7. Simulation results on tool deterioration: (a) setting tool as flexible and workpiece as rigid, (b) both tool and workpiece were set as flexible.

E.4 Conclusion

The simulation of drilling with ANSYS could not achieve the main goal, i.e. a serrated chip formation. However, some points of note could be learned from the simulation result so far:

a. A smoother mesh on the workpiece required a longer time for the simulation to run. In this simulation the mesh size of 0.2 mm for the workpiece and 1.0 mm for the tool resulted in the optimum performance of the tool-workpiece-chips; a mesh size of less than 0.2 mm would be very time consuming due to the capacity of the memory of the computer used;
b. A balance between linear and angular speed of the tool along with the time set for the simulation is very essential to achieve the correct movement of the drill in simulation;
c. Setting the tool as flexible to simulate tool deterioration resulted in the tool being blasted into dust, regardless of the workpiece as flexible or rigid.